

University of Windsor

Scholarship at UWindor

Electronic Theses and Dissertations

Theses, Dissertations, and Major Papers

2014

Effect of Roll Material on Surface Quality of Rolled Aluminum

Qi Zhao

University of Windsor

Follow this and additional works at: <https://scholar.uwindsor.ca/etd>



Part of the [Materials Science and Engineering Commons](#)

Recommended Citation

Zhao, Qi, "Effect of Roll Material on Surface Quality of Rolled Aluminum" (2014). *Electronic Theses and Dissertations*. 5080.

<https://scholar.uwindsor.ca/etd/5080>

This online database contains the full-text of PhD dissertations and Masters' theses of University of Windsor students from 1954 forward. These documents are made available for personal study and research purposes only, in accordance with the Canadian Copyright Act and the Creative Commons license—CC BY-NC-ND (Attribution, Non-Commercial, No Derivative Works). Under this license, works must always be attributed to the copyright holder (original author), cannot be used for any commercial purposes, and may not be altered. Any other use would require the permission of the copyright holder. Students may inquire about withdrawing their dissertation and/or thesis from this database. For additional inquiries, please contact the repository administrator via email (scholarship@uwindsor.ca) or by telephone at 519-253-3000ext. 3208.

Effect of Roll Material on Surface Quality of Rolled Aluminum

by

Qi Zhao

A Thesis

Submitted to the Faculty of Graduate Studies
through Engineering Materials
in Partial Fulfillment of the Requirements for
the Degree of Master of Applied Science at the
University of Windsor

Windsor, Ontario, Canada

2014

©2014 Qi Zhao

Effect of Roll Material on Surface Quality of Rolled Aluminum

by

Qi Zhao

APPROVED BY:

A. T. Alpas
Mechanical, Automotive, and Materials Engineering

S. Chowdhury
Electrical and Computer Engineering

A.R. Riahi, Advisor
Mechanical, Automotive, and Materials Engineering

April 4, 2014

DECLARATION OF ORIGINALITY

I hereby certify that I am the sole author of this thesis and that no part of this thesis has been published or submitted for publication.

I certify that, to the best of my knowledge, my thesis does not infringe upon anyone's copyright nor violate any proprietary rights and that any ideas, techniques, quotations, or any other material from the work of other people included in my thesis, published or otherwise, are fully acknowledged in accordance with the standard referencing practices. Furthermore, to the extent that I have included copyrighted material that surpasses the bounds of fair dealing within the meaning of the Canada Copyright Act, I certify that I have obtained a written permission from the copyright owner(s) to include such material(s) in my thesis and have included copies of such copyright clearances to my appendix.

I declare that this is a true copy of my thesis, including any final revisions, as approved by my thesis committee and the Graduate Studies office, and that this thesis has not been submitted for a higher degree to any other University or Institution.

ABSTRACT

The surface defects of aluminum alloys that have undergone hot rolling were studied.

The effects of different roll materials, of the number of rolling passes and of lubrication on surface defects of hot rolled aluminum alloys were investigated by laboratory hot rolling. Two different aluminum alloys, Al-Mn and Al-Mg, were each rolled against three different steel alloy rolls, AISI 52100, AISI 440C and AISI D2. The results showed that different roll materials do affect the morphology of the mating aluminum alloy surface with apparent surface defects, which included magnesium and oxygen rich dark regions on both alloys. The carbide protrusions in 440C and D2 steel rolls are confirmed to be responsible for the dark, rich magnesium and oxygen regions on both the rolled Al-Mn and Al-Mg alloy surfaces. As the number of passes increases, Mg and O deposit in the form of patches and grain boundaries near the surface area.

DEDICATION

To my parents;

Without my loving parents unconditional love, support, and encouragement, I wouldn't have been able to continue my study.

I dedicate my dissertation work to my advisor Dr. A Riahi. He is my respected advisor for my academic career.

I also dedicate my dissertation work to my colleague Olufisayo Gali, without his help I would be like a ship on the sea with no compass.

ACKNOWLEDGEMENTS

I would like to give my sincere gratitude to Dr. Riahi; without his support and encouragement, I wouldn't have finished my research work. His mentorship and knowledge have been a great help to my career. I would also like to thank Dr. Alpas for his continual support, and his valuable suggestions have indeed been an inspiration to my study. My thanks to Dr. Hunter and Dr. Shafiei from Novelis Global Research and Technology Center, as well for their comments, support and vital suggestions during this work.

I would like to express my gratitude to Dr. Chowdhury, giving thanks for his time and his constant suggestions and inspiration to me. My thanks also to Dr. Northwood for his time and aid on my final defence as well as my dissertation.

My special thanks to Olufisayo Gali for training me on the experiments, for valuable suggestions and for inspiring ideas in my work. I would also like to thank the members of the whole tribology group. They were always kind to provide equipment and guidance during my research.

Financial support for this research is provided by Ontario Centers of Excellence (OCE), Natural Sciences and Engineering Research Council of Canada (NSERC) and Novelis Global Research and Technology Center.

TABLE OF CONTENTS

DECLARATION OF ORIGINALITY	III
ABSTRACT.....	IV
DEDICATION.....	V
ACKNOWLEDGEMENTS	VI
LIST OF FIGURES	IX
LIST OF TABLES	XV
NOMENCLATURE.....	XVI
CHAPTER 1 INTRODUCTION.....	1
1.1 Background	1
1.1.1 Aluminum alloys	1
1.1.2 Heat-treatable and non-heat-treatable alloys.....	1
1.1.3 Rolling process	4
1.1.4 Steel roller alloys.....	6
1.2 Thesis objective	7
1.3 Organization of thesis.....	8
CHAPTER 2 REVIEW OF LITERATURE	10
2.1 Introduction of disturbed layer	10
2.2 Microstructure of the disturbed layer.....	12
2.3 Content distribution in disturbed layer of aluminum alloy under rolling	15
2.4 Mechanisms of disturbed layer formation.....	22
2.5 Optical appearance	26
2.6 Effect of disturbed layer to filiform corrosion (FFC).....	27
2.7 Rolling parameters that affect the surface layer.....	32
2.7.1 Heat treatment and strain effect.....	33
2.7.2 Material transfer and adhesion	36
2.7.3 Grinding effect	39
2.8 Summary of literature survey.....	40

CHAPTER 3 DESIGN AND METHDOLOGY	41
3.1 The workpiece	41
3.2 The roller	41
3.3 Laboratory simulation	42
CHAPTER 4 RESULTS	46
4.1 Results with Al-Mn alloy	46
4.2 Results with Al-Mg alloy	48
CHAPTER 5 DISCUSSION	74
CHAPTER 6 CONCLUSION	79
REFERENCES	80
VITA AUCTORIS	90

LIST OF FIGURES

Figure 1. Optical micrographs of the two alloys a) AA3104, b) AA5182, c) Phase diagram of binary Al–Mg system, d) Phase diagram of binary Al–Mn system [11,14].....	4
Figure 2. Typical process route for can body stock [15,16]	5
Figure 3. Schematic representation of subsurface layer containing microcrystalline oxides mixed with small grained material and covered with a continuous surface oxide. Layer A represents the surface oxide layer and layer B represents the subsurface ultrafine grained layer [28]	13
Figure 4. SEM backscattered micrograph of the surface of Aluminum alloy AA5050: (a) as-cast; (b) hot roll after first pass. [16].....	14
Figure 5. Schematic diagrams showing the microstructure of near-surface deformed layer introduced by rolling: (a) type A is hot rolling involved and (b) type B under cold rolling without hot rolling involved [27]	15
Figure 6. Quantitative r.f. GDOES depth profile of hot rolled AA1050 [39].....	17
Figure 7. a) Metallic element distribution as a wt% amount of the total metal content in the subsurface layer of the laboratory rolled sample of aluminium alloy AA3104 [1]. b) Distribution of Mg in the surface layer of aluminium alloy AA3104 measured for only reheated and reheated followed by laboratory rolled specimens [42]	18
Figure 8. a) FIB image of AA3104 surface hot rolled in 1 pass at 753 K and with forward speed 12%; b) EDS analysis from the area marked as "d" in image a; the elements Pt and Ga are from the protective coating and the ion source respectively; and c) EDS analysis from the area marked as "e" (bulk material) in image a; d) evolution of AA3104 surface hot rolled in 2 passes in the same direction, temperature and forward speed; e) EDS analysis of the area marked as "d" in image d [29]	19

Figure 9. (a) GDOES depth profile analysis from the surface of an as-polished sample; (b) GDOES depth profile analysis from the surface of a sample polished and heated to 753 K for 840s [29] 20

Figure 10. Image showing material transferred from the stock surface to the work roll surface after the two-pass rolling on the Robertson mill [15]..... 21

Figure 11. Schematic representation of the roll-bite. Cross-sectional TEM analysis was carried out along the planes A (just before entry), B (just after entry), C (neutral plane) and D (just after exit) [41]..... 23

Figure 12. AA3104 surface hot rolled in 1 pass at 753K and with 12% forward speed; (a) localized shear deformations in the form of shingles; the inserted image magnifies the area in the bracket; (b) low magnification image of the trench after FIB milling; the surface was platinum coated first in order to avoid damage due to exposure to ion beam; (c) cracks formed beneath and parallel to the surface [29] 24

Figure 13. Schematic of the influence of rolled-in oxides on the Total Reflectance (TR) [41,50] 27

Figure 14. Schematic view of a filiform filament on aluminum [56]..... 28

Figure 15 Effects of intermetallic particles on the propagation behavior of filiform filaments [56] 29

Figure 16. Surface-active filiform corrosion (left side figure): (a) SEM of cross-section show the initial stages of filiform corrosion with attack of grain boundaries in the deformed layer; (b) TEM showing the dispersoids (indicated by the arrows) in the corrosion product. SEM of successive-pitting filiform corrosion (right side figure): (c) corrosion initiated at a grain

boundary of the aluminum matrix after the near-surface deformed layer has been consumed; (d) corrosion growth into one of the grains [33]	31
Figure 17. Optical micrographs of the 6082 alloy after homogenization: (a) rapidly-heated specimen; (b) slowly-heated specimen. PFZ stands for precipitate free zones [40].....	34
Figure 18. RF GDOES qualitative depth profiles of a hot-rolled AA3005 aluminum alloy: (a) "as received"; (b) after annealing for 2 h at 500 °C [63]	35
Figure 19. Friction coefficient for polished samples; solid curves for tests with Somentor 32 base oil, dashed curves for Somentor 32 plus a boundary additive [68]	39
Figure 20. General view and schematic of experimental setup of hot rolling simulation	44
Figure 21. a) WYKO images of surface profilometry of AISI 440C, D2 and 52100 steel rolls (as-polished), surface roughness of 440C Ra = 0.0148, D2 Ra = 0.0108, 52100 Ra = 0.0089, b) Micro graphs of 52100, c)440C, and d) D2	50
Figure 22. WYKO images of surface profilometry of Al-Mn alloy after rolled 1 pass with AISI 440C, D2 and 52100 steel rolls, rolled with 440C Ra = 0.285, D2 Ra= 0.303, 52100 Ra = 0.286, pits are observed covering the surface of the Al-Mn alloy after deformation with 440C and D2, but not with 52100	51
Figure 23. The SEM images of Al-Mn alloy rolled with 440C roll after 1 pass, order of magnification from low to high for a) to d)	52
Figure 24. The SEM images of Al-Mn alloy rolled with D2 roll after 1 pass, order of magnification from low to high for a) to d)	53
Figure 25. The SEM images of Al-Mn alloy rolled with 52100 roll after 1 pass, order of magnification from low to high for a) to d)	54

Figure 26. Comparison of the SEM images of Al-Mn alloy rolled with 440C, D2 and 52100, a) and B) for rolled with 440C, c) and d) rolled with D2, e) and f) rolled with 52100 55

Figure 27. The SEM images of a) and b) for 440C steel alloy surface after rolled with Al-Mn alloy after 1 pass, c) and d) for D2 steel alloy surface after rolled with Al-Mn alloy after 1 pass, e) and f) for 52100 steel alloy surface after rolled with Al-Mn alloy after 1 pass..... 56

Figure 28. The comparison of a) 440C, b) D2 and c) 52100 steel alloy surface after rolled with Al-Mn alloy after 1 pass 57

Figure 29. EDS mapping of 440C steel alloy surface after rolled with Al-Mn alloy after 1 pass 57

Figure 30. EDS mapping of D2 steel alloy surface after rolled with Al-Mn alloy after 1 pass.... 58

Figure 31. EDS mapping of 52100 steel alloy surface after rolled with Al-Mn alloy after 1 pass 58

Figure 32. Comparison of EDS mapping of D2 and 440C steel alloy surface after rolled with Al-Mn alloy after 1 pass with elements of O, Cr and V..... 59

Figure 33. SEM images of Al-Mg alloy surface rolled with 52100 steel roll after 1 pass, order of magnification from low to high for a) to d) 60

Figure 34. SEM images of Al-Mg alloy surface rolled with 440C steel roll after 1 pass, a) SEM image taken at 12 kV and b) SEM image taken at 5 kV, f) and h) are EDS analysis on surface features at e) and g), respectively 61

Figure 35. SEM images of 440C steel alloy surface after rolled with Al-Mg alloy after 1 pass.. 62

Figure 36. EDS mapping of 440C steel alloy surface after rolled with Al-Mg alloy after 1 pass 63

Figure 37. SEM images of Al-Mg alloy surface rolled with 440C steel roll after 1 pass and 4 passes, a) and b) after 1 pass, c) and d) after 4 passes, magnification from low to high: 1 pass for a) to b) and 4 passes for c) to d)..... 64

Figure 38. SEM images of Al-Mg alloy surface rolled with D2 steel roll after 1 pass and 4 passes, a) and b) after 1 pass, c) and d) after 4 passes, magnification from low to high: 1 pass for a) to b) and 4 passes for c) to d) 65

Figure 39. SEM images of Al-Mg alloy surface rolled with 52100 steel roll after 1 pass and 4 passes, a), b) and c) after 1 pass, d), e) and f) after 4 passes, magnification from low to high: 1 pass for a) to c) and 4 passes for d) to f) 66

Figure 40. EDS analysis of Al-Mg alloy surface features rolled with 440C steel roll after 4 passes, a) at normal rolled surface region, b) at darkened grain boundary region, c) at dark patch area . 67

Figure 41. EDS analysis of Al-Mg alloy surface features rolled with D2 steel roll after 4 passes, a) at normal rolled surface region, b) at darkened grain boundary region 67

Figure 42. EDS analysis of Al-Mg alloy surface features rolled with 52100 steel roll after 4 passes, a) at darkened grain boundary, b) at normal rolled surface region 68

Figure 43. WYKO images of surface profilometry of Al-Mg alloy after rolled a) 1 pass at 550 °C Ra = 0.206, b) 2 passes at 525 °C Ra = 0.132, c) 3 passes at 500 °C Ra = 0.196, d) 4 passes at 475 °C Ra = 0.186, all with 440C, e) 5 passes at 475 °C Ra = 0.198, all with 440C, and f) 6 passes at 475 °C Ra = 0.203, all with 440C 69

Figure 44 SEM images of Al-Mg alloy surface rolled with 440C steel roll after 1 pass, 2 passes, 3 passes and 4 passes, a), b) and c) after 1 pass, d), e) and f) after 2 passes, g), h) and i) after 3 passes, j), k) and l) after 4 passes. Magnification from low to high: 1 pass for a) to c), 2 passes for d) to f), 3 passes for g) to i) and 4 passes for j) to l) 70

Figure 45. Different conditions of lubrication a) nozzle close to roll, b) nozzle far from roll 71

Figure 46. SEM images of Al-Mg alloy surface rolled with 440C steel roll after 1 pass with far nozzle distance lubrication condition, order of magnification from low to high for a) to d) 72

Figure 47. SEM images of Al-Mg alloy surface rolled with 440C steel roll after 1 pass with close nozzle distance lubrication condition, order of magnification from low to high for a) to d) 73

LIST OF TABLES

Table 1. Classification of the tendency of adhesion and transfer of work material to the surface of the five tool steel treatments, thin layer transfer (TLT), small patch transfer (SPT), extensive patch transfer (EPT), and full width transfer with local patches (FWT). [64].....	37
Table 2. Elemental composition distribution of Al-Mn and Al-Mg alloy	41
Table 3. Elemental composition distributions of 52100, 440C and D2 steel rolls	42
Table 4. Variable process parameters of all experiments done in this study (the empty block is tests that were not done, and the temperature is the last pass temperature).....	45
Table 5. Hardness of AISI 52100, 440C and D2 steel alloy rollers.....	45

NOMENCLATURE

COF	Coefficient of Friction
EDS	Energy Dispersive X-Ray Spectroscopy
EPT	Extensive Patch Transfer
FFC	Filiform Corrosion
FIB	Focused Ion Beam
FWT	Full Width Transfer
GDOES	Glow Discharge Optical Emission Spectroscopy
PFZ	Precipitate Free Zones
RS	Relative Softening
SEM	Scanning Electron Microscope
SPT	Small Patch Transfer
TEM	Transmission Electron Microscope
TLT	Thin Layer Transfer
TR	Total Reflectance

CHAPTER 1 INTRODUCTION

1.1 Background

1.1.1 Aluminum alloys

Aluminum alloys have a very wide application in engineering structures and components where a light weight or corrosion resistance is required. For example, aluminum alloys containing magnesium have a high strength to weight ratio and are much less flammable than other alloys that contain the same percentage of magnesium; that makes these alloys lighter than other aluminum alloys and make them favored in aerospace applications [1-3]. The typical aluminum alloying elements are copper, magnesium, manganese, silicon and zinc. The aluminum alloys can be divided by heat-treatable and non-heat-treatable. Almost 85% of aluminum is used for wrought products, such as foils, rolled plate and extrusions [3-5].

1.1.2 Heat-treatable and non-heat-treatable alloys

Alloys that respond to thermal treatment are based on phase solubility such as solution heat treatment, quenching and age hardening. Whether they are cast or wrought, they are referred to as heat treatable. Many wrought aluminum alloys created mainly through work hardening by mechanical reduction, as well as some casting alloys, are not as heat treatable; they usually appear to be non-brittle metals with a reasonably high melting point. Alloys not amenable to heat treatment are referred to as non-heat-treatable [3,4].

Heat treatable aluminum alloys represent alloys that can be hardened by a controlled cycle of heating and cooling; as the strength increases by heat treating, the formability may sometimes be affected. Usually aluminum alloys in the 2000, 6000 and 7000 series are heat treatable. Non-heat-treatable aluminum alloys are hardened by strain hardening without heat treatments, while aluminum alloys in the 1000, 3000, 4000 and 5000 series are strengthened by

work hardening [1,3,4,6]. The 3000 series is widely used in cooking utensils and chemical equipment, due to its superiority in handling many foods and chemicals; the AA3104 or 3004 in particular is the largest volume alloy combination in the industry, with applications in the bodies of beverage cans. The 5000 alloys have wide applications in the top of the beverage can, automotive, building and construction areas [4,5].

The aluminum alloy compositions are registered with the Aluminum Association (AA). The 3000 and 5000 series are alloyed with manganese and magnesium respectively. Both of these additions increase strength primarily by solid solution hardening and by forming precipitates such as $Al_6(Mn,Fe)$, $\alpha-Al_{15}(Fe,Mn)_3Si_2$ and Al_3Mg_2 which could control recrystallized grain size by pinning grain and subgrain boundaries. At the Eutectic temperature, the limit of manganese solubility is 1.5 wt% and magnesium solubility is 17.4 wt% in aluminum (Figure 1) [7-10]. The present system utilized to identify wrought aluminum alloys is the four digit designation system, shown below:

- The 1000 series are essentially pure aluminum with a minimum 99% aluminum content by weight and can be work hardened.
- The 2000 series are alloyed with copper and can be precipitation hardened to strengths comparable to steel. Formerly referred to as duralumin, they were once the most common aerospace alloys, but were susceptible to stress corrosion cracking. They are increasingly replaced by 7000 series in new designs.
- The 3000 series are alloyed with manganese, and can be work hardened.
- The 4000 series are alloyed with silicon. They are also known as silumin and are heat treatable.
- The 5000 series are alloyed with magnesium and can be work hardened.

- The 6000 series are alloyed with magnesium and silicon, are easy to machine, and can be precipitation hardened, but not to the high strengths that 2000 and 7000 can reach.
- The 7000 series are alloyed with zinc, and can be precipitation hardened to the highest strengths of any aluminum alloy.
- The 8000 series is a category mainly used for lithium alloys, heat treatable.
- The 9000 series is reserved for future use [1,2,4]

The work hardening rates can be different for different alloy series, for instance, AA3104, AA5182 and AA9111 have high work hardening rates at low temperatures and the work hardening amount decreases while temperature increases, due to the dynamic recovery [11]. The compositions and grain sizes between different series are different, as shown in Figure 1; even in the same series, the composition can be very different [12,13].

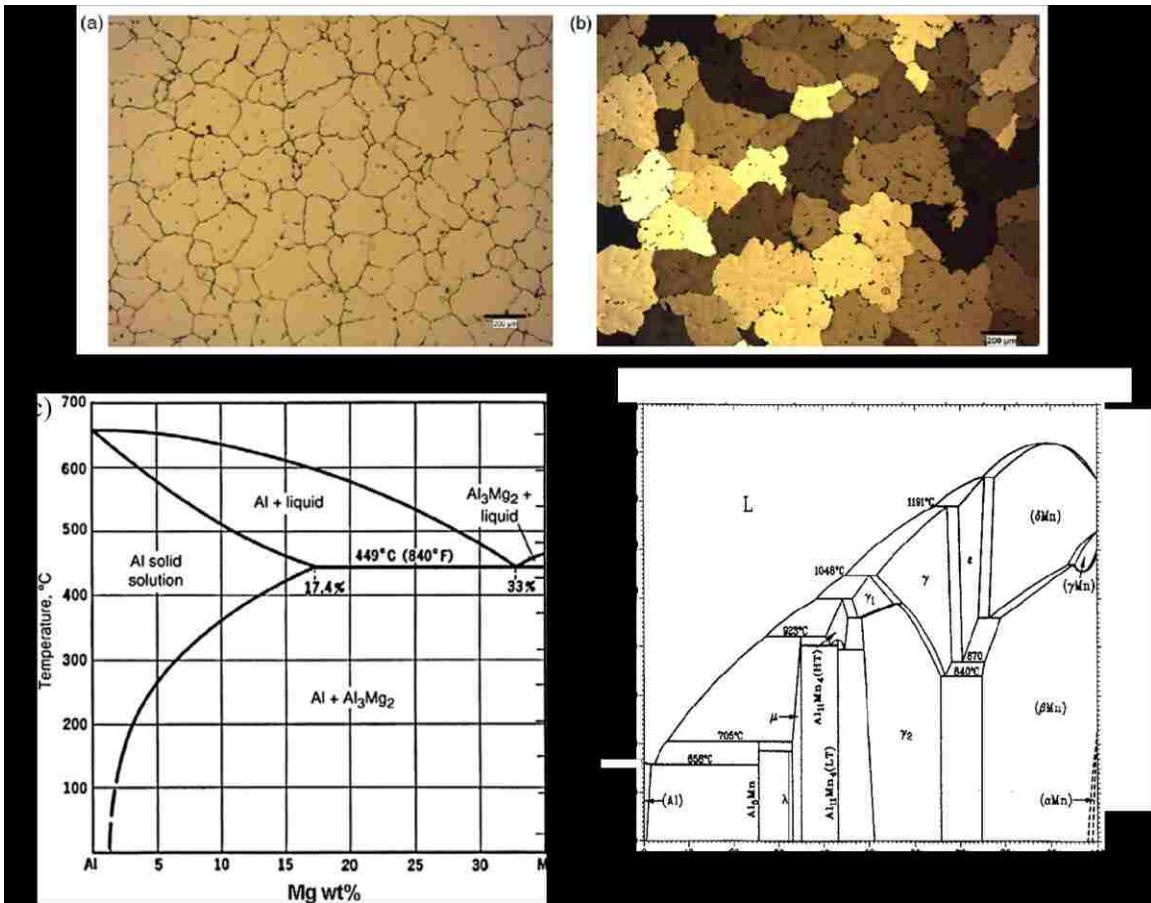


Figure 1. Optical micrographs of the two alloys a) AA3104, b) AA5182, c) Phase diagram of binary Al–Mg system, d) Phase diagram of binary Al–Mn system [11,14]

1.1.3 Rolling process

For most non-heat-treatable aluminum alloys, the process usually first involves hot rolling, which leads to significant thickness reduction and preparation for the later forming process. Rolling is a typical metalworking process and the most common method of work-hardening (cold-rolling) non-heat-treatable alloys. It has wide industrial application. Figure 2 is a schematic diagram of the process route for the production of can body stock [15]. It can be divided into two stages according to the temperature of the work metal. If the temperature is above the recrystallization temperature, the process is referred as hot rolling; if the temperature is below the recrystallization temperature, the process is cold rolling. Rolling of aluminum is an

integral part of manufacturing of wrought aluminum alloy sheets, and the main purpose of hot rolling is gauge reduction. Rolling could change the morphological, optical, microstructural and electrochemical properties of the surface and near-surface regions compared to the bulk, by exerting a load and a shear stress on the surface of the workpiece. There are many types of rolling processes, including ring rolling, roll bending, roll forming, profile rolling and controlled rolling [1].

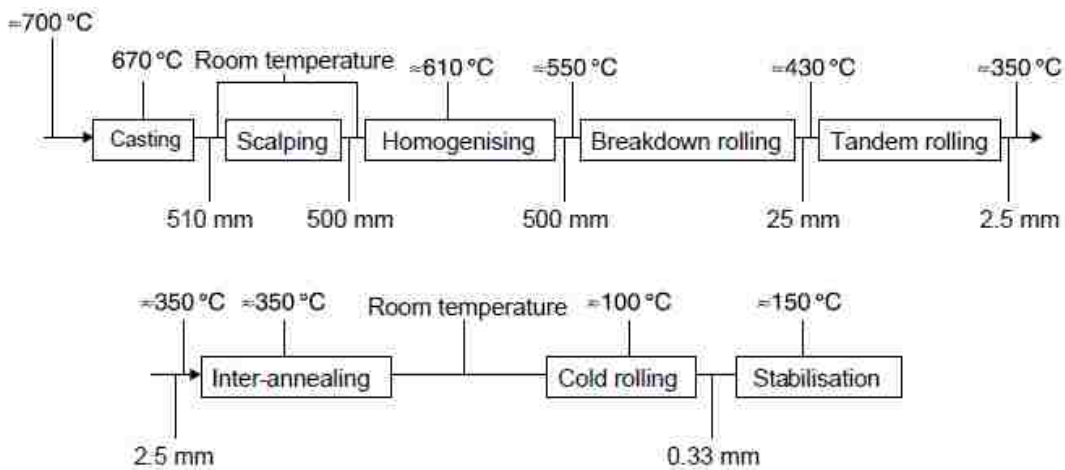


Figure 2. Typical process route for can body stock [15,16]

Hot rolling occurs only above the recrystallization temperature of the workpiece material, which is usually in the range of $0.6T_m$, where T_m is the melting temperature in Kelvin. When the temperature is above recrystallization temperature, the grains deform into equiaxed microstructures during processing and impede the metal from work hardening. The temperature must be controlled to remain above the recrystallization temperature, so the finishing temperature is usually defined 50-100 °C above the recrystallization temperature. Usually, a multi stand rolling mill is used in industrial manufacturing. However, the alternating cycles of deformation and recrystallization generated during hot rolling have a strong influence on the

overall microstructure and texture evolution. The recrystallization between two consecutive tandem passes could be diminished by modern high-speed tandem mills [17]. However, the surface of the finished product is always covered with an oxide layer, so pickling or a smooth cleaning of surface process is needed to reveal a smooth surface [1].

Cold rolling occurs below recrystallization, usually at room temperature. It increases the alloy strength up to 20%, usually by strain hardening and improving the surface finish. There are different levels for cold rolling, which are full-hard, half-hard, quarter-hard and skin-rolled. The full-hard level reduces the thickness by 50%, while the skin-rolled level only does so by 0.5%-1%. The skin-rolled is always used to attain a smooth surface, a uniform thickness and the reduction of the yield point phenomenon [1].

1.1.4 Steel roller alloys

Steel are used in a variety of mechanical applications due to their high strength, hardness and other properties. In the rolling process, steel alloys play an important role in the rolling of the tool piece. Although AISI 52100, D2 or 440C steel alloys could be used as tool steel for rolling aluminum, they have been found, respectively, to contain different levels of chromium content of an order from low to high. AISI 52100 was one of the first alloys developed for commercial use as a bearing material composed of 1 wt% carbon and 1.5 wt% chromium. AISI D2 is also a high-carbon chromium alloy steel, alloyed with molybdeum and vanadium, and it is a cold work tool steel containing 12 wt% chromium and 1.5 wt% carbon. The AISI 440C can attain the greatest hardness of any stainless steel after the heat treatment, and can be used for bearing assemblies such as the ball bearings [18-21]. More chromium content is added to steel alloys to obtain high corrosion resistance. For example, AISI 440C, which contains about 17 wt% chromium and a carbon content of 1.05 wt% to maintain hardenability. However, only dissolved

chromium content in the matrix is effective, and in the cases of both 440C and D2, with a combination of high chromium and carbon contents, Precipitates form carbide [22-24]. Carbides in 440C are reported to be $M_{23}C_6$ and M_7C_3 , and in D2 to be M_7C_3 , where M refers to metallic elements that can form carbides. Elements such as Cr, Fe, Mo, V, W, Nb, Ti and Zr are all typical carbide forming elements, but in these two alloys, M would be mostly chromium [23]. M_7C_3 carbide is larger and possesses a hexagonal or an orthorhombic unit cell, while $M_{23}C_6$ is smaller and possesses an FCC unit cell [23,25]. These carbides could become sources of stress concentration and could form prominent voids in the near regions, which would have a negative effect on the durability of the steel alloy, but a high population density of carbides could improve the hardness behaviors of the steel [23]. The different amount of chromium content allows these different roll materials to obtain different hardnesses and surface morphologies that could significantly affect rolled aluminum surface defects.

1.2 Thesis objective

There has been limited study done in the area of surface defects of hot rolling aluminum alloys under the effects of different roll materials. This study examines the surface defects that occur during the hot rolling of Al-Mn and Al-Mg alloys. Both of the alloys are widely used in the production of beverage cans.

The roller currently used in the industry is the steel alloy roll. Usually, a higher roll hardness gives more thickness reduction to rolled aluminum and enhances metal working efficiency during hot rolling. AISI 52100, D2 and 440C steel alloys have been found to contain, respectively, different levels of chromium content of an order from low to high. The different concentrations of chromium content and elemental composition means that these different roll materials obtain different hardnesses and surface morphologies. The different types of carbide

attributed to the varieties of surface morphology could significantly affect rolled aluminum surface defects.

The objective of this research pertains to how processing parameters such as roll materials, number of passes and lubrication conditions affect the development of surface defects.

1.3 Organization of thesis

This thesis is arranged into six different chapters, each of which is briefly described below.

Chapter 1 introduces the background information related to this thesis and the research objectives and organization of the thesis.

Chapter 2 provides a literature survey related to this thesis and includes information on previous research that has been done so far. It focuses on the disturbed layer and surface defects occurring in aluminum alloy surfaces during thermo-mechanical processing along with how the disturbed layer affects the mechanical properties of the aluminum alloy. It also looks at how some factors affect the formation of the disturbed layer.

Chapter 3 introduces the experimental procedures. It includes descriptions of the experimental setup and sample preparation as well as the aluminum alloys and steel roll alloy elemental composition details. It describes the working principles of the hot simulation used in this research as well as the analytical tools used to examine the surface defects on the specimen surfaces.

Chapter 4 describes the results obtained by WYKO, SEM, and EDS. This chapter is divided into two parts. One is the results related to the Al-Mn alloy, and one is the results related to AA5182.

Chapter 5 discusses the results obtained. It first discusses the effect of three different roll materials on the two different aluminum alloy surfaces. It then moves to the effect of number of the passes along with lubrication effects during hot rolling simulation.

Chapter 6 summarizes the conclusions of this research. It presents a summary of the results obtained from the research and the conclusions drawn from discussions.

CHAPTER 2 REVIEW OF LITERATURE

2.1 Introduction of disturbed layer

During metal working, the surface and subsurface regions of a metal sheet are always subjected to different conditions and treatments. Material transfer has been a long term problem due to the interactions between the metal and the tool surface. The material transfer can take place through a variety of mechanisms: microcutting, adhesion, delamination, etc. The transferred metal can be oxidized and retransferred back to the workpiece surface, resulting in distinct surface disturbance, which adversely influences the properties of the surface. Rolling is an integral part of a wrought aluminum alloy sheet, and the main purpose of hot rolling is gauge reduction. Rolling could change the morphological, optical, microstructural and electrochemical properties of the surface and near-surface regions compared to the bulk by exerting a load and a shear stress on the surface of the workpiece. Both hot and cold rolling could induce the formation of a disturbed layer, and the subsequent cold rolling after hot rolling always provides strain hardening [16,26,26,27]. In earlier research into the disturbed layer, Fishkis and Lin [28] found that a subsurface was formed in the process of rolling a magnesium-containing aluminum alloy that had a different microstructure, oxide content and alloy distribution from the bulk material. The thickness of the subsurface layer was non-uniform and decreased as the rolling pass increased.

Deformation of the aluminum surface during hot rolling provides high compressive and surface shear stresses resulting from the friction between the rolls and the metal. The formation of the disturbed layer is attributed to these stresses coupled with the high temperatures involved and it is responsible for altering the local composition and microstructure of the surface and subsurface (i.e., several micrometers below the surface) regions. This disturbed layer consists of

a surface region of continuous metal oxide, which has nanocrystalline oxide grains 25-150 nm in size, and a subsurface region of a "refined" grain structure with 50-200 nm diameter grains, rolled-in oxide particles and a fine distribution of intermetallic particles. The thickness of the disturbed layer varies from 200 nm to 8 μm [29].

The disturbed layers induced by rolling are relevant for the productivity of the aluminum alloy sheet since the deformed layer is not always removed by post-production treatment such as anodizing or caustic etching [30]. This layer also has a strong influence on the adhesion, corrosion resistance, optical appearance and weldability of the metal. It is important to investigate this rolling induced disturbed layer [28,29,31-33].

The mechanical properties of the disturbed layer are different from the properties of the bulk alloy in several respects. Observation of the disturbed layer of rolled aluminum after a tensile test showed fibres connecting in cracks; this formation of elongated fibres indicates the ductile behaviour of the disturbed layer during plastic deformation of the aluminum alloy [32]. However, this surface layer also holds the property of a higher strength than that of the bulk alloy, due to the ultra-fine equiaxed grains of the microstructure [34].

There are various techniques by which to study the disturbed layer, such as cross-sectional transmission electron microscopy (TEM), which can indicate the presence of disturbed layers characterized by a refined grain structure with rolled-in oxide particles and a fine distribution of intermetallics. Scanning electron microscopy can be used in identifying shingles and transverse cracks on the surface of the alloy which have been identified as an indication of the disturbed layer [27-29]. Various depth profiling techniques can be applied as well, like qualitative glow discharge optical emission spectroscopy (GD-OES), which has been used to study the in-depth behaviour of specific elements of rolled Al alloys. However, GDOES cannot

determine whether the segregated alloying element is present in a solid solution or as second phase particles. Checking the total reflectance (TR) can also examine for the existence of rolled in oxides [16,35].

2.2 Microstructure of the disturbed layer

The structure of the disturbed layer depends on the alloy composition and also the process conditions. Typically, a multilayer structure is always obtained by the rolling process. The outermost deformed layer is characterized by ultrafine, equiaxed grains. Then, a transition region is sandwiched between the outermost deformed layer and the bulk microstructure, which is characterized by microbands consisting of elongated grains aligned parallel to the working surface due to the shear stress generated during rolling. The precise mechanism of the formation of the microbands observed by Zhou et al. [27] remains unclear, but the most widely suggested theory is that dynamic recovery effects and dislocation loss may be responsible for their formation. The change of dislocation density strongly affects materials' mechanical properties and influences microstructures such as the orientation of grains [36-39].

Fishkis and Lin [28] observed that the grain size of the disturbed layer materials was more than 25 times smaller than the grain size of the bulk, which contributes to Zener pinning. The deformed surface layer has extremely fine grains compared to the bulk, and these ultra-fine grains are pinned by rolled-in oxides and intermetallics or dispersoids. These second phase particles may be caused by the secondary precipitation during heating [40], preventing grain growth of the surface layer during subsequent heat treatment, which referred to as Zener pinning [16]. These fine second phase particles present within the subsurface layer acting as Zener barriers by locking the grain boundaries and thereby preventing further recrystallization [16,26-28,41].

Figure 3 shows the microstructure of the subsurface region schematically. The subsurface layer contains the microcrystalline oxides mixed with small grained metal and covered by a continuous oxide layer. The thickness of the continuous oxide layer decreases as the rolling processes [28].

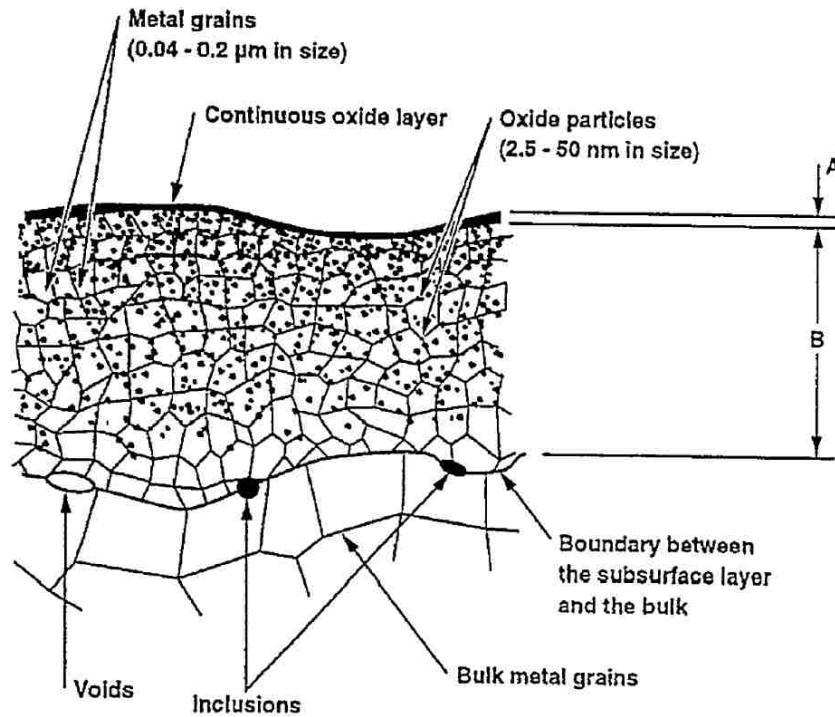


Figure 3. Schematic representation of subsurface layer containing microcrystalline oxides mixed with small grained material and covered with a continuous surface oxide. Layer A represents the surface oxide layer and layer B represents the subsurface ultrafine grained layer [28]

The intermetallics appearing on the surface of the material surface region after rolling are fine and irregularly shaped, as Figure 4b shows. This is due to the breaking up and smearing out of the intermetallics during rolling [16].

The size and distribution of intermetallics, rolled-in oxide particles or dispersoids have a strong effect on the recovery, recrystallization and grain growth, which results in an uncertain grain size in the disturbed layer [40].

The second-phase particles are usually sufficiently small [26,42], and if the oxide particle diameter exceeds a critical diameter, the boundary migration can occur so that grain growth restarts:

$$r_{cr} = \frac{6R_0}{\pi} f \left(\frac{3}{2} - \frac{2}{Z} \right)^{-1} [28]$$

Where R_0 is the mean grain radius, f is the volume fraction of the second-phase (oxides) particles, and Z is the ratio of the radius of a growing grain to that of its neighbors. Anderson et al. [1] found the fraction of second-phase particles between pinned grains is significantly greater than between random intersections. Therefore, the limited grain diameter after being pinned by second-phase particles can be calculated by Anderson et al.'s equation:

$$R_{limit} = r(4.5 \pm 0.8)/f^{(0.31 \pm 0.02)} [28]$$

The volume fraction of oxide incorporated into the near-surface deformed layer is associated with process parameters such as abrasive medium, temperature, roll grinding, inter-annealing treatment, lubrication regime and lubricant formulation [27].

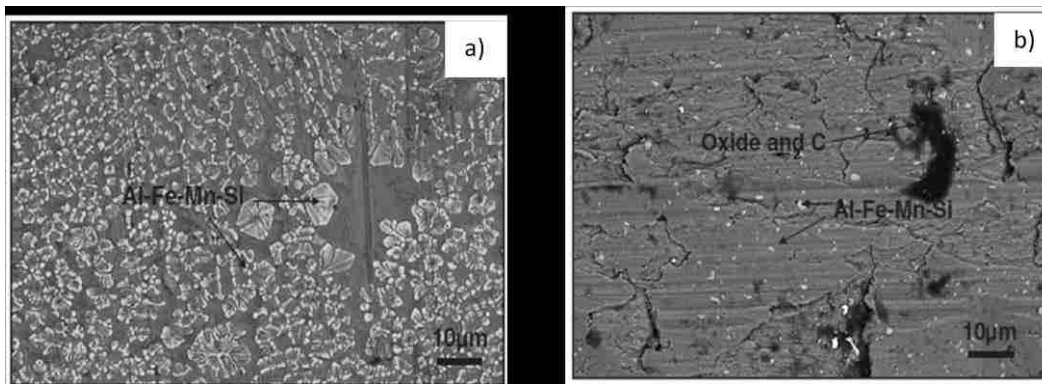


Figure 4. SEM backscattered micrograph of the surface of Aluminum alloy AA5050: (a) as-cast; (b) hot roll after first pass. [16]

The subsequent cold rolling can distribute the fine micrograined layer over a larger surface area and reduces the thickness of the deformed layer. Nevertheless, cold rolling alone without the previous hot rolling process, cannot incorporate second-phase particles that are necessary to pin the refined grain growth in the deformed subsurface layer [26,27,35]. Moreover, the oxides formed after hot rolling are crystalline, but after cold rolling, the subsurface oxide particles are amorphous, as the temperature at the cold rolling stage is indeed too low to initiate oxide crystallization [43]. Figure 5 systematically shows the condition of the different microstructures of the disturbed layer (near surface) formed when hot rolling is involved and when it is not involved. Type A is the microstructure disturbed layer with hot rolling is involved, and type B is under cold rolling only; at lower temperatures, there are no precipitates or oxides in the grain boundaries.

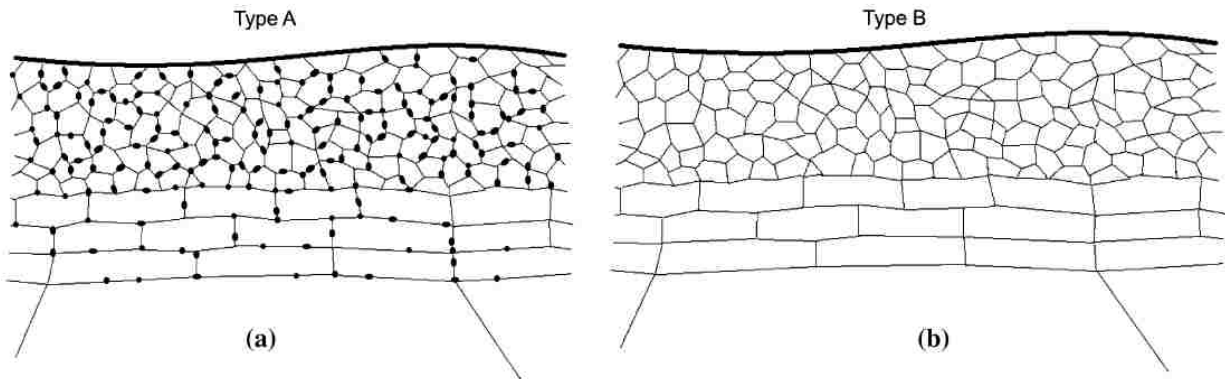


Figure 5. Schematic diagrams showing the microstructure of near-surface deformed layer introduced by rolling: (a) type A is hot rolling involved and (b) type B under cold rolling without hot rolling involved [27]

2.3 Content distribution in disturbed layer of aluminum alloy under rolling

The disturbed layer formed during rolling contains both oxide particles and a different intermetallic particle distribution compared to the bulk material. Therefore, the mixed phases of the disturbed layer of aluminum alloy under rolling contain not only very fine magnesium and

aluminum oxide particles [26,28], but almost all the intermetallics are rich in Al, Mg, Fe, Mn and Si (depending on aluminum alloy content distribution); these includes $AlMn_6$, $AlSi$, Mg_2Si and $AlMnSi$ [34]. The increased number of fine intermetallic particles is due to the fragmentation of existing particles, nucleation and the growth of new precipitates [16,35,44]. The composition of the precipitates remains almost constant during the subsequent rolling [41]. The difference of particle distribution between the bulk and the disturbed layer is due to the plastic strain induced by continuous enhanced shear deformation in the surface and near the surface region. During rolling, the intermetallic phases are smeared over and covered with the softer aluminum matrix, and then break up into smaller fragments. By exposure to the high temperature process, the large plastic strain results in the increase of secondary precipitation of fine dispersoid particles; this contributes to different particle distribution between the bulk and the disturbed layer [26].

Al, C, O, Si, Fe, Mg, Cu and Pb are discovered in the surface and near surface layer after rolling, according to Buytaert's study, which use the aluminum alloy of AA1050 that contains 0.075% Si, 0.34% Fe, 0.005% Mn, 0.008% Ti, 0.003% Cu, 0.003% Zn, 0.002% Cr, 0.001% Mg, 0.001% Pb and 99.5% Al [39]. The presence of carbon could be the result of rolling lubricants [29]. Figure 6 shows that there is always an increasing tendency of Al with depth, and oxygen displays a strong decreasing evolution away from the surface, which could confirm the presence of an oxygen-rich layer that is only present in the subsurface, due to rolled-in oxide particles.

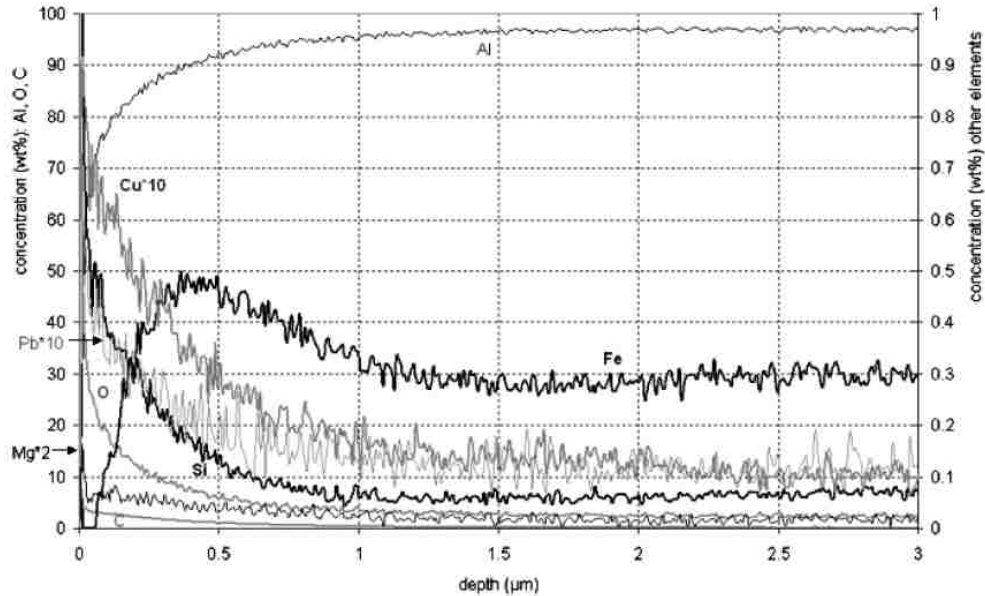


Figure 6. Quantitative r.f. GDOES depth profile of hot rolled AA1050 [39]

Both the rolling and the heating process for aluminum alloy induces significant Mg enrichment at the surface and in the near regions. Al_2CuMg is a typical precipitate formed at low temperature, but usually Mn dispersoids exist at a higher temperature [45]. The diffusion of Mg to the surface during heating and hot rolling is responsible for magnesium oxide formation, which contributes to the formation of the disturbed layers, since Mg reacts with the oxygen and aluminum to produce MgO and $MgAl_2O_4$; this provides the Zener pinning that establishes the fine-grain surface structures. Also, the fine-grained material always has a larger interdiffusion coefficient than coarse-grained material which leads the Mg diffusion to the aluminum surface as well [33,46]. The raised magnesium content has an inverse ratio with the depth below the surface (Figure 7), and this depth is related to the thickness of the subsurface particle layer in each case [15,16,35,42]. Although other metal oxide particles also exist in the subsurface region, Mg always has the second-most particles in the aluminum alloy; thus, the subsurface structure and morphology relates to the depth of the Mg enrichment due to rolling passes as well [16].

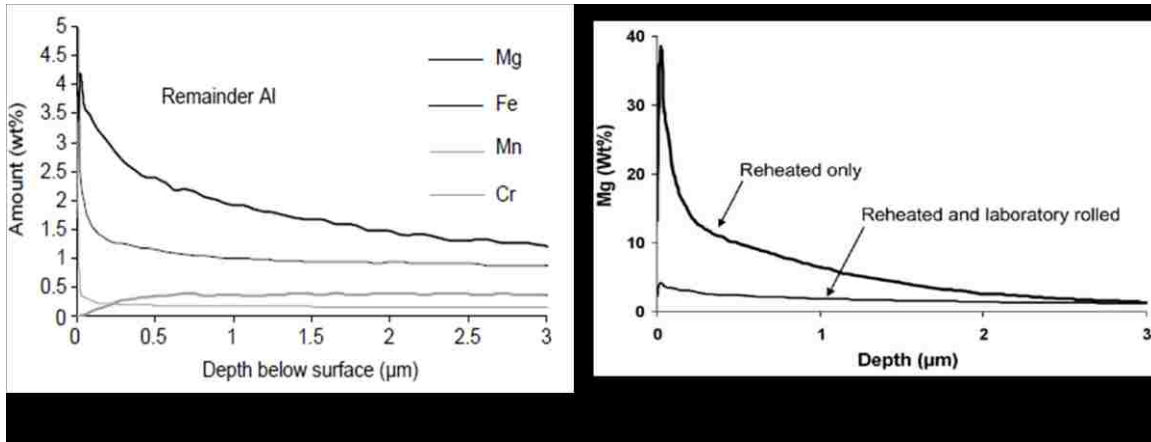


Figure 7. a) Metallic element distribution as a wt% amount of the total metal content in the subsurface layer of the laboratory rolled sample of aluminium alloy AA3104 [1]. b) Distribution of Mg in the surface layer of aluminium alloy AA3104 measured for only reheated and reheated followed by laboratory rolled specimens

[42]

For aluminum alloys that contain magnesium, the continuous oxide layer that covers the subsurface layer is comprised predominantly of MgO. The composition of the oxide-metal mixed layer is not homogeneous, and it is found to be a mixture of MgO, $\gamma\text{-Al}_2\text{O}_3$, MgAl_2O_4 and amorphous aluminum oxide [15,28,42]. However, only the MgO content increases as the rolling process continues, due to lower temperatures during the later passes and due to the increasing magnesium content in the oxide layer (Figure 8) [12,27,28]. The MgO dominated oxide layer contains a considerable amount of porosity and cracks in order to allow oxygen to react with magnesium and other metals, to grow the oxide layer [12]. The magnesium content also results in magnesium enrichment on the roll surface via material transfer [29].

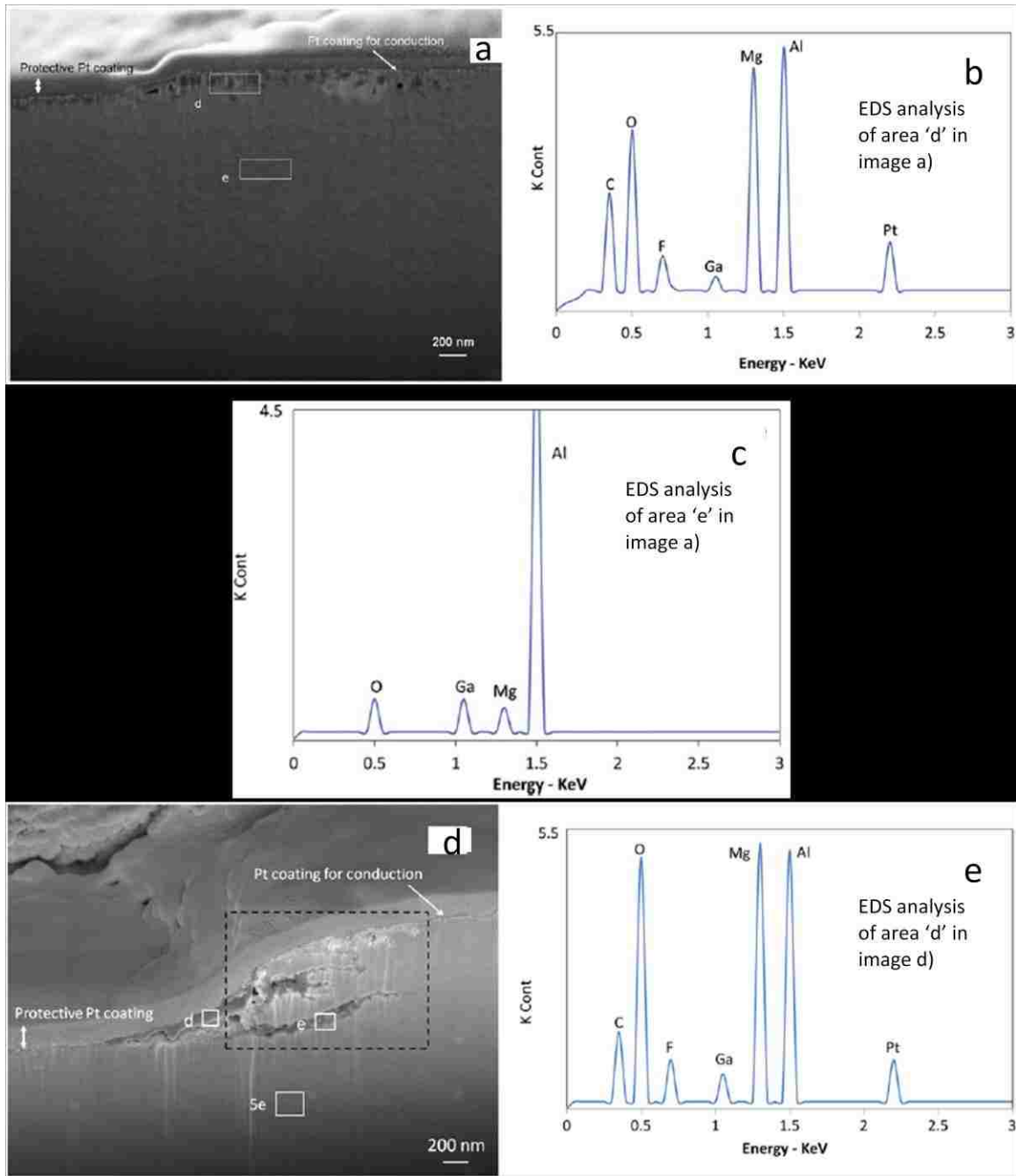


Figure 8. a) FIB image of AA3104 surface hot rolled in 1 pass at 753 K and with forward speed 12%; b) EDS analysis from the area marked as "d" in image a; the elements Pt and Ga are from the protective coating and the ion source respectively; and c) EDS analysis from the area marked as "e" (bulk material) in image a; d) evolution of AA3104 surface hot rolled in 2 passes in the same direction, temperature and forward speed; e) EDS analysis of the area marked as "d" in image d [29]

However, aluminum alloy surfaces could oxidize either with or without heating. The fresh surface of Al-Mg alloys always tends to generate a thin, amorphous layer of aluminum oxide during the initial stages of oxidation, without tribo-layers. If the heating is continually applied, the magnesium atoms diffuse to the surface, as shown in Figure 9, and promote the formation of MgO on the surface and $MgAl_2O_4$ at the interface between the oxide layer and the bulk material. The thickness of the magnesium rich oxide layer and the magnesium oxide contents increase with the rising magnesium content in the alloy [32]. The oxidation rate decreases during the reheating process, but the rates of magnesium diffusion to the alloy surface increase with temperature, unlike steel, in which the oxide layer becomes thinner with a higher oxidation temperature [27,42,47].

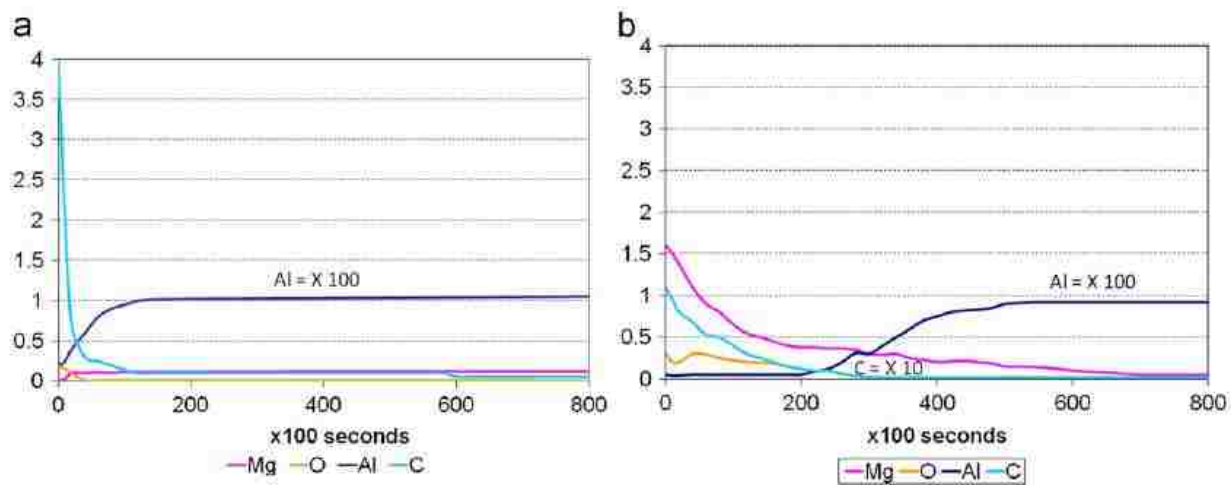
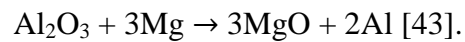


Figure 9. (a) GDOES depth profile analysis from the surface of an as-polished sample; (b) GDOES depth profile analysis from the surface of a sample polished and heated to 753 K for 840s [29]

The Mg content reduces along with the reduction in disturbed layer thickness through rolling deformation. There are two main possible reasons for the decreasing Mg content: the first

reason is that the Mg content is diluted by the inevitable introduction of fresh metal by the increasing of the surface area caused by the deformation process, and the second is that some surface materials are transferred on to the rolling tools and form a surface coating, as shown in Figure 10 [15,29,42].

Moreover, subsequent cold rolling can break up and smear out rolled-in oxide islands in the near-surface of rolled aluminum [35,39]. In aluminum alloys containing magnesium, Plassart et al. [43] observed aluminum nanocrystals in the intermetallic particles, found to be caused by a reduction of Al_2O_3 reacting with metallic Mg that occurred during cold rolling, according to the following:



which, on the other hand, proved the Mg diffusion and subsequent oxidation.



Figure 10. Image showing material transferred from the stock surface to the work roll surface after the two-pass rolling on the Robertson mill [15]

The lubricant in aluminum hot rolling is usually in the form of an oil-water emulsion. There is lubricant entrapment on the surface and in the near surface region as well. It may be caused by the reaction of the lubricant with the surface oxide film during rolling, by the entrapment of lubricant in surface defects such as holes, cracks, etc., or by closure due to the smearing out of the surface during subsequent rolling. The different surface structure of rolled metal and the surface geometry of the rolls could also attenuate or accentuate lubricant capture on the rolled surface area [29,41,48] .

2.4 Mechanisms of disturbed layer formation

Since the majority of the subsurface deformation takes place at earlier stages of hot rolling, the mechanisms of these earlier stages of hot rolling are always investigated most thoroughly and considered most significant [26]. The surface damage is very severe during earlier rolling passes, and then the damage is distributed to a larger surface area due to further rolling passes, which makes it less severe after later passes. The percentage gauge reduction is always highest at the first roll pass and decreases as subsequent passes proceed, and the deformation is most severe in the roll-bite part of the workpiece surface, as shown in Figure 11. The thickness of the surface layer decreases, and properties became more distinct compared to the underlying bulk as the rolling proceeds [41].

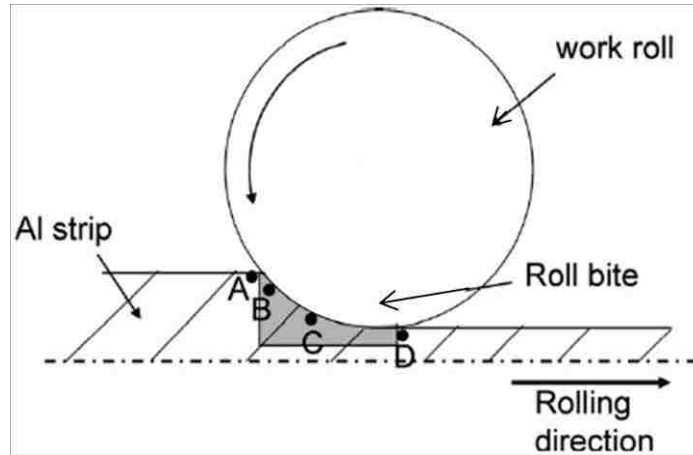


Figure 11. Schematic representation of the roll-bite. Cross-sectional TEM analysis was carried out along the planes A (just before entry), B (just after entry), C (neutral plane) and D (just after exit) [41]

First, it is known that the subsurface layer is always covered with a continuous oxide layer. The thickness of the continuous oxide layer decreases as the rolling proceeds. This is explained by the breaking up of the original thick oxides formed during earlier rolling passes and their distribution to a larger surface due to further rolling, as well as by the descending oxidation rate due to the lower temperature at later passes [27,28].

Since the rough roll has a grooved structure on the surface, the hot aluminum squeezes into the grooves and forms micro wedges (shingles) during the initial stages of surface damage from rolling as shown in Figure 12a. These wedges deform more easily than the flat surfaces, due to lower constraints, and when the micro wedges slide against the groove on the roll surface they experience more severe plastic deformation. This is even more severe if the groove depth is high or if a lubricant breakdown occurs[29].

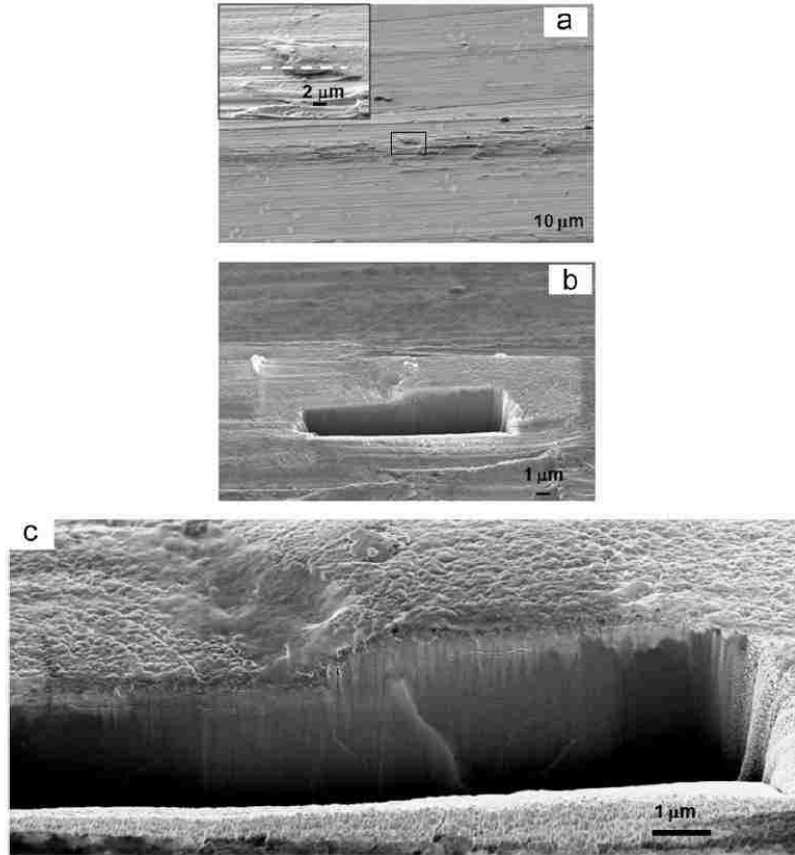


Figure 12. AA3104 surface hot rolled in 1 pass at 753K and with 12% forward speed; (a) localized shear deformations in the form of shingles; the inserted image magnifies the area in the bracket; (b) low magnification image of the trench after FIB milling; the surface was platinum coated first in order to avoid damage due to exposure to ion beam; (c) cracks formed beneath and parallel to the surface [29]

Fishkis and Lin [28] concluded that there was a three-step process to the mechanism of subsurface layer formation during rolling. First, transverse surface cracking and adhesive and delamination wear occurs on the surface and near surface region. After that, surface defects are filled with wear debris, consisting of fine intermetallic, dispersoid and oxide particles. Eventually, thin metal layers cover all surface defects during the continuous rolling process leading to a "shingled" surface appearance (Figure 8).

The holes then develop into sub-surface cracks in subsequent rolling passes. The transverse surface cracking is the initial stage, and also the most important stage, of the formation of the disturbed layer. It is caused by the lower ductility that contributes to the surface cooling, by the brittleness of the surface oxide layer of the surface layer and by shear stress obtained during rolling [27,28,41]. As the rolling passes increase, some of the localized shear deformed areas can delaminate, as Figure 12c shows; they transfer onto the roll surface and back to the sheet surface during the subsequent rolling process. This delaminated debris oxidizes and contaminates the lubricant and then embeds in the rolled surface, becoming part of the disturbed layer as rolling continues. The re-deposited layer also contributes to the increasing thickness and structural changes of the disturbed layer[29].

There are always fine grained structures and incorporated oxide particles in the surface and near surface layers after the rolling process. They are caused by large shear deformation combined with repeated fracturing and re-welding of the surface material due to friction between the aluminum sheet and the work-roll surface during heat treatment. The shear strains generated in the surface and near-surface regions are severe, with a gradient distribution that gradually decreases from a maximum at the surface to zero in the bulk alloy. This is sufficient to cause the geometric dynamic recrystallization of the grain, resulting in significant microstructure refinement and the formation of the deformed layer. It initiates near the surface before extending gradually towards the centre [49]. Therefore, the microstructure variation at various depths from the surface is continuously a reflection of the strain distribution [50-52]. Alloying elements or impurities in the alloy in the form of intermetallics can act as grain refiners, then oxide and lubricants introduced to the surface could pin the subgrain structure and also act as grain refiners as well. However, the purer grade such as the 1000 series aluminum alloys do not easily form a

grain refined surface layer, because they do not have sufficient impurities to act as grain refiners [53].

2.5 Optical appearance

Usually, the aluminum alloy surface will keep an apparent shine with a high level of optical reflectance in a dry environment due to the formation of the protective oxide layer of aluminum. The optical reflectance of the surface layer after the rolling process has been found to be much less than that of the bulk alloy predominantly due to the presence of rolled-in oxides [16]. The oxide particles mixed in the subsurface highly decrease the total reflectance (TR) upon the rolling of aluminum (Figure 13), so that the oxide-rich subsurface is the main reason for the reduction of TR in rolled aluminum alloys. The TR can be increased by removing more material in order to gradually remove the incorporated oxide particles. Therefore, lower TR values indicate the presence of a higher number of incorporated oxide particles in the respective sample, so the method of TR for the optical reflectance can be used to evaluate the presence of subsurface oxide-rich layers upon the cleaning and etching treatments of rolled aluminum alloys. Since the TR value is inversely proportional to the number of incorporated oxide particles, it could also be used to calculate the thickness of the surface layer, which appears to be a cost-effective, quick and reliable technique for the estimation of the thickness of the subsurface layer [41].

Surface treatment on the alloy, such as alkaline etching or chemical cleaning with Nabuclean and CrO_3 or H_3PO_4 , could be an effective way to affect the surface appearance of rolled aluminum alloy. Buytaert et al. [54] found that the alkaline etching preferentially attacks the aluminum matrix and preserves the rolled-in oxide rich subsurface regions, and CrO_3 or

H_3PO_4 dissolves the oxide-rich regions leaving the aluminium matrix un-attacked, and form a layer containing Cr on surface.

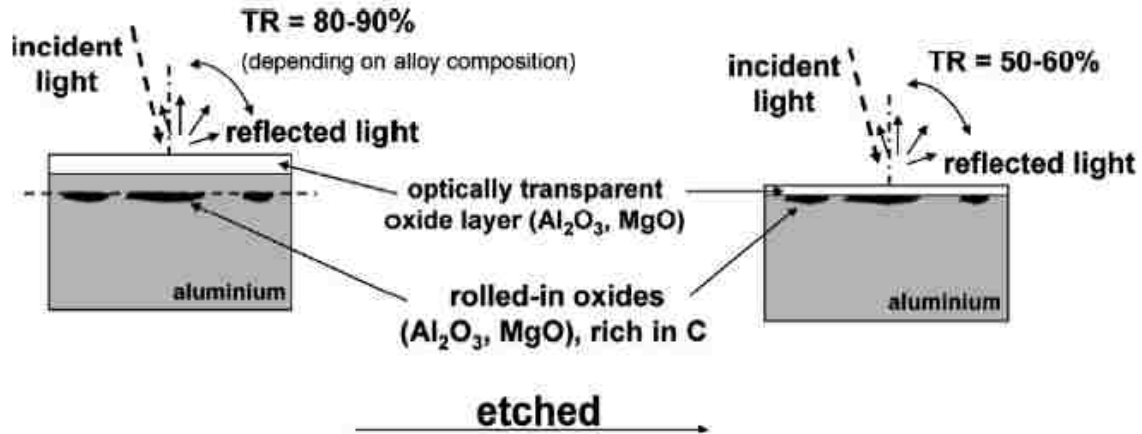


Figure 13. Schematic of the influence of rolled-in oxides on the Total Reflectance (TR) [41,50]

2.6 Effect of disturbed layer to filiform corrosion (FFC)

Filiform corrosion (FFC) on aluminum alloys can be severe in marine, tropical or coastal areas, because it also depends on humidity and the formation of hygroscopic corrosion products in the head of the filament. The filiform corrosion can even propagate at a relative humidity as low as 30%, since the dissolution point of aluminum chloride is approximately at 30-35% relative humidity at 25 °C, and it will form an aqueous solution above with a solid salt below. Therefore, increasing the humidity and decreasing the pH value may increase the propagation rate of the filiform corrosion. However, it may propagate again even after a dry period, unless a complete hydrolysis of the corrosion products in the head of the filaments leads to a repassivation. In that case, the FFC process is dominant during dry conditions and starts to propagate when the environment becomes humid again, meaning that it could restart without an initiation process [55].

The anodic activity is the leading factor for the propagation behavior of FFC on aluminum, as Figure 14 shows. The aluminum is dissolved in the head of a filament and oxygen is reduced, while the corrosion products are deposited in the tail and the oxygen is mainly passed through the tail, since it is much easier for oxygen to go through the porous corrosion products than the coating. Therefore, the initiation of filiform filaments is reduced for the thicker porous layer [56].

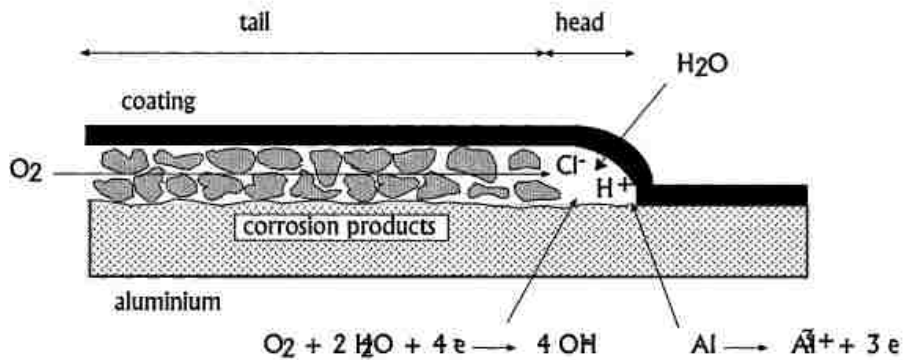


Figure 14. Schematic view of a filiform filament on aluminum [56]

The susceptibility to corrosion and surface reactivity are not particularly related to grain size but to differences in the intermetallic particle distribution and the solid solution content. The matrix and particles such as precipitates, dispersoids and intermetallic particles in an alloy can have a significant influence on its corrosion behavior [56,57].

Intermetallic particles can increase the probability of the initiation of FFC, whereas the 1000 series aluminum alloys (containing mainly pure aluminum) have better FFC resistance. The intermetallic particles can act either as cathodes or anodes in order to affect the rate of electrochemical processes by promoting the dissolution of aluminum. Thus, they may play an important role in the location of filiform corrosion initiation[26,55,56]. As Figure 15 shows, the intermetallic particles in the front of the filiform head serve as local cathodes for the hydrogen

reduction reaction. The intermetallics are surrounded by dissolved aluminum until the cathode is detached or a new one is reached. As the cycle continues, the anodic section could turn to cathodic in order to take the reaction for oxygen reduction. As more intermetallic particles become available and the cathodic and anodic surface areas increase, then the corrosion current density increases [56,58,59].

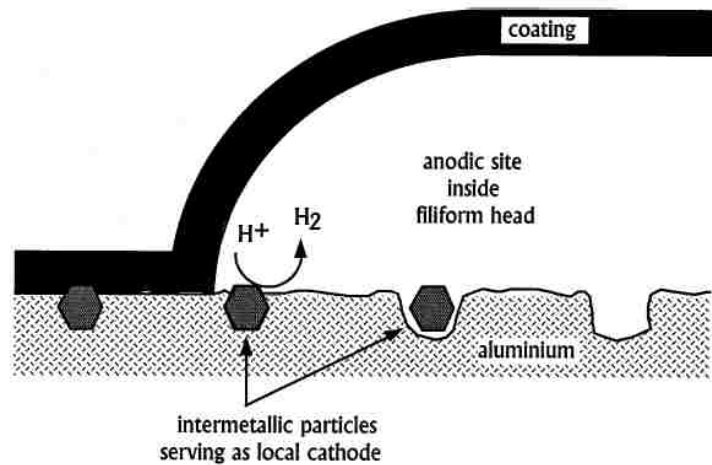
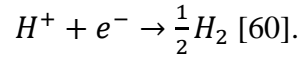
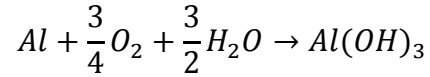
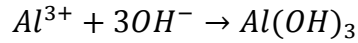
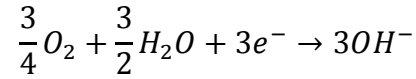
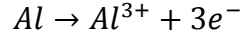


Figure 15 Effects of intermetallic particles on the propagation behavior of filiform filaments [56]

The altering of the surface layer makes it more prone than the bulk material to corrosion attacks. Therefore, thin surface layer corrosion always leads to a rapid and extensive propagation of underfilm corrosion [16]. The hot-rolled material has more susceptibility to filiform attack than cold-rolled material, and this susceptibility further increases with heat-treatment [44]. The filiform corrosion usually starts at discontinuities, breaks, etc in the surface area. It needs sufficient relative humidity, oxygen, temperature and surface defects as well as the right material to be induced. Under filiform corrosion, aluminum exhibits small hydrogen bubbles at filament heads, and the whole solution at the heads is acidic. The reactions are shown below:



The corrosion first propagates along preferred grain boundaries and then develops into the bulk grains. Figure 16 below shows the two stages of filiform corrosion after hot rolled aluminum alloy, which are surface-active filiform corrosion and successive-pitting filiform corrosion. At the surface-active stage, the localized corrosion attack is intergranular and very superficial, having less than 2 μm depth; it propagates at or adjacent to grain boundaries along the near-surface layer, accelerated by the rapid dissolution of magnesium oxide and the presence of manganese/iron-rich dispersoids, with no penetration into the bulk metal. After the near-surface deformed layer is corroded, the stage of successive-pitting corrosion occurs. The depth of penetration may even reach to 10 μm , and the corrosion attack is preferred at grain boundaries as well. The intergranular corrosion could result from the density change of dislocations during shear deformation in rolling, since the grain stored energy is determined by the density of the dislocations. Therefore, the microstructural differences between grains, such as size and dislocation capacities, makes one more susceptible to corrosion than another [33]

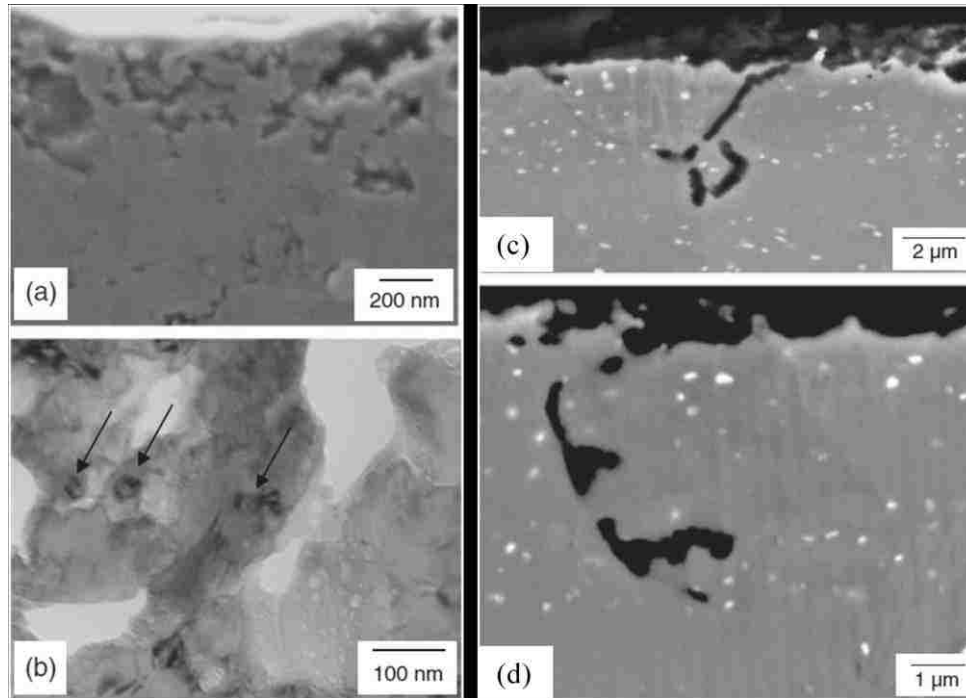


Figure 16. Surface-active filiform corrosion (left side figure): (a) SEM of cross-section show the initial stages of filiform corrosion with attack of grain boundaries in the deformed layer; (b) TEM showing the dispersoids (indicated by the arrows) in the corrosion product. SEM of successive-pitting filiform corrosion (right side figure): (c) corrosion initiated at a grain boundary of the aluminum matrix after the near-surface deformed layer has been consumed; (d) corrosion growth into one of the grains [33]

Afseth et al. [26] found that high temperature heat treatment for the aluminum alloy AA3005 results in a drastic loss of FFC resistance, and that is attributed to the higher plastic deformation undergone by the near surface layer, caused by the secondary precipitation of manganese bearing intermetallic particles in this region. Therefore, the FFC properties of rolled aluminum are strongly influenced by the intermetallic particles and the solid solution levels of impure elements in the near surface region; for instance, a higher density of fine intermetallic particles and lower manganese solid solution content than that of the underlying bulk metal usually causes poor FFC properties in the metal alloy.

The higher corrosion rate contributes to the higher cathodic or anodic activity on the surface during the rolling process due to an increased number of Fe- and Mn-rich precipitates for some Mn containing aluminum alloys [16,44]. Alloys with a high level of manganese, such as AA3005, always have a higher susceptibility to filiform corrosion [30,57]. α -AlMnSi could be the point at which the corrosion process is induced. It is believed that this type of corrosion is promoted by the electrical potential between the α -AlMnSi and the matrix. These preferential precipitation dispersoids can be prevented by controlling the level of manganese in solid solution or by reducing the manganese in the alloy [57]. However, the depletion of Mn from solid solution into the second phase particles in the deformed surface layer also enhances FFC susceptibility, but since the Mn content does not change continuously during the rolling, the depletion of Mn is not the main factor that is responsible for enhanced FFC susceptibility [16]. Therefore, a simple method of rendering aluminum sheet surfaces resistant to FFC is to remove the active layer by caustic etching or by using other appropriate treatments [15,53,61].

Coating is an efficient way to prevent filiform corrosion; the degree of adhesion related to the surface roughness of the coating could be a principle influence on the filiform corrosion rate. The coating usually breaks down above the filiform corrosion heads and tails, and the same phenomenon may occur in the disturbed layer [62]. Chromatizing the aluminum alloy could improve the resistance to FFC as well, due to the formation of a stable oxide layer by the remaining hexavalent chromium ions serving as active corrosion inhibitors [56].

2.7 Rolling parameters that affect the surface layer

The rolling parameters such as temperature, rolling geometry, roll surface morphology, state of lubrication, forward speed, number of rolling passes, roughness of the rolls and the roll speed are important to the formation and properties of the surface and near-surface regions

[29,32]. For instance, increasing rolling passes can increase the generation of localized shear deformed areas, which makes the alloy more prone to form the disturbed layer. Also rolling in different directions elongates the surface, embedding the shear deformed areas more deeply into the surface than if rolled in same direction. Furthermore, the thickness of the disturbed layer is extremely commercially important in order to minimize the cost of post-production treatment such as anodizing, caustic etching, etc. [41]. The hot rolling process is more significant for the formation of the micrograined surface layers than is subsequent cold rolling. The thickness of the disturbed layer is greater at higher forward rolling speeds [29]. Process parameters such as the type of rolling schedule and equipment that represents forward, reverse or and multistand milling can also significantly affect the microstructure [49].

2.7.1 Heat treatment and strain effect

The recrystallization of grains has two critical prerequisites; one is to have a critical deformation, and the other is to reach a critical temperature. Therefore, the heat treatment of a rolled aluminum piece has significant effects on the microstructure of both the bulk alloy and the disturbed layer. The greater the deformation produced, the higher the nucleation sites and the nucleation rate of the recrystallizing grains will be. The rates of magnesium oxidation and diffusion to the alloy surface increase with temperature, so that the thickness of the oxide layer and quantity of rolled in oxide particles decreases in the later passes since the temperature goes down [27]. However, the grain size becomes stabilized, since the second-phase particles present in the disturbed layer act as grain refiners; the grain size does not change with further annealing [34].

As in the literature mentioned above, the size and distribution of the dispersoids in an alloy have strong effects on the recovery, recrystallization and grain growth during heat

treatment, and the heating rate strongly affects the size and distribution of the dispersoids. For instance, the Mn-containing dispersoid Mg_2Si is preferentially formed on the area on which Mg and Si lie on while heating at a fast rate, but it nucleates in a uniform distribution in the matrix at a slow heating rate (as shown in Figure 17) [40]. At initial stages of precipitation by annealing, there are multiple kinds of intermetallics or dispersoids, but as the temperature rises, only the Mn precipitation process occurs [45].

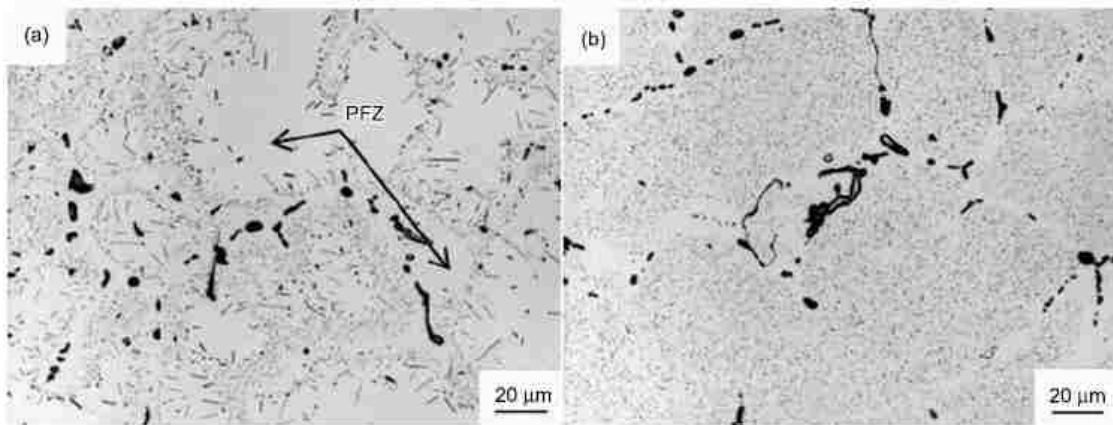


Figure 17. Optical micrographs of the 6082 alloy after homogenization: (a) rapidly-heated specimen; (b) slowly-heated specimen. PFZ stands for precipitate free zones [40]

Annealing promotes the preferential precipitation of intermetallic particles in the disturbed layer, which increases the density of cathodic sites in the surface layers to induce corrosion. This preferential precipitation can be prevented by controlling the level of manganese in solid solution or by reducing the manganese in the alloy [57]. However, annealing has little or no effect on the thickness of the subsurface layer and does not significantly affect the examined elemental distribution; apparently, only the magnesium, carbon and oxygen are affected, but intermediate annealing appears to have a small increasing influence on the subsurface layer's thickness [35].

Figure 18 shows the contrast of the GDOES qualitative depth profiles between the AA3005 aluminum alloy "as received" and after annealing of the hot-rolled AA3005 aluminum alloy (max. 0.28 wt% Si, 0.60 wt% Fe, 1 wt% Mn, 0.25 wt% Mg) for 2h at 500°C. Carbon has almost the same tendency as oxygen; this is probably caused by the entrapped contaminants and rolling lubricants. Si declines for the first micrometer and then remains constant, which agrees with the Si contents of the alloy, and Fe does the same. There is only a small copper enrichment in the near-surface region [39,63]. Moreover, the evolution of the texture orientations during hot rolling could influence the recrystallization behavior of the structure from the surface even to the mid-thickness depth, due to the subsequent annealing process [50].

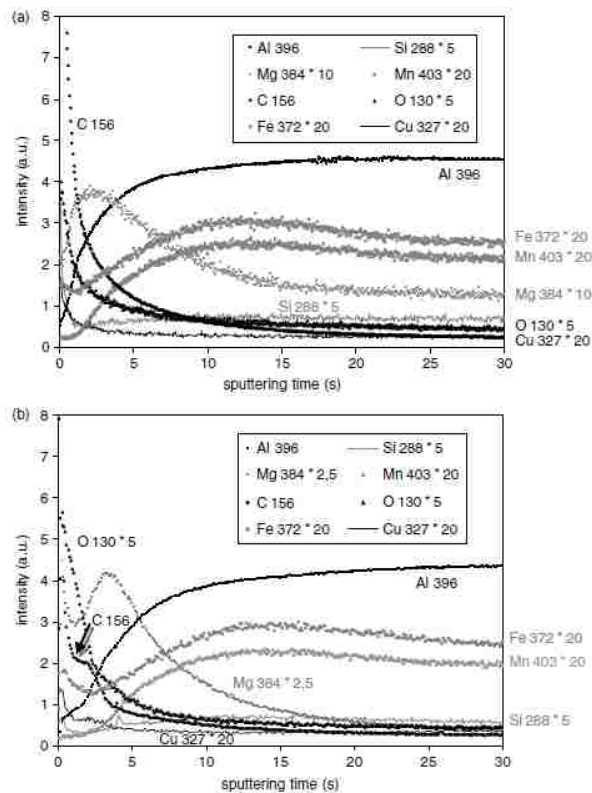


Figure 18. RF GDOES qualitative depth profiles of a hot-rolled AA3005 aluminum alloy: (a) "as received"; (b) after annealing for 2 h at 500 °C [63]

Furthermore, since heat treatable aluminum alloys are strengthened by precipitation hardening, the evolution of damage in aluminum alloys under mechanical loading by rolling could be dependent both on the previous heat treatment condition and on strain rates. The naturally aged (cooling at room temperature) alloy shows a higher susceptibility to strain localization than the artificially aged alloy, the grain size and degree of recrystallization are influenced by the tempered condition of the alloy as well [17].

2.7.2 Material transfer and adhesion

The transfer and adhesion of material to tool surfaces during rolling or any kind of process of hot forming aluminum alloy sheets could be the major problem in impeding high production rates, since this reduces the surface quality of the finished product [12]. The workpiece material may experience several kinds of hardening mechanisms such as work hardening, grain refinement, and oxide particle incorporation during transfer and adhesion. The hardening work done by transfer and adhesion could cause the formation of scratches and indentations that could induce damage in subsequent work. Adhesion for aluminum is always even more severe and occurs even when the roller is very smooth [64]. Table 1 shows the tendencies of adhesion and material transfer from the work material to the tool rod, obtained by the sliding experiment. PM-A to E stands for powder metallurgical steel, which is much harder than stainless steel and aluminum alloys, and A to E represents an increasing sequence of surface roughness. It is apparent that aluminum is transferred the most easily since it is softer than steel.

Table 1. Classification of the tendency of adhesion and transfer of work material to the surface of the five tool steel treatments, thin layer transfer (TLT), small patch transfer (SPT), extensive patch transfer (EPT), and full width transfer with local patches (FWT). [64]

	PM-A	PM-B	PM-C	PM-D	PM-E
SS	TLT or SPT	SPT	EPT	EPT	EPT
Al	FWT	No test	FWT	FWT	No test

However, the bonding strength between the work and the tool interface should be higher than the internal strength of the work material. This is a prerequisite for initiating the material transfer. It is usually characterized by the oxide layer on top of the contacting materials. Therefore, two kinds of work material transfer are summarized: the first is when the work material oxide layer is softer than the bulk material if the tool surface is smooth. Then a prow can form and grow as the shear zone beneath it grows, and after the fracture of the shear zone occurs, the prow will adhere to the tool surface. So the oxide thickness is a key to avoiding adhesion and metal transfer if the oxide is soft. The second kind of transfer is when the oxide layer is substantially harder than the bulk metal. The hard oxides may form a mechanical grip on the tool surface, which makes the strength of the interface bonding between the work and the tool surface stronger than the internal strength [64].

During rolling aluminum, the aluminum adheres to the roll surface as soon as there is a lubricant breakdown. The transferred material on the roll surface forms a film that contains C, O, Mg and Al, covering the surface, and reduces the coefficient of friction in subsequent rolling. This film can also act as a barrier to prevent the further adhesion of more aluminum to the roll surface. Hence, the aluminum transfer on the roll surface is most severe at the first pass of rolling [29].

Using coatings and lubricants can be an efficient way to prevent material transfer or adhesive junction formation by reducing the coefficient of friction. Transfers between steel and aluminum alloys are especially difficult to diminish without using lubricants. In addition, applying a coating to the tool surface with a hardness higher than the work material oxides is also recommended to reduce transfer [64-66]. However, a rolling lubricant with poor properties cannot form an effective lubricating oil film, which may induce lubrication failure; this failure could lead to many irregularly shaped microcracks on the aluminum surface because of the adhesive wear produced by direct contact between the work and tool piece after such a lubricant failure. The lubricant, which is usually an oil-water mixture, could also become trapped in cracks formed during rolling because of the high carbon content found in cracks on the disturbed layer. These are possible factors believed to lead to color changes on the aluminum surface [67].

Friction is important for controlling the aluminum rolling process. A high friction coefficient is never desirable, not only because of the energy wasted but also because of the increasing rate of material transfer between the workpiece and the tool surface. As a result, the addition of lubricant is always the primary, significant way of reducing the coefficient of friction, since it can reduce material transfer from the sample to workpiece. The addition of a boundary additive can reduce the COF as well [68-71]. Figure 19 shows the difference between adding lubricant only and adding lubricant with boundary additives.

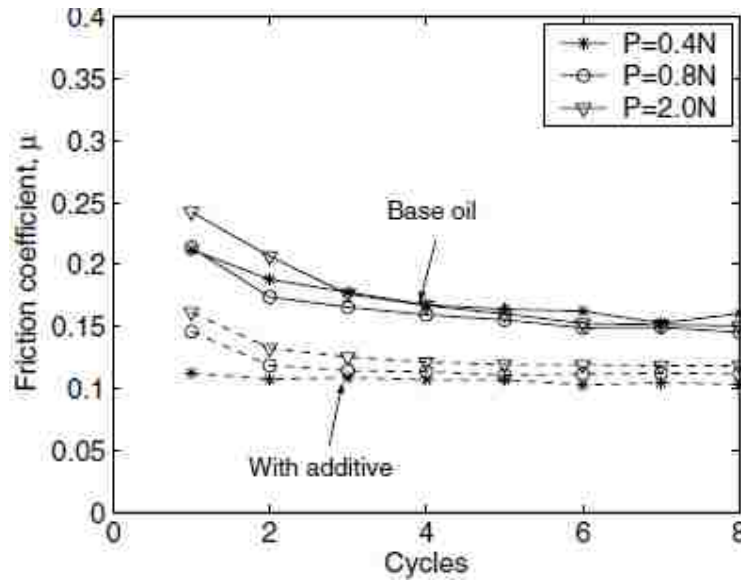


Figure 19. Friction coefficient for polished samples; solid curves for tests with Somentor 32 base oil, dashed curves for Somentor 32 plus a boundary additive [68]

2.7.3 Grinding effect

The technique of grinding and polishing the tool piece and workpiece samples can provide different advantages. In the rolling process, grinding a roller can induce varying topographies (roughness) on the roller in order to fulfill different industrial needs. In general, friction increases with the roughness, especially when rolling aluminum alloys where friction can remain high even with a smooth roller [64]. Therefore, grinding the tool piece or rolling samples may also be a concern that affects the surface and near-surface layers. Lee et al. [72] showed that grinding could reduce the thermal stresses induced by annealing the aluminum metal matrix composite and that the effect of grinding is diminished as the depth increases. Hot rolled aluminum alloys that are mechanically ground always show very little corrosion. At the same time, aluminum samples that have a finer surface finish prior to heat treatment show much less filiform corrosion susceptibility compared to samples that are not mechanically ground [57].

2.8 Summary of literature survey

Rolling aluminum alloy could generate a disturbed layer on the surface region, and this disturbed layer has different microstructure and content distribution compare to bulk alloy. It affects the mechanical properties of the surface region such as corrosion resistance, weldability and optical appearance. The formation of disturbed layer during rolling is dynamic along with different mechanisms, which could be affected by many variable rolling parameters such as forward speed or lubrication conditions. However, there is very limited research works done in the rolling parameter of different roll materials, as a result, study of rolling with different roll materials is needed.

CHAPTER 3 DESIGN AND METHDOLOGY

3.1 The workpiece

The alloys investigated were an Al-Mn and an Al-Mg alloy. Their approximate compositions are shown in Table 2. The alloys were provided by Novelis Global Technology Centre and machined to the required dimensions of 10.5 x 30 x 96 mm. The roll contact surface (10.5 x 96 mm edge face) was polished to a mirror surface finish, using 1 μm diamond paste, and was cleaned ultrasonically in acetone for 10 minutes to remove surface contaminants.

Table 2. Elemental composition distribution of Al-Mn and Al-Mg alloy

Alloy	Si	Fe	Cu	Mn	Mg	Zn	Ti	Ga	V	others		Al
										each	total	
Al-Mn alloy	0.6	0.8	0.05- 0.25	0.8- 1.4	0.8- 1.3	0.25	0.1	0.05	0.05	0.05	0.15	Remainder
Al-Mg alloy	0.2	0.4	0.15	0.2- 0.5	4-5	0.25	0.1	-	-	0.05	0.15	Remainder

3.2 The roller

The rollers used in these experiments were steel alloy AISI 52100, 440C and D2, with their approximate compositions given in Table 3. They were all polished to a mirror surface, using 1 μm diamond paste, to a surface roughness of $R_a = 0.0089 \mu\text{m}$ for 52100, $R_a = 0.0148 \mu\text{m}$ for 440C, and $R_a = 0.0108 \mu\text{m}$ for D2. Table 5 showed the hardness of each steel roller, all of them were in annealed condition. They all had a diameter of 21 mm and were less than 1/20 the size of rolls used in the industry.

Table 3. Elemental composition distributions of 52100, 440C and D2 steel rolls

Alloy	Cr	Ni	C	Mn	Cu	Mo	Si	S	P	Other
52100	1.3-	0-	0.93-	0.25-	0-	0-0.1	0.15-	0.025	0.025	0-0.05 Al
	1.6	0.25	1.10	0.45	0.03		0.35			0-0.0015 O
440C	16-18	0- 0.75	0.95-1.2	0-1	0-0.5	0-0.75	0-1	0- 0.03	0-0.04	-
D2	11-13	0-0.3	1.40- 1.65	0.6	-	0.5- 1.2	0.3-0.6	0.03	0.03	0.5-1.10% V

3.3 Laboratory simulation

The experiments were carried out using a CNC machine with a stage built on it to hold an aluminum block sample. The stage was made of stainless steel and was fixed on the controlled stage of the machine. Movement of the stage was controlled along both the x and y axes. Two load cells were attached to the stage to measure the normal and shear forces. Two cartridge heaters were placed in sample holders attached to the stage, while a thermocouple was placed into the sample via a 10 mm deep 1 mm diameter hole located at the side of the aluminum sample, in order to monitor the surface temperature. The schematic and image of the experimental setup are shown in Figure 20.

Prior to each experiment the roller was cleaned with a 15 % (wt/wt) sodium hydroxide solution to remove any transferred aluminum while the aluminum samples were ultrasonically cleaned for 10 minutes, using acetone. Two kinds of oil-in-water emulsion were used as lubricant and were applied continuously during the tests. They were acquired from different sources and were named lubricant A and lubricant B, and were provided by the Novelis Global Technology Centre, and all were prepared by shearing neat oil in water, usually at a 4 % (v/v) concentration,

using a homogenizer at 15,000 rpm for approximately five minutes. Lubricant A was heated to 50°C before blending in the homogenizer.

During the rolling simulation, the aluminum alloy block sample was held between two holders and heated to the required temperature. After the temperature was reached, the emulsion flow and roller rotation were started, while the stage simultaneously moved towards the roller. To avoid excess lubricant being burned into the surface of the sample during rolling, pressurized air was sprayed on the sample surface immediately after the contact with the roller. The time required to reach 550°C was 14 to 15 minutes. During the rolling process the load was 860 -1130 N, providing a contact pressure of 30.7 - 40.4 MPa. The degree of deformation was always set previously. Table 4 shows the variable process parameters considered in the experiments. The forward speed was determined by the difference between the speed of the stage and the linear speed of the roller, and was then divided by the speed of the stage multiplied by 100. The forward speeds of all experiments in this study were 7%.

A scanning electron microscope (SEM) equipped with energy dispersive X-ray spectroscopy (EDS) was used to study the sample surfaces after each test. The surface topographies were investigated with an optical profilometer (WYKO NT1100).

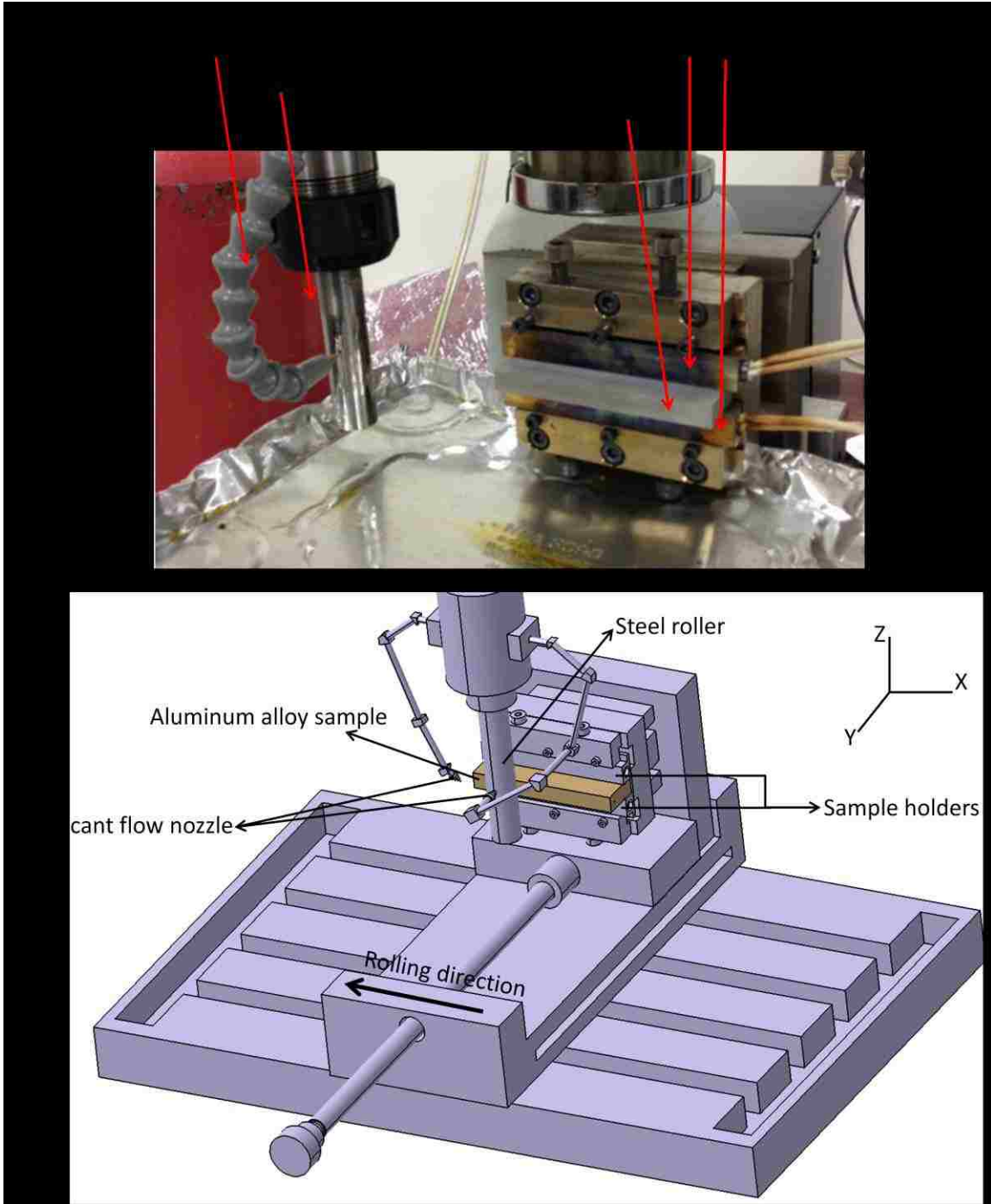


Figure 20. General view and schematic of experimental setup of hot rolling simulation

Table 4. Variable process parameters of all experiments done in this study (the empty block is tests that were not done, and the temperature is the last pass temperature)

	AISI 52100	AISI 440C	AISI D2	Temperature	lubricant
Al-Mn alloy	1 pass	1 pass	1 pass	550 °C	Lubricant A
Al-Mg alloy	1 pass	1 pass		550 °C	Lubricant A
Al-Mg alloy	1 pass	1 pass	1 pass	550 °C	Lubricant B
Al-Mg alloy		2 pass		525 °C	Lubricant B
Al-Mg alloy		3 pass		500 °C	Lubricant B
Al-Mg alloy	4 pass	4 pass	4 pass	475 °C	Lubricant B

Table 5. Hardness of AISI 52100, 440C and D2 steel alloy rollers

Steel roller hardness		
52100	440C	D2
C23.2 Rockwell	C24.1 Rockwell	C21.8 Rockwell

CHAPTER 4 RESULTS

4.1 Results with Al-Mn alloy

As mentioned in the literature, there is possibly undissolved chromium content that precipitates to carbides in the steel alloys 440C and D2. The surface topography profile and micrographs of the steel surfaces 440C, D2 and 52100 (before rolling) in Figure 21 shows protrusions suspected to be carbides observed on 440C and D2, but not with the 52100 roll. These protrusions appear more prominent in 440C, but they appear to have a higher population density on D2.

An examination of the surface of the Al-Mn alloy after one hot rolling pass was made with surface profilometry. The surface profile images of the rolled Al-Mn alloy surface of the steel alloy rolls 440C, D2 and 52100 are shown in Figure 22. Pits are observed covering the surface of the Al-Mn alloy after deformation with 440C and D2, but not with 52100.

Figure 23 shows the SEM images of the Al-Mn alloy surface rolled with the 440C roll after one pass. Grain boundary sliding (GBS), grain overlapping and cracks at the surface were observed after the first pass. A high percentage of broken precipitates and darkened patches was found on the surface. The dark patches on the surface were observed to be rich in Mg and O and occurred especially around precipitates. The roughened surface displayed in the surface profilometry image was observed to be due to pits and crevices on alloy surface. Figure 24 shows the SEM images of the Al-Mn alloy surface rolled with the D2 roll, after one pass. It appears similar in its features to the Al-Mn alloy samples rolled with 440C. GBS, grain overlapping and cracks at the surface were observed after the first pass. A high percentage of broken precipitates and darkened patches was found on the surface. Patches of roughened areas around grains and precipitates were observed on the surface. These areas are rich in Mg and O.

Roughened surfaces were observed to be due to pits, crevices and micro-cracks on the alloy surface as well. Figure 25 shows the SEM images of the Al-Mn alloy surface rolled with the 52100 roll, after one pass. GBS, grain overlapping and cracks were observed on the surface, similar to the surfaces deformed with the D2 and 440C steel. The surface was covered with micro and nano-cracks. Nano-cracks can be observed on the surface at a higher magnification (Figure 25 d).

Figure 26 compares the SEM images of the Al-Mn alloy surface rolled with 440C, D2 and 52100 after one pass. Cracks at the grain boundaries and broken precipitates were observed on all surfaces. Darkened patches were observed on the surface of the D2 rolled sample, with fewer on the 440C rolled sample and none on 52100 rolled sample.

Figure 27a-b shows the SEM images of the 440C steel alloy surface after being rolled with the Al-Mn alloy, after one pass. Broken carbides were observed on the roll surface, and aluminum transfer was observed on a few areas of the roll surface. Light circular areas on the steel surface were identified by EDS as carbon deposits from the lubricant. Figure 27c-d shows the D2 surface in the same condition, with broken carbides observed as well and rich carbon deposits from the lubricant covering the surface. The surface features of the 52100 roll with the same condition are shown in Figure 27e-f; no carbides were observed on the roll surface, and rich carbon deposits from the lubricant covered the surface as well.

The comparison of these three rolls is shown in Figure 28, where a surface densely covered in large carbides in D2 and M_7C_3 is suspected. However, the carbides on 440C are not as large or as dense as on D2, and M_7C_3 and $M_{23}C_6$ are suspected and silicon particles are also observed on the surface. No carbides are observed on the 52100 surface.

The EDS map of the steel roll (Figures 29-31) shows that the Mg adhesion appears to cover 50% of the surface and to coincide with carbides. The carbides appear to be rich in oxygen. However, Al and Mg adhesion appears across the roll surface, with oxides spread more across the surface of the roll for 52100. The EDS map in Figure 32 shows that the D2 carbides contain C, Cr, and V, but that the 440C carbides contain C and Cr. Carbides on both steel rolls were observed to contain O.

4.2 Results with Al-Mg alloy

Figure 33 shows the SEM images of the Al-Mg alloy surface rolled with the 52100 steel roll, after one pass. The surface shows GBS occurring on the surface; the dark spots are observed to be depressions on the alloy surface, and cracks were also observed within grains. The dark depressions are rich in Mg. Figure 34 shows the SEM images and EDS analysis of the Al-Mg alloy surface, rolled with the 440C steel roll, after one pass. Figure 34 contains a comparison of images made with the 5kV and 12 kV electron beams, with 5 kV providing a better topological view of the surface features than the 12 kV. Spots observed on the surface with 12 kV are better observed 5 kV to be spherical bumps on the surface; these spherical bumps and a dark patchy network are observed covering the surface. From the EDS analysis, spherical bumps have the same Al-Mg concentration as the surface, while the patches are observed to be rich in Mg.

Figure 35 shows the SEM images of the 440C steel alloy surface after being rolled with the Al-Mg alloy, after one pass. Al-Mg adhesion was found either on the carbide edges or covering the whole surface. Moreover, the EDS mapping in Figure 36 shows that Mg adhesion better coincides with carbides than with the Al-Mn alloy, and Al adhesion on carbides also been confirmed.

The hot rolling simulation lubricant was changed to lubricant B for the experiments below. This reduced the frequency of the appearance of Al-Mg micro-ball features on the surface of the rolled Al-Mg alloy.

Figures 37d-e, 38d-e and 39d-f show the Al-Mg alloy surface rolled with 440C, D2 and 52100 after four passes; grain boundaries appear darkened and distinct compare to their appearance after one pass, and dark patches are observed within grains as well. From the EDS analysis in Figures 40-42, darkened grain boundaries and patches appear continually rich in Mg and O. The pits or crevices are mostly observed at the darkened Mg and O areas at higher magnification. All Al-Mg alloy surfaces rolled with 440C, D2 and 52100 after one pass are shown in Figures 37a-b, 38a-b and 39a-c. These show GBS, while grains are surrounded by cracks occurring at the boundaries and at higher magnifications, rich Mg and O patches are observed.

The Al-Mg alloy rolled with the 440C steel roll was chosen to investigate the surface evolution of each pass up to four passes, because of the similar carbide protrusion structures of 440C and D2. The surface profile in Figure 43 shows that the surface roughness decreases after the second pass, but it increases again at the third pass and decreases again after the fourth pass. Figure 44 shows the surface of the Al-Mg alloy rolled with 440C after one pass, two passes, three passes and four passes. The grain boundaries and patches grow darker as the number of passes increases, while the Mg and O rich dark patches cover more surface area as well.

Since the Al-Mg micro-ball features appeared less often on the surface of the rolled Al-Mg alloy when the lubricant had been changed, the experiments with different lubrication conditions confirmed that the Al-Mg micro-ball features on the surface of the Al-Mg alloy rolled with the 440C steel roll were observed due to the lack of lubrication. Figure 45 shows the two

different conditions of lubrication; one uses an emulsion nozzle close to the steel roll, and the other is far from the steel roll. The results in Figure 46 show that no ball features formed on the surface of the Al-Mg alloy during the experiment with the emulsion nozzle close to the roll, compared to Figure 47 and the condition in which the surface was rolled with the nozzle far from the roll.

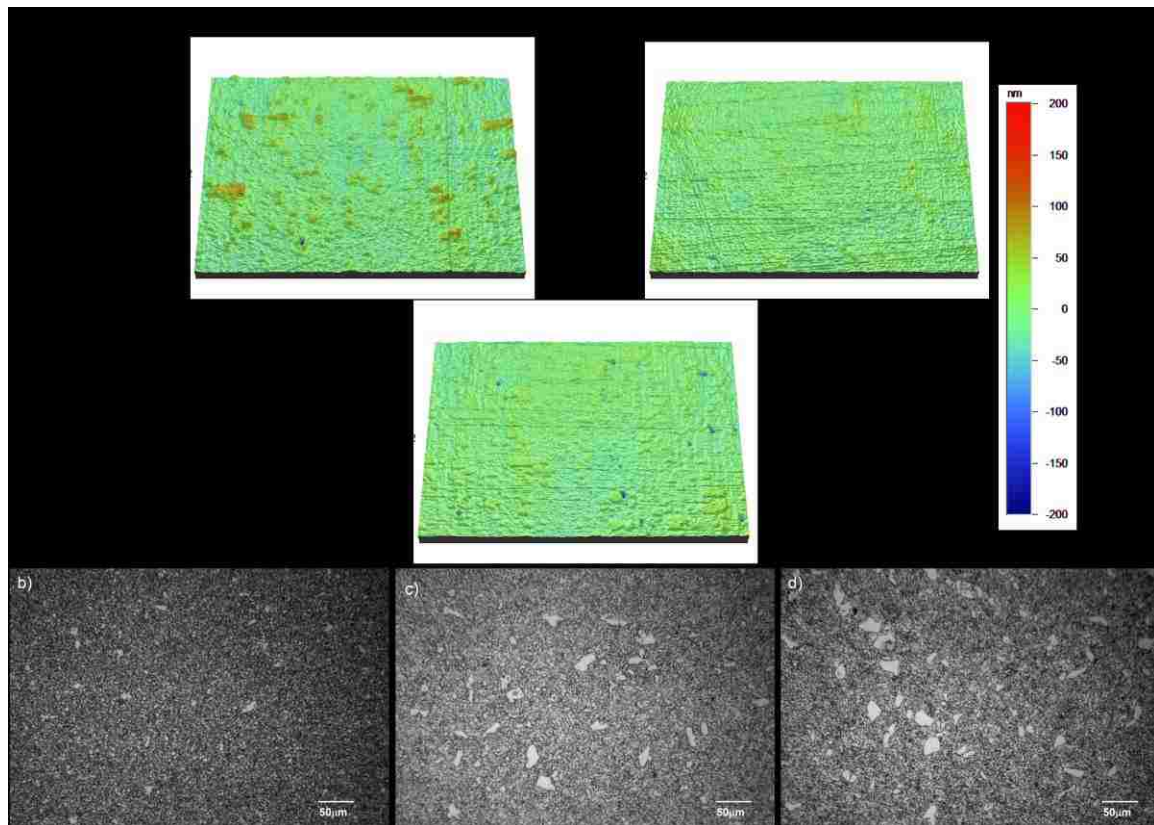


Figure 21. a) WYKO images of surface profilometry of AISI 440C, D2 and 52100 steel rolls (as-polished), surface roughness of 440C $R_a = 0.0148$, D2 $R_a = 0.0108$, 52100 $R_a = 0.0089$, b) Micro graphs of 52100, c)440C, and d) D2

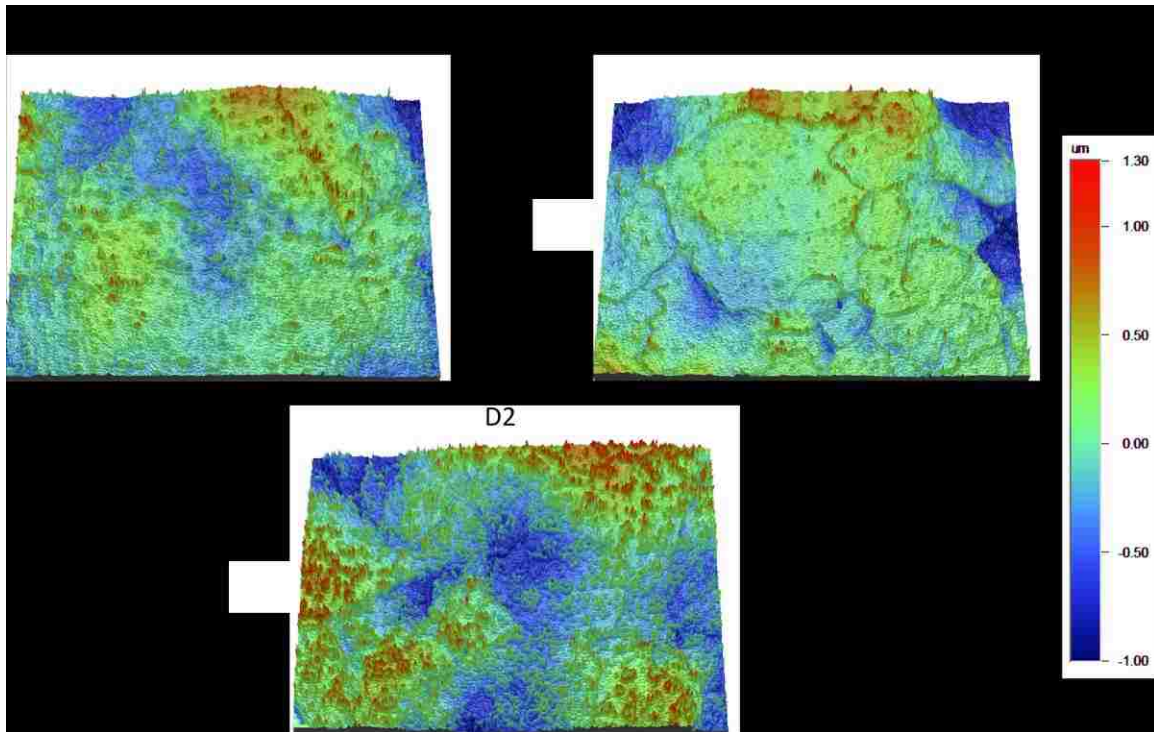
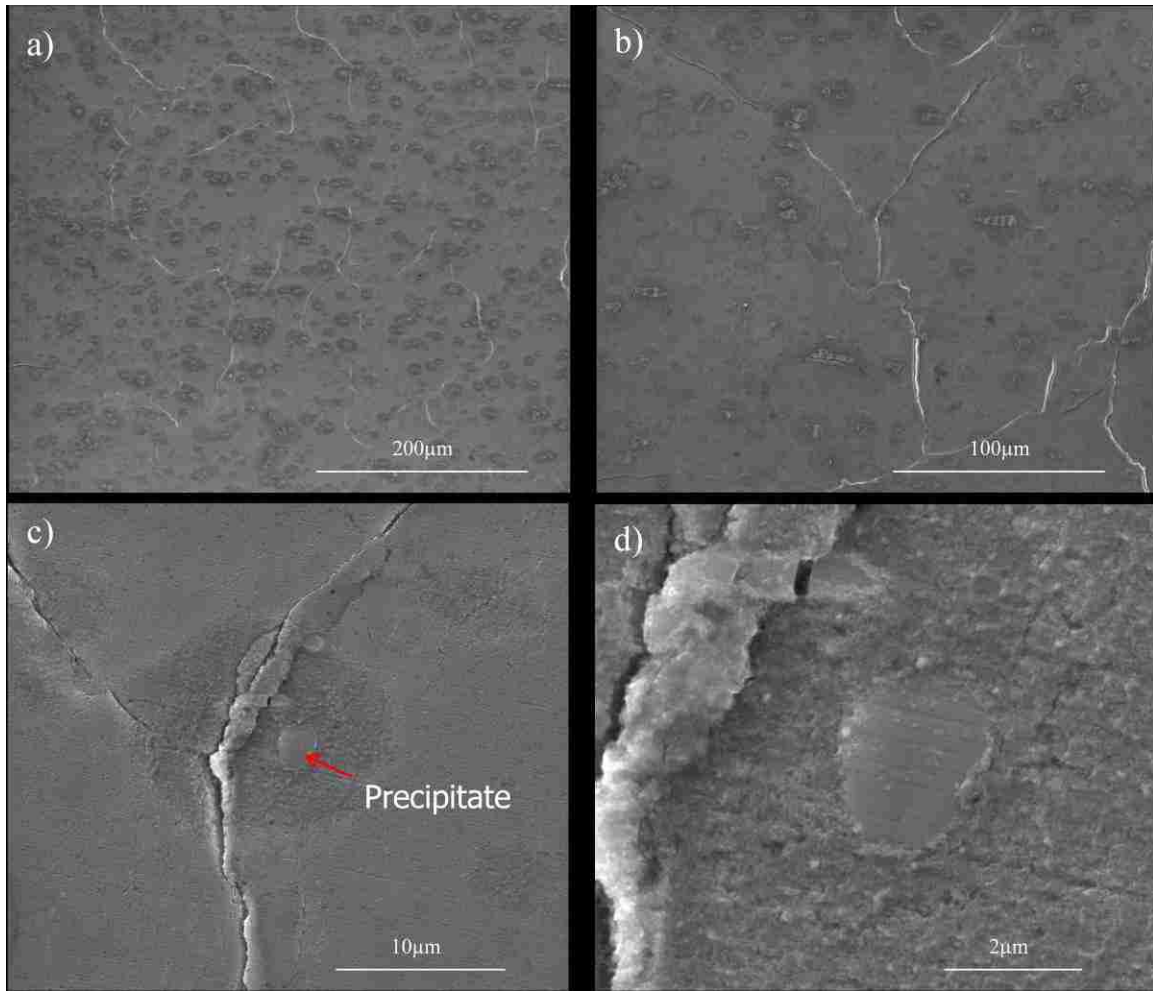


Figure 22. WYKO images of surface profilometry of Al-Mn alloy after rolled 1 pass with AISI 440C, D2 and 52100 steel rolls, rolled with 440C Ra = 0.285, D2 Ra= 0.303, 52100 Ra = 0.286, pits are observed covering the surface of the Al-Mn alloy after deformation with 440C and D2, but not with 52100



←
Rolling direction

Figure 23. The SEM images of Al-Mn alloy rolled with 440C roll after 1 pass, order of magnification from low to high for a) to d)

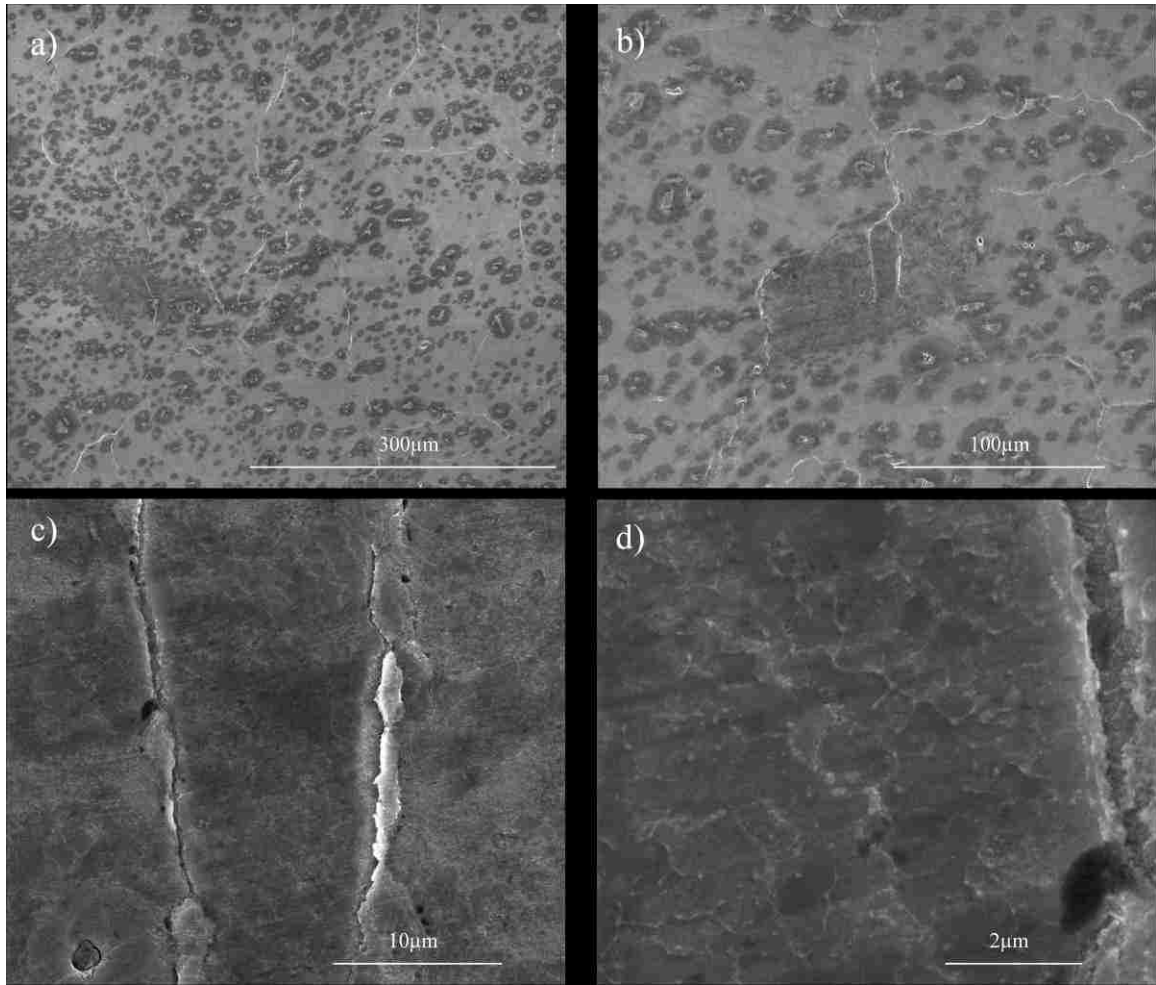
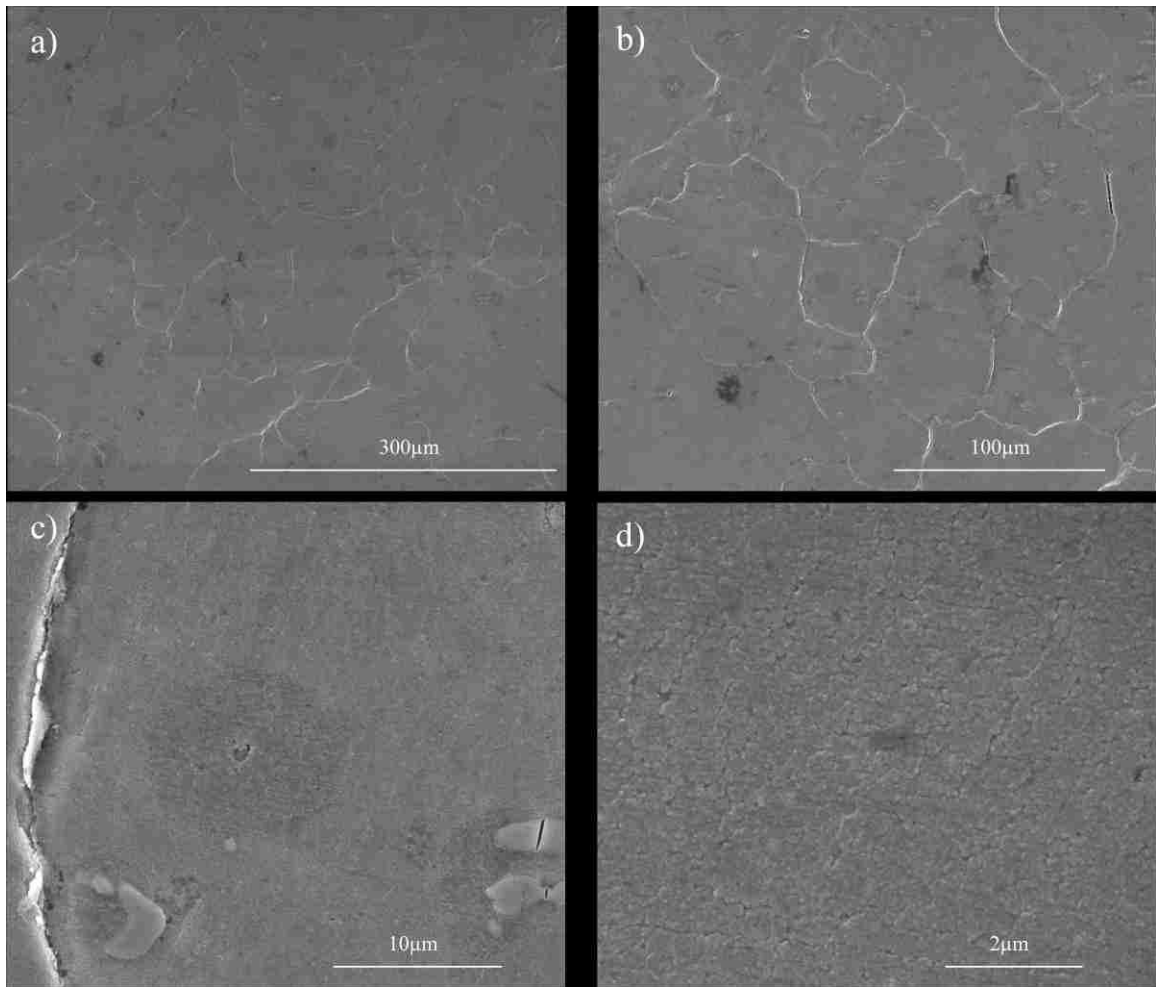


Figure 24. The SEM images of Al-Mn alloy rolled with D2 roll after 1 pass, order of magnification from low to high for a) to d)



← Rolling direction

Figure 25. The SEM images of Al-Mn alloy rolled with 52100 roll after 1 pass, order of magnification from low to high for a) to d)

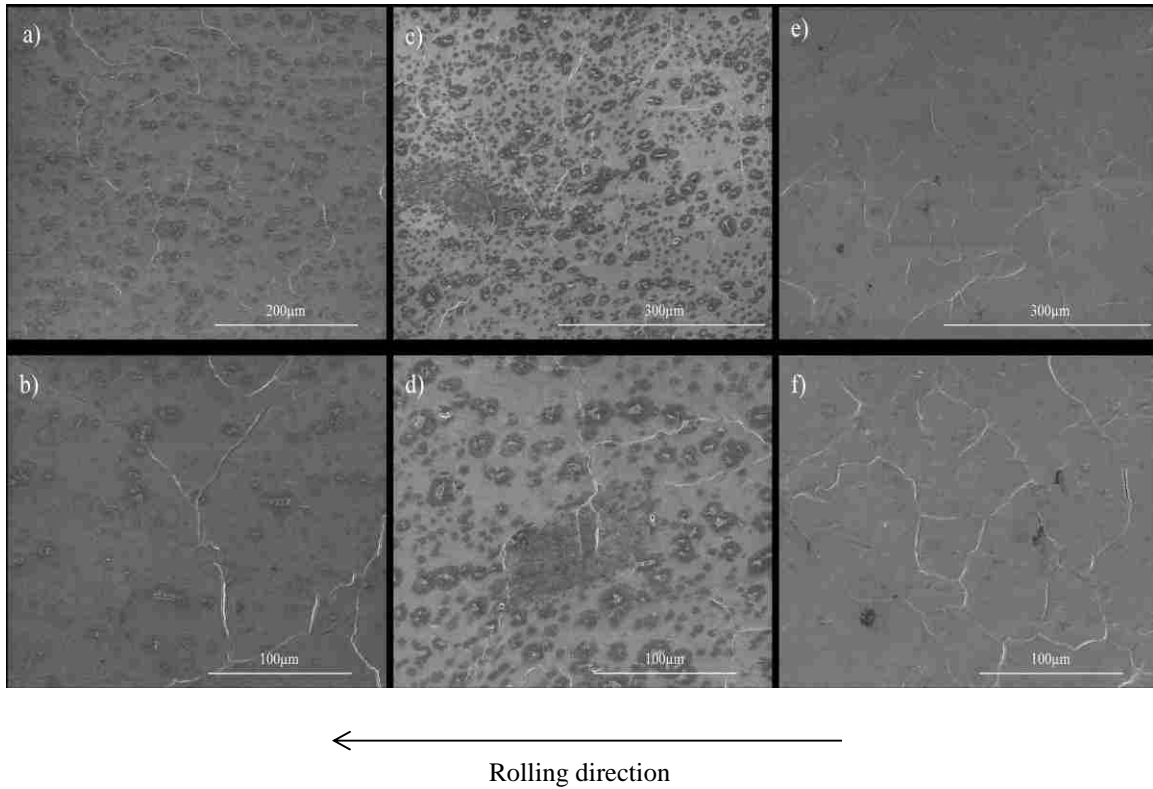


Figure 26. Comparison of the SEM images of Al-Mn alloy rolled with 440C, D2 and 52100, a) and B) for rolled with 440C, c) and d) rolled with D2, e) and f) rolled with 52100

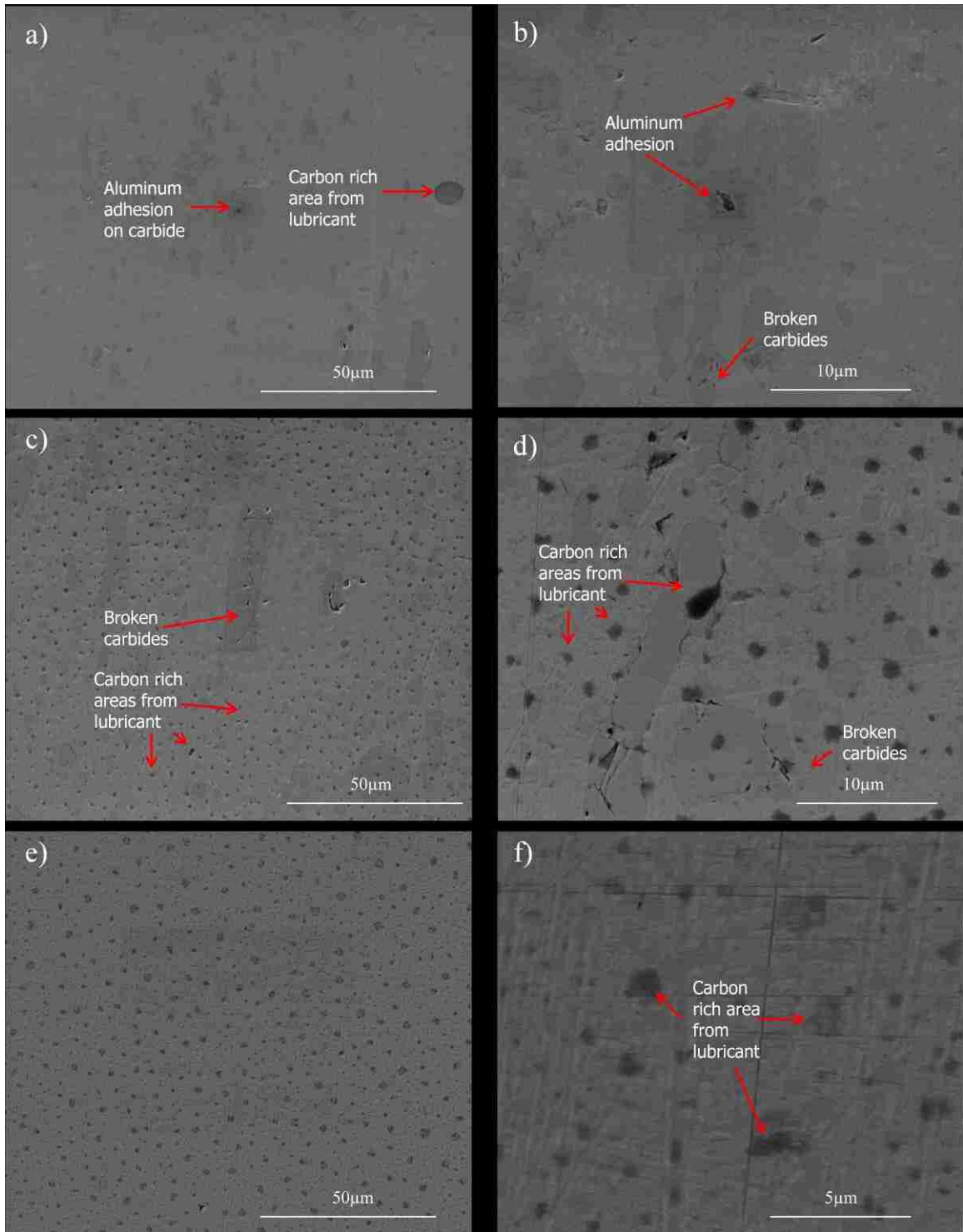


Figure 27. The SEM images of a) and b) for 440C steel alloy surface after rolled with Al-Mn alloy after 1 pass, c) and d) for D2 steel alloy surface after rolled with Al-Mn alloy after 1 pass, e) and f) for 52100 steel alloy surface after rolled with Al-Mn alloy after 1 pass

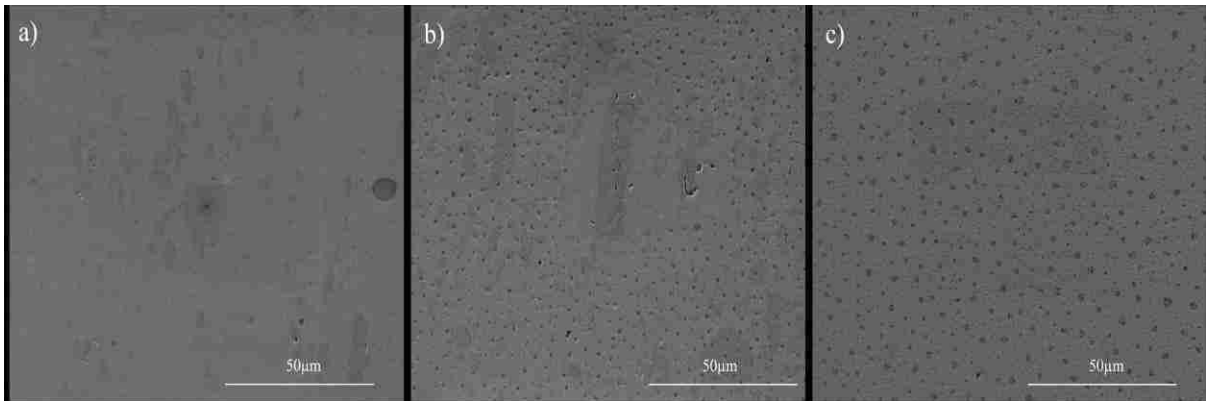


Figure 28. The comparison of a) 440C, b) D2 and c) 52100 steel alloy surface after rolled with Al-Mn alloy after 1 pass

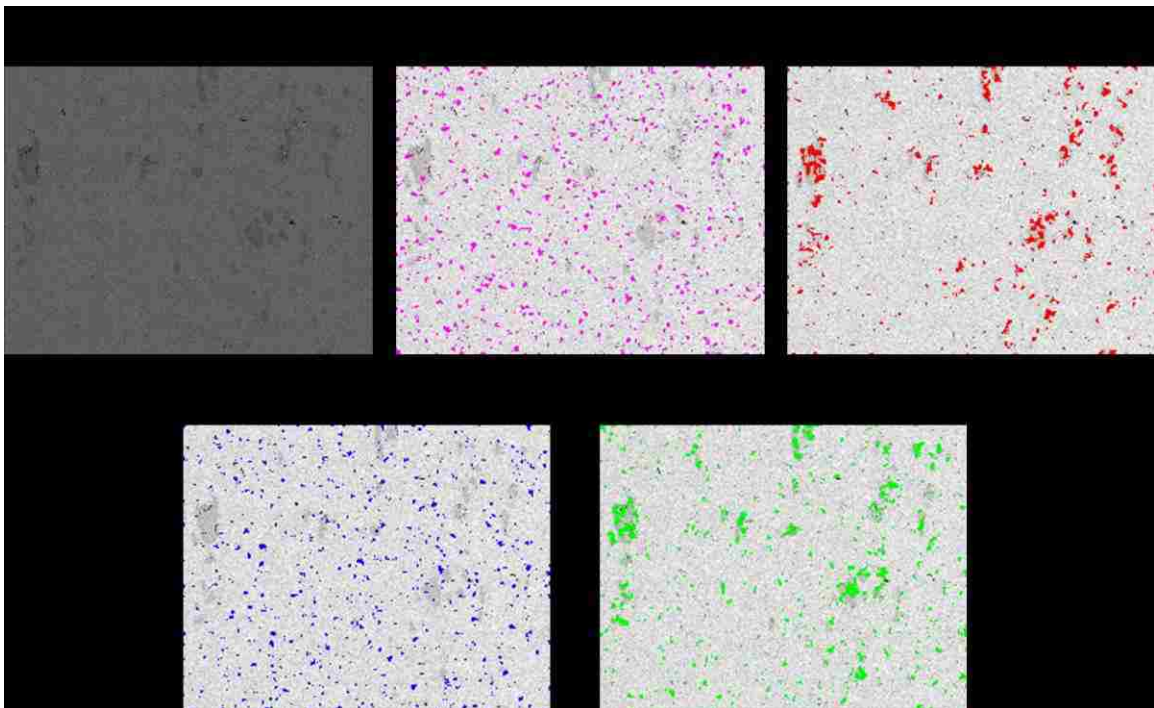


Figure 29. EDS mapping of 440C steel alloy surface after rolled with Al-Mn alloy after 1 pass

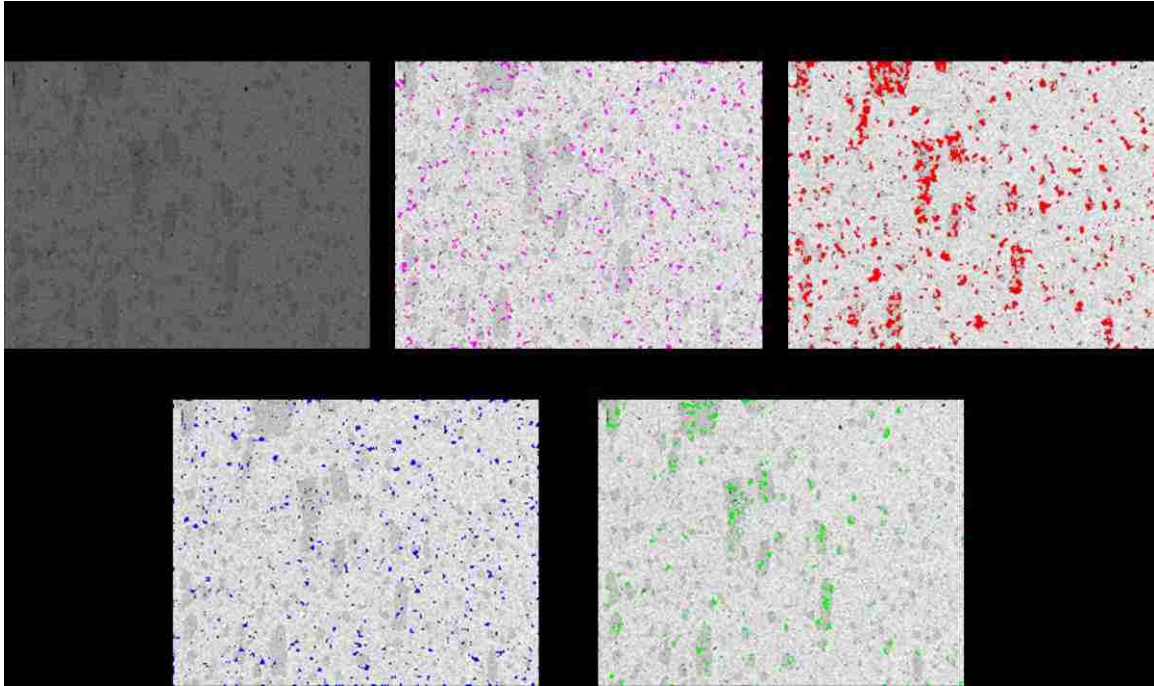


Figure 30. EDS mapping of D2 steel alloy surface after rolled with Al-Mn alloy after 1 pass

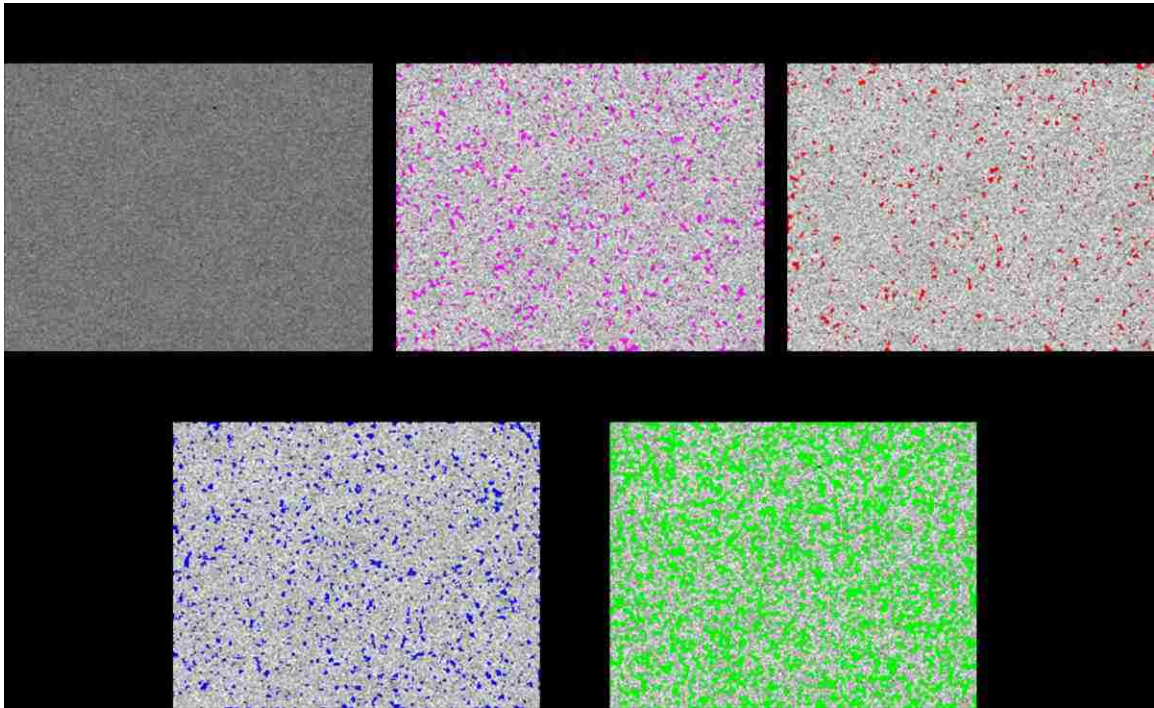


Figure 31. EDS mapping of 52100 steel alloy surface after rolled with Al-Mn alloy after 1 pass

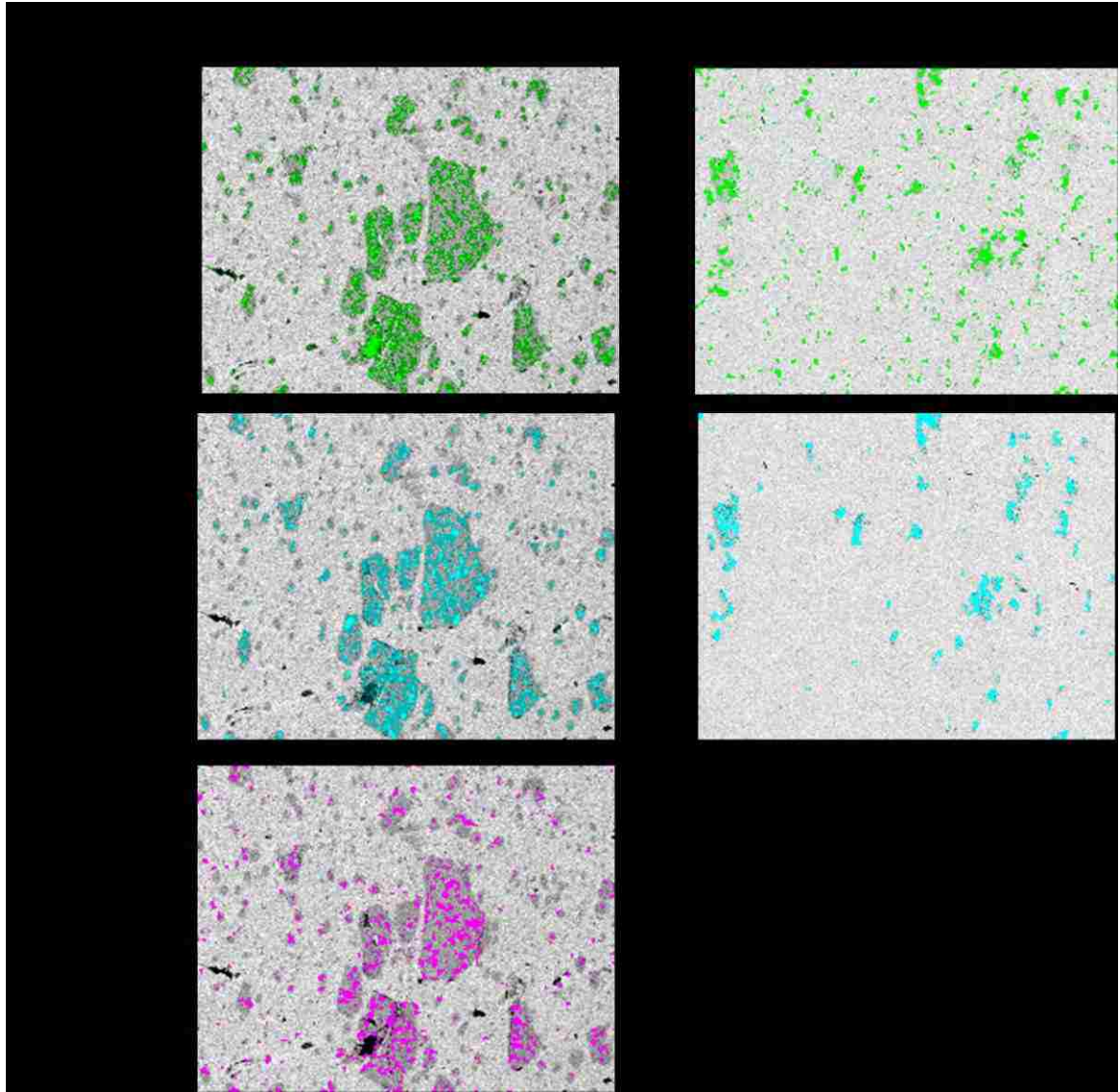
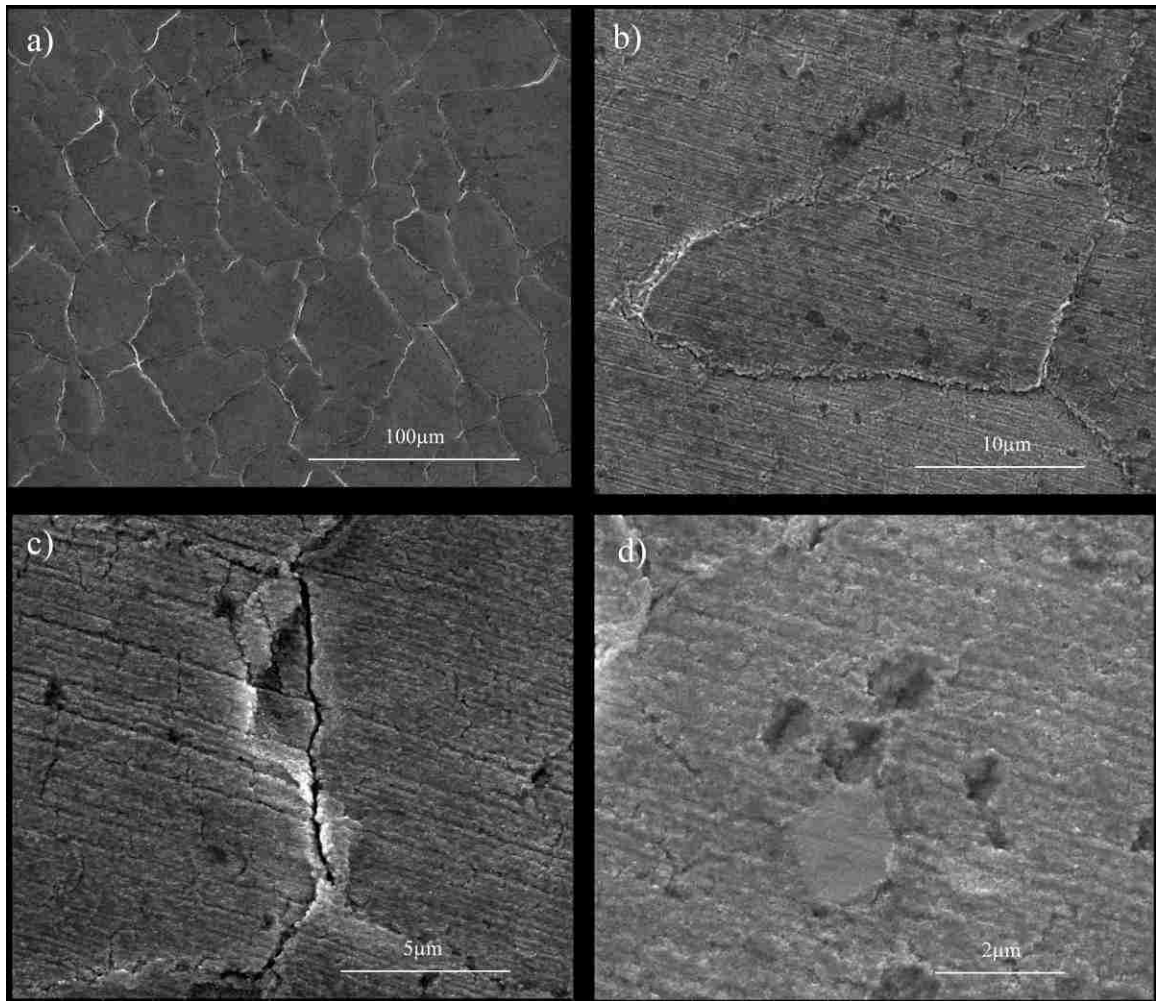


Figure 32. Comparison of EDS mapping of D2 and 440C steel alloy surface after rolled with Al-Mn alloy after 1 pass with elements of O, Cr and V



←
Rolling direction

Figure 33. SEM images of Al-Mg alloy surface rolled with 52100 steel roll after 1 pass, order of magnification from low to high for a) to d)

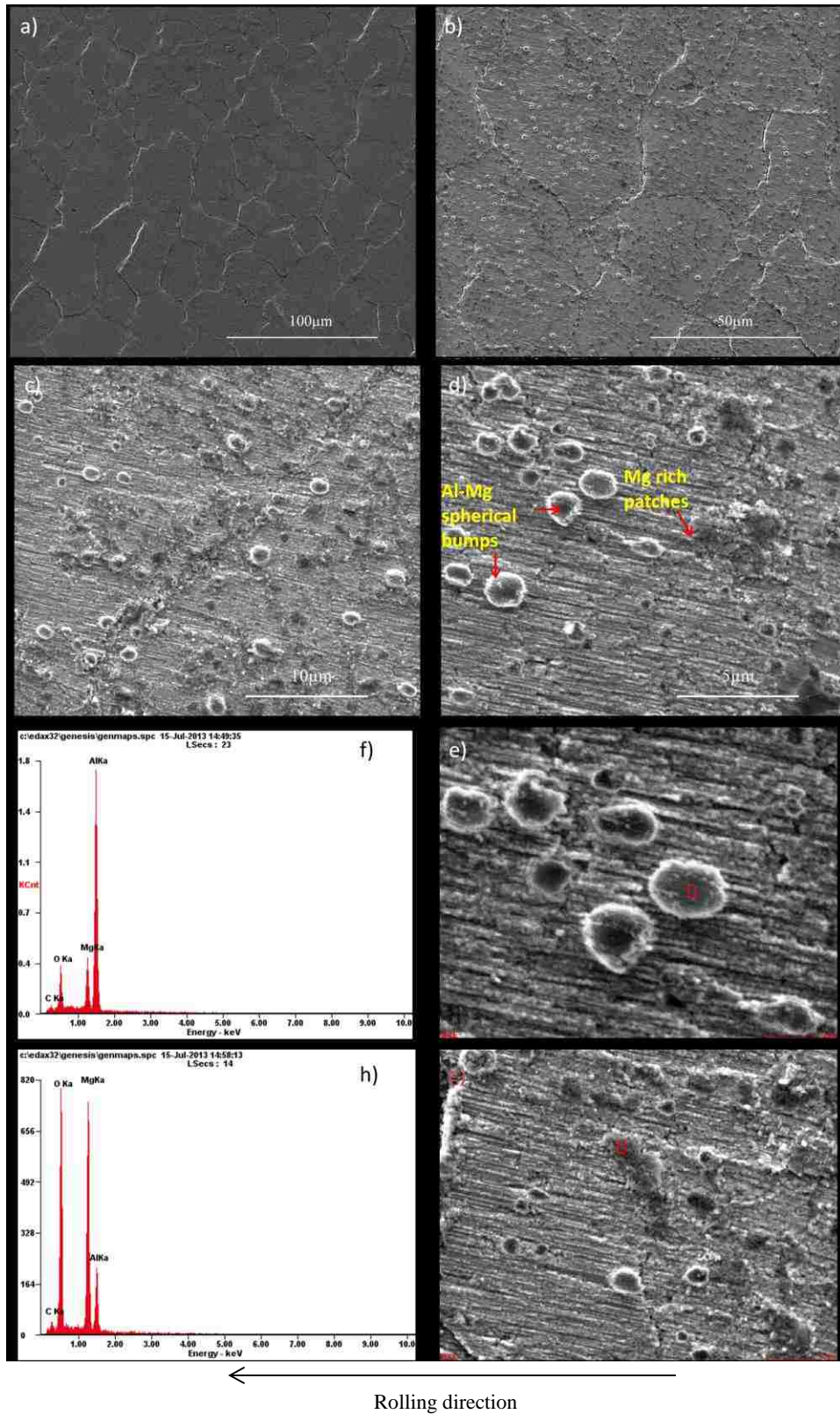


Figure 34. SEM images of Al-Mg alloy surface rolled with 440C steel roll after 1 pass, a) SEM image taken at 12 kV and b) SEM image taken at 5 kV, f) and h) are EDS analysis on surface features at e) and g), respectively

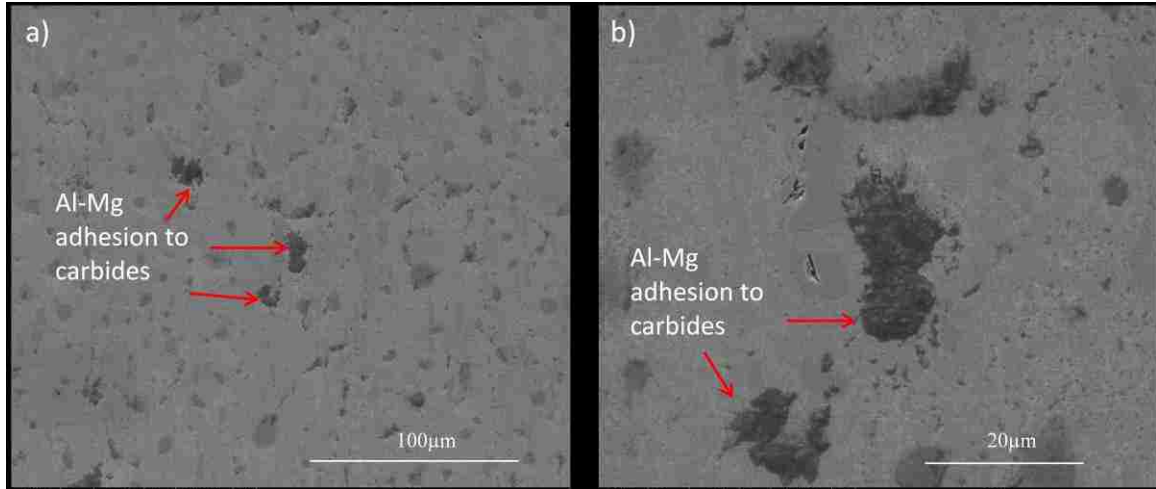


Figure 35. SEM images of 440C steel alloy surface after rolled with Al-Mg alloy after 1 pass

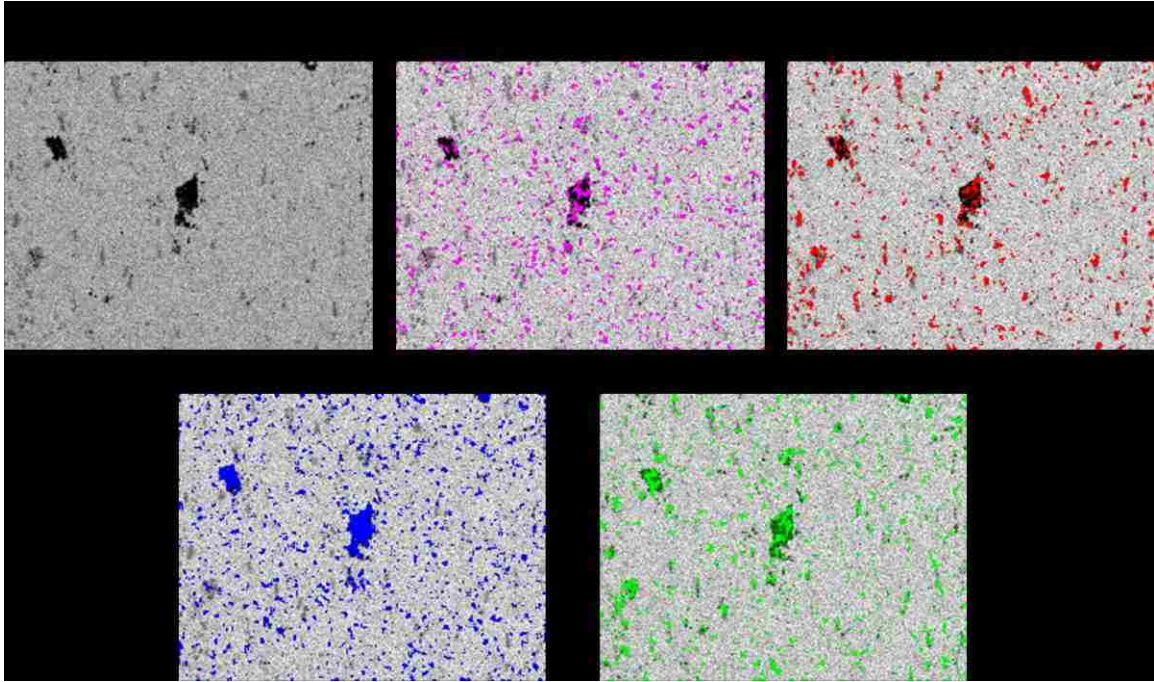
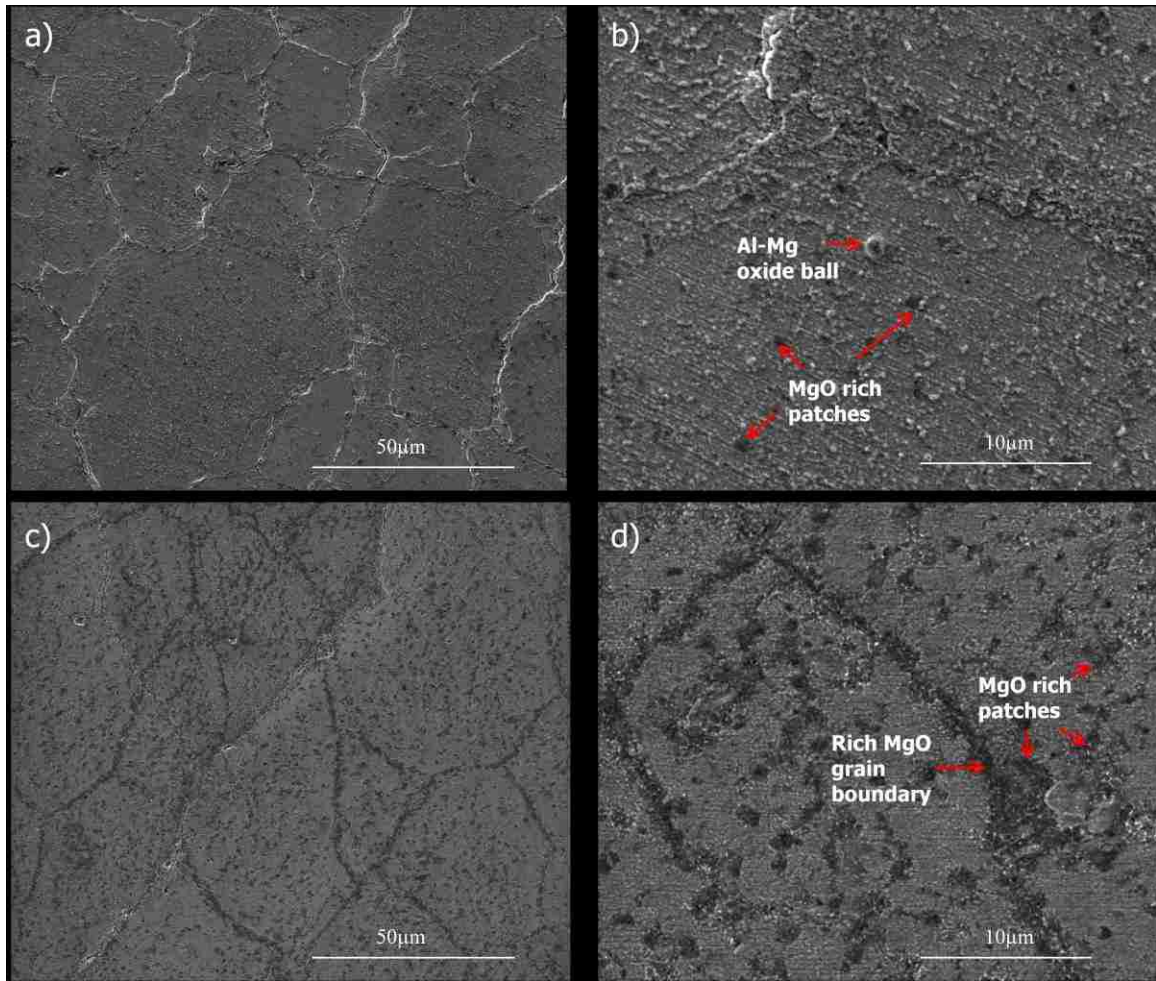


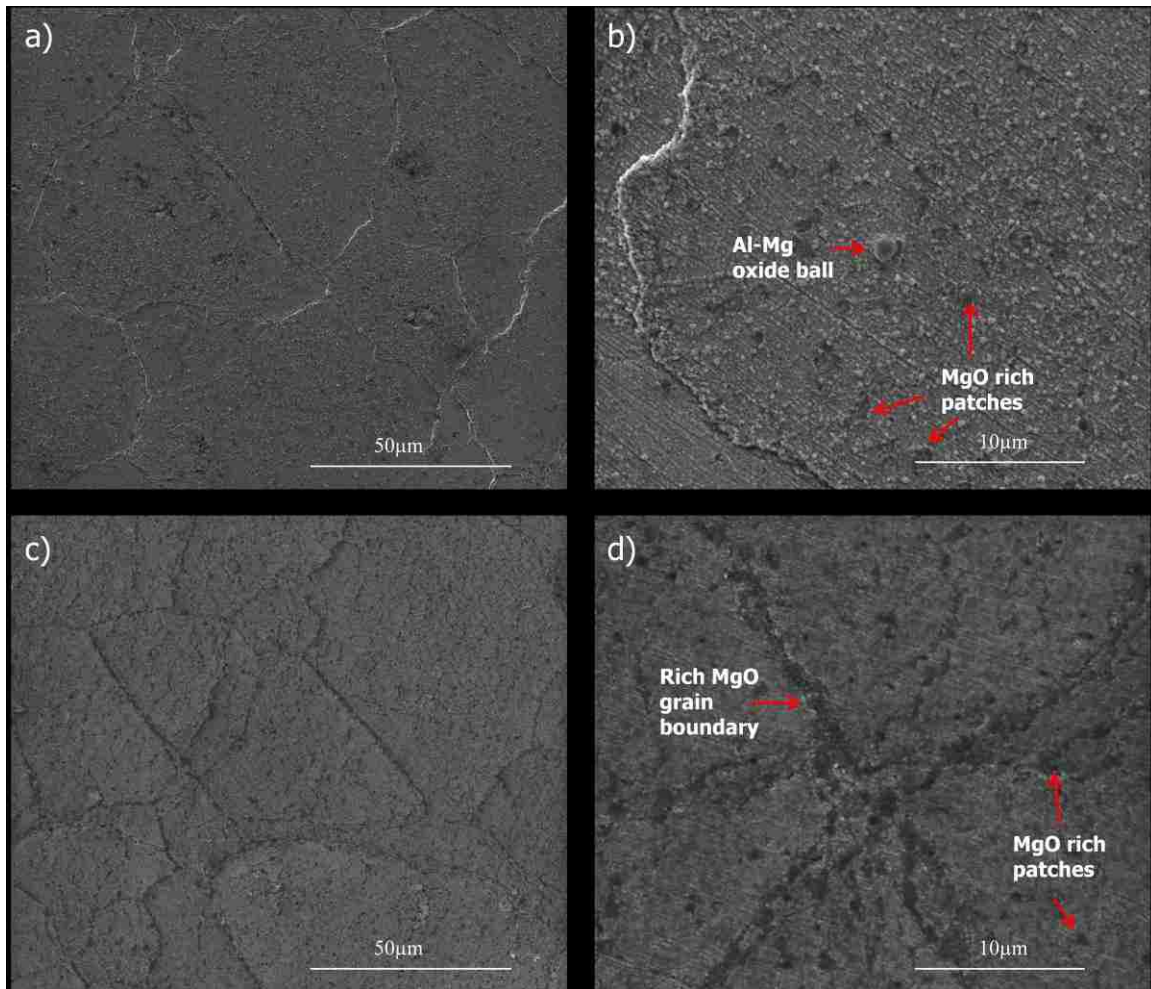
Figure 36. EDS mapping of 440C steel alloy surface after rolled with Al-Mg alloy after 1 pass



←
Rolling direction

Figure 37. SEM images of Al-Mg alloy surface rolled with 440C steel roll after 1 pass and 4 passes, a) and b) after 1 pass, c) and d) after 4 passes, magnification from low to high: 1 pass for a) to b) and 4 passes for c) to

d)



←
Rolling direction

Figure 38. SEM images of Al-Mg alloy surface rolled with D2 steel roll after 1 pass and 4 passes, a) and b) after 1 pass, c) and d) after 4 passes, magnification from low to high: 1 pass for a) to b) and 4 passes for c) to d)

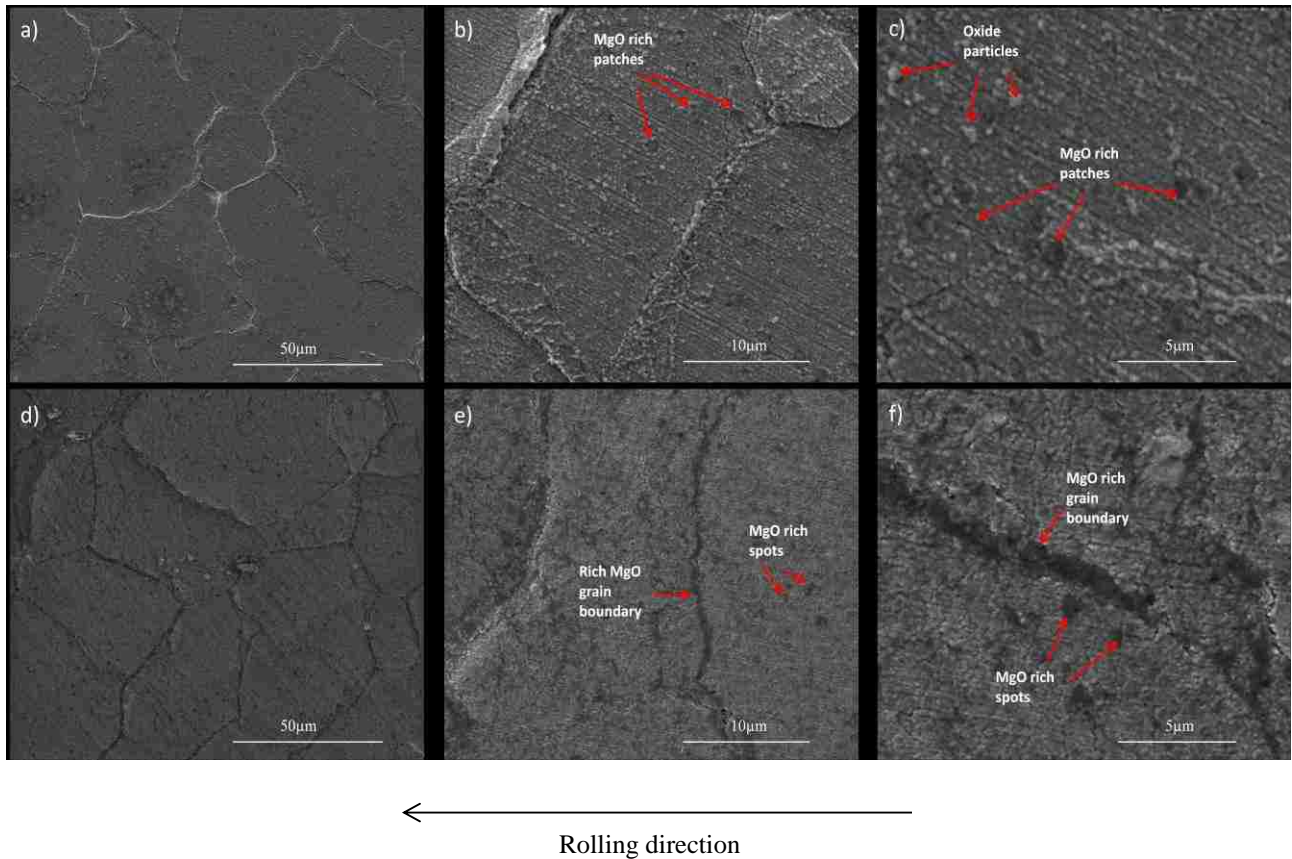


Figure 39. SEM images of Al-Mg alloy surface rolled with 52100 steel roll after 1 pass and 4 passes, a), b) and c) after 1 pass, d), e) and f) after 4 passes, magnification from low to high: 1 pass for a) to c) and 4 passes for d) to f)

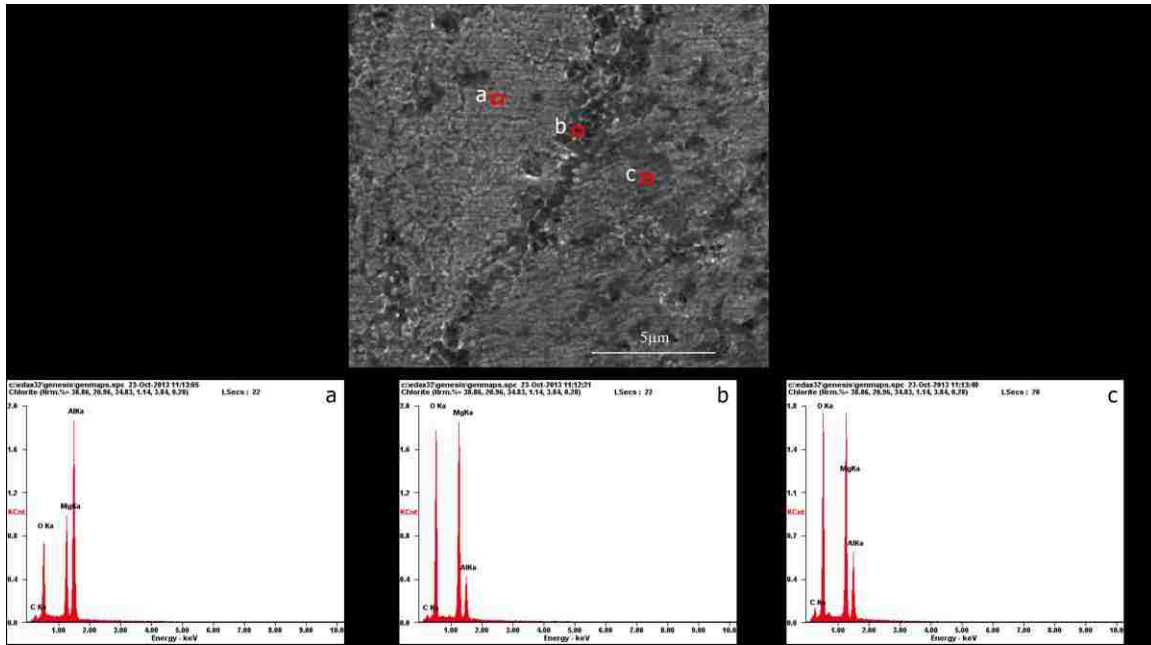


Figure 40. EDS analysis of Al-Mg alloy surface features rolled with 440C steel roll after 4 passes, a) at normal rolled surface region, b) at darkened grain boundary region, c) at dark patch area

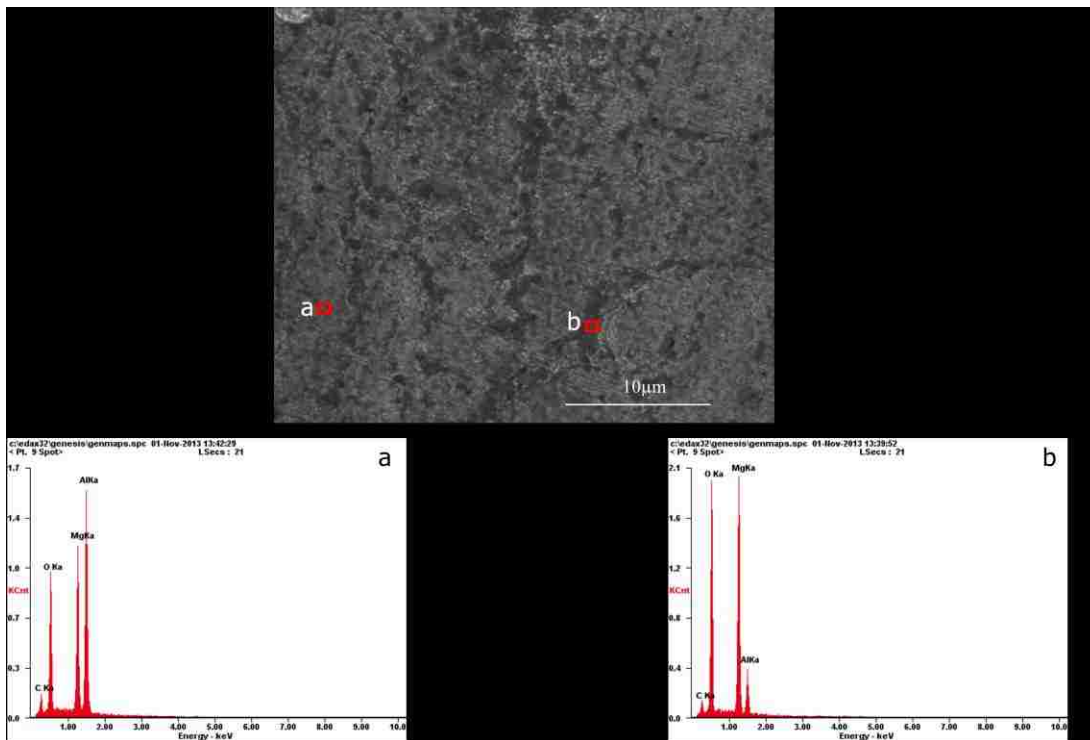


Figure 41. EDS analysis of Al-Mg alloy surface features rolled with D2 steel roll after 4 passes, a) at normal rolled surface region, b) at darkened grain boundary region

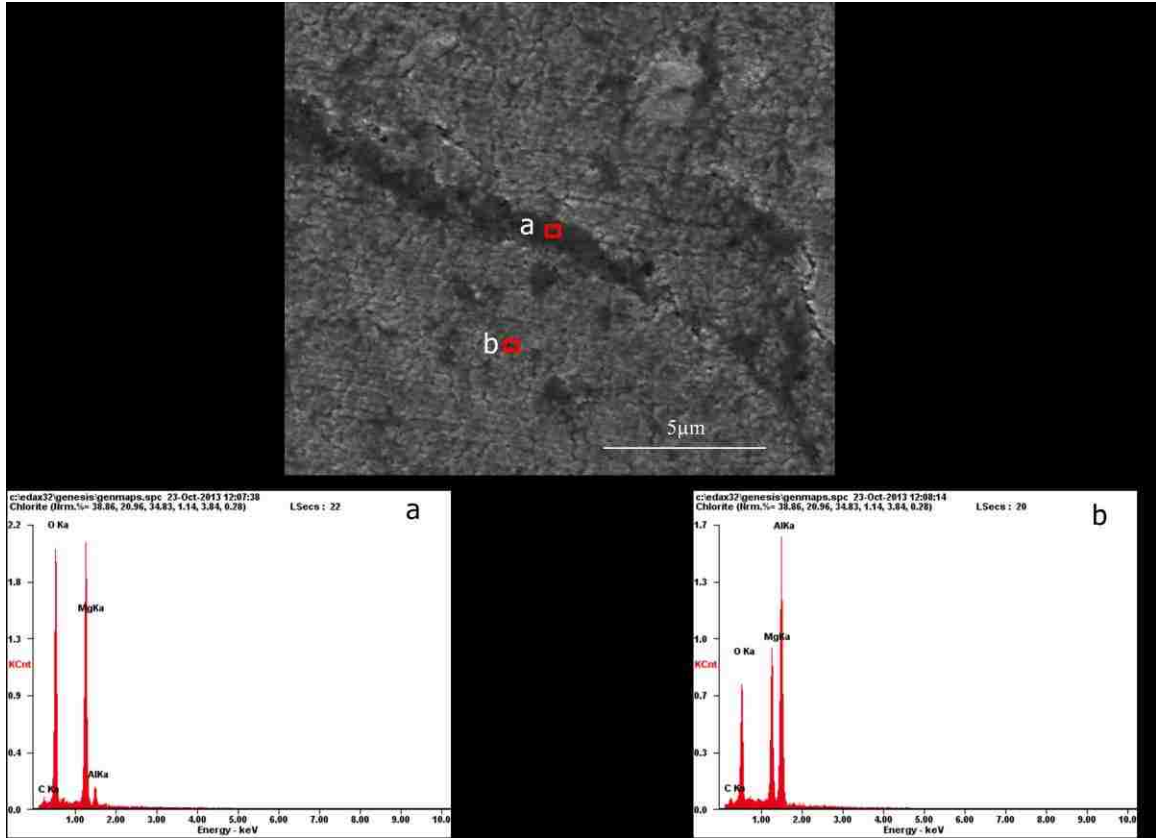


Figure 42. EDS analysis of Al-Mg alloy surface features rolled with 52100 steel roll after 4 passes, a) at darkened grain boundary, b) at normal rolled surface region

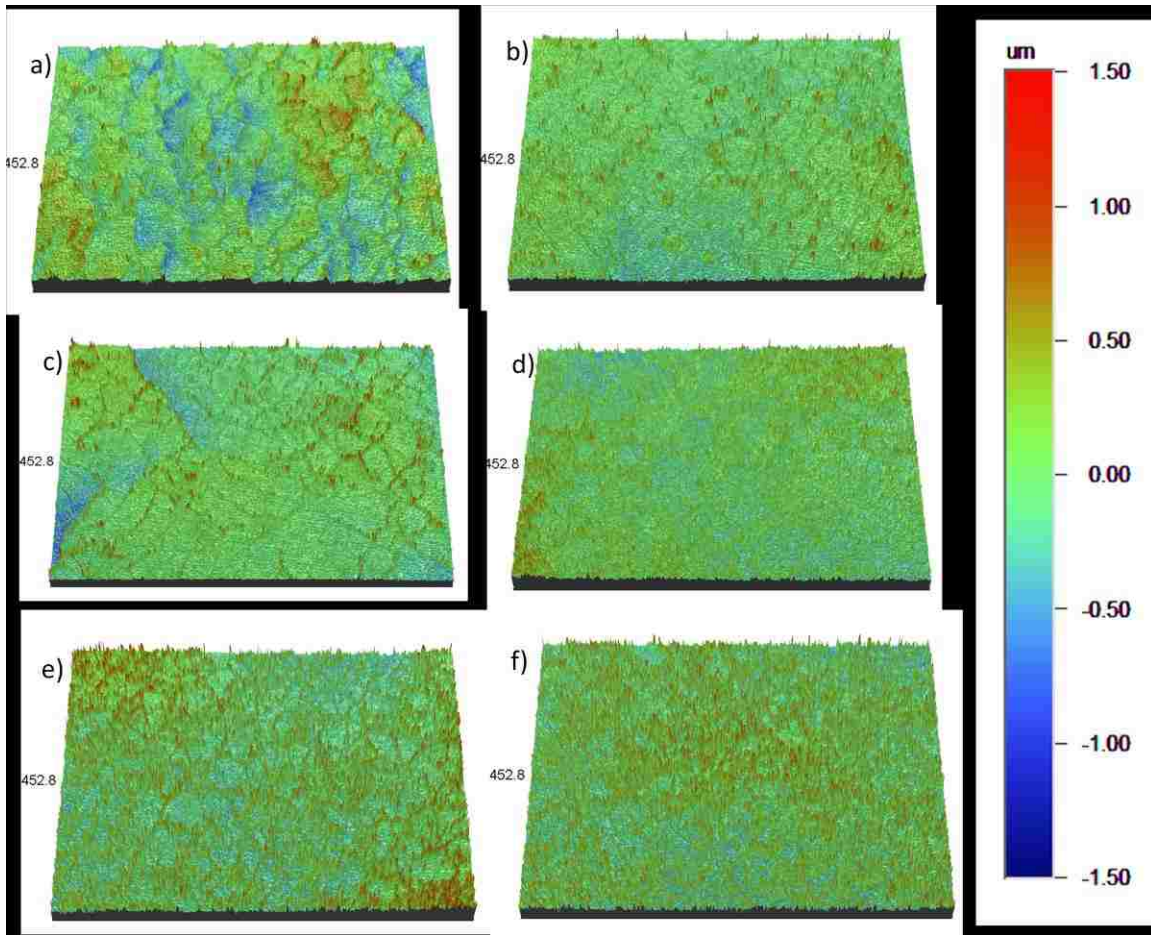
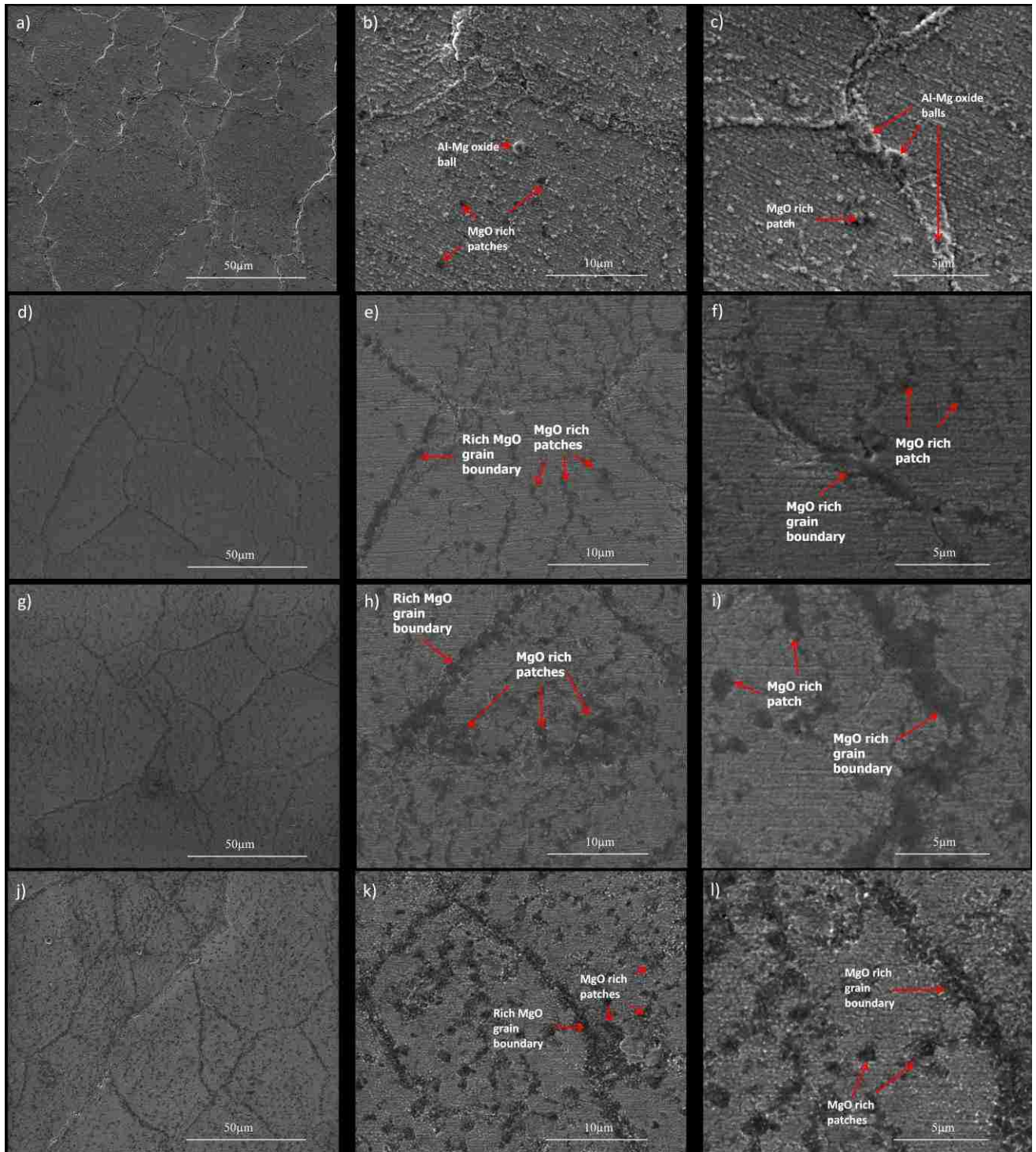


Figure 43. WYKO images of surface profilometry of Al-Mg alloy after rolled a) 1 pass at 550 °C Ra = 0.206, b) 2 passes at 525 °C Ra = 0.132, c) 3 passes at 500 °C Ra = 0.196, d) 4 passes at 475 °C Ra = 0.186, all with 440C, e) 5 passes at 475 °C Ra = 0.198, all with 440C, and f) 6 passes at 475 °C Ra = 0.203, all with 440C



Rolling direction ←

Figure 44 SEM images of Al-Mg alloy surface rolled with 440C steel roll after 1 pass, 2 passes, 3 passes and 4 passes, a), b) and c) after 1 pass, d), e) and f) after 2 passes, g), h) and i) after 3 passes, j), k) and l) after 4 passes. Magnification from low to high: 1 pass for a) to c), 2 passes for d) to f), 3 passes for g) to i) and 4 passes for j) to l)

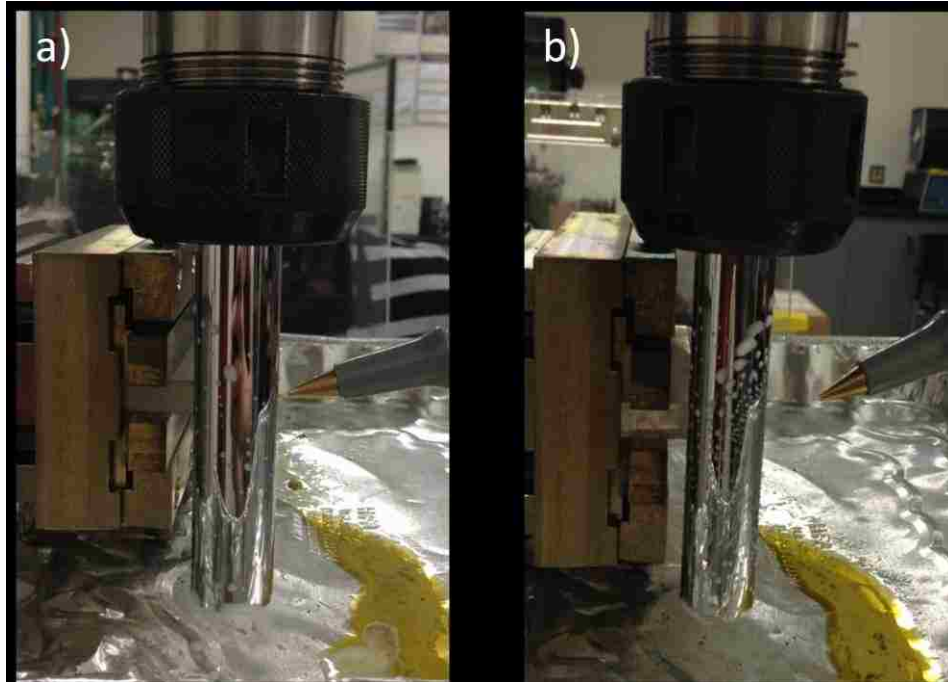


Figure 45. Different conditions of lubrication a) nozzle close to roll, b) nozzle far from roll

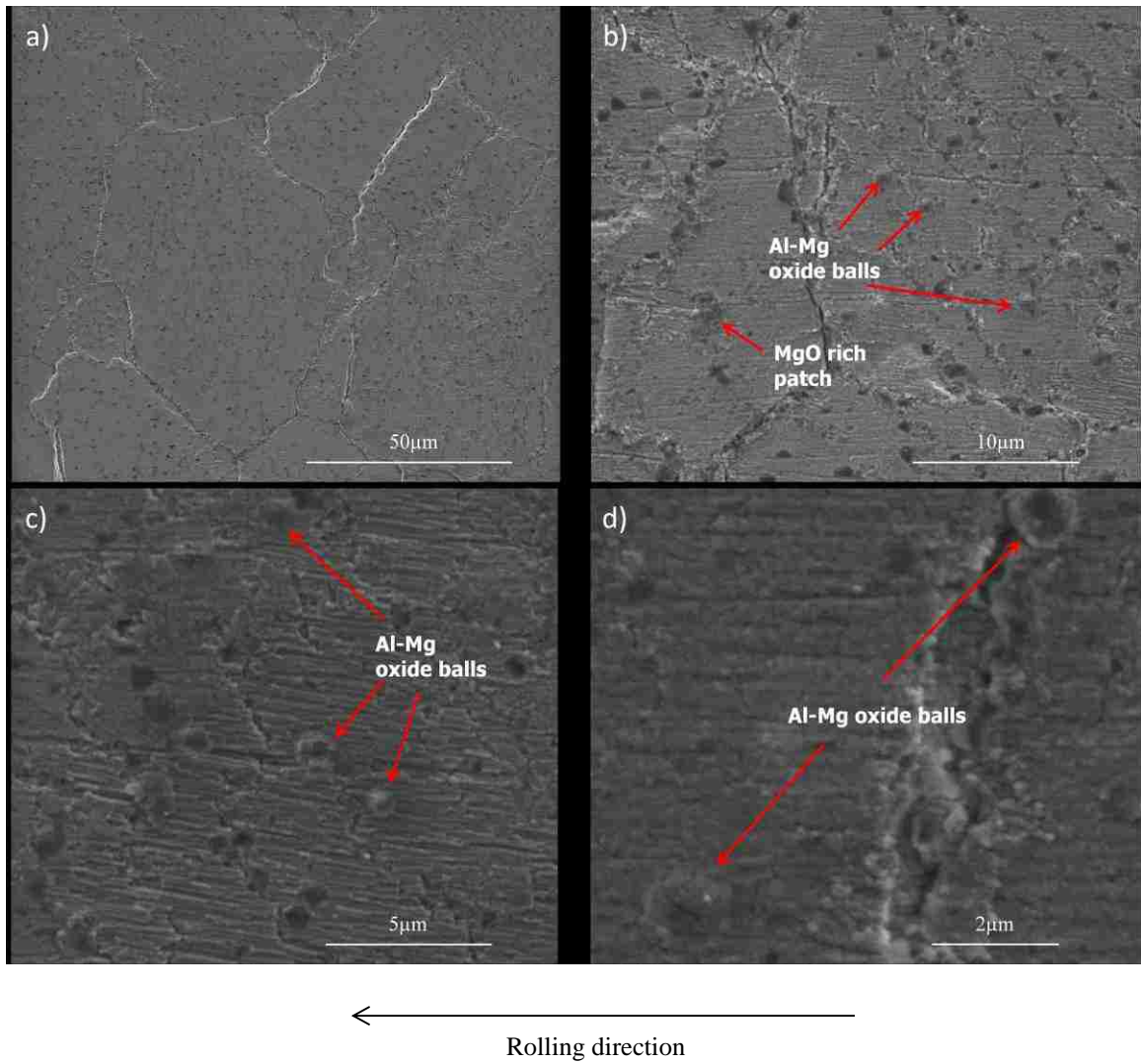


Figure 46. SEM images of Al-Mg alloy surface rolled with 440C steel roll after 1 pass with far nozzle distance lubrication condition, order of magnification from low to high for a) to d)

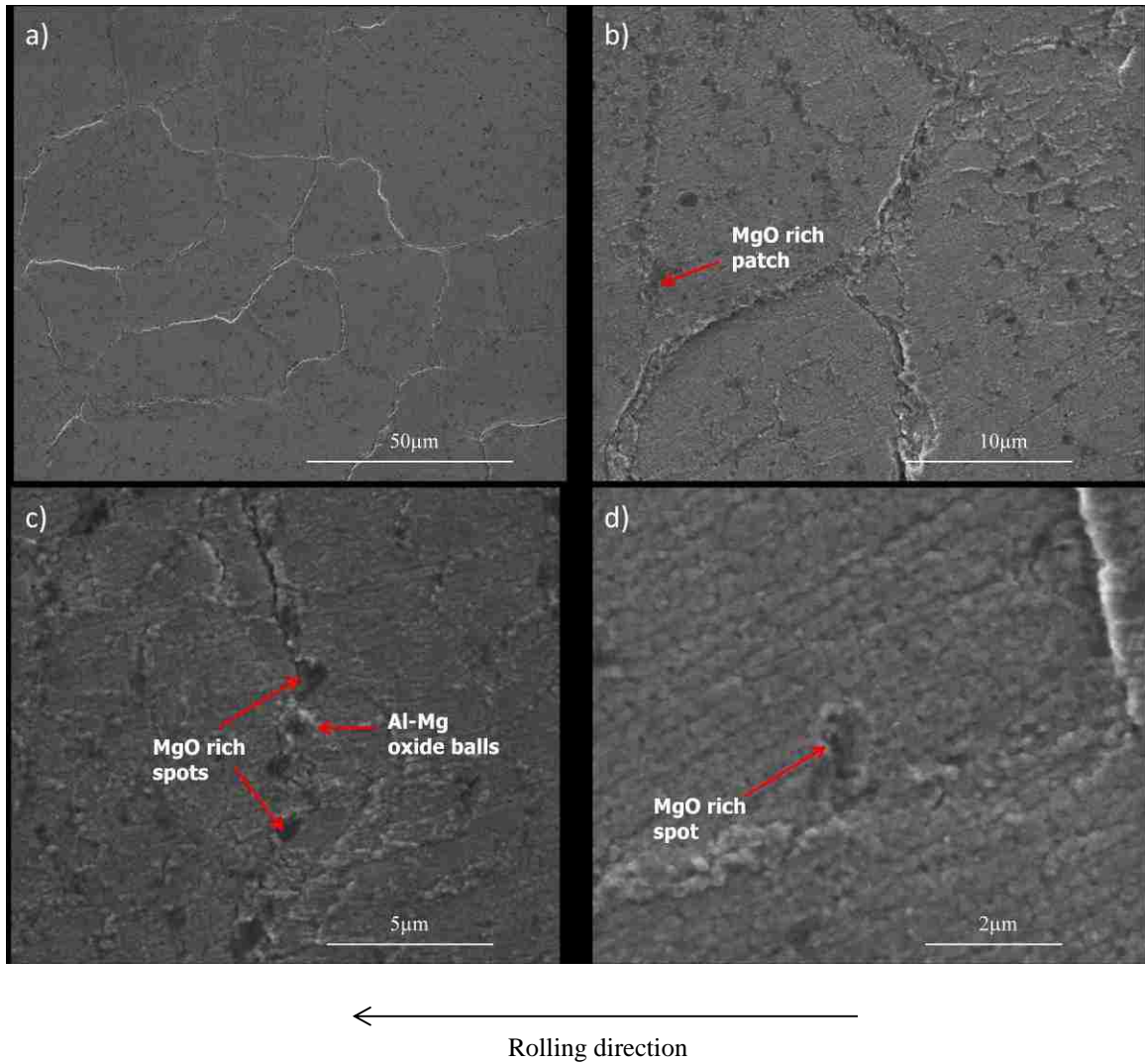


Figure 47. SEM images of Al-Mg alloy surface rolled with 440C steel roll after 1 pass with close nozzle distance lubrication condition, order of magnification from low to high for a) to d)

CHAPTER 5 DISCUSSION

In this study, the most important variable parameter was the roll materials, which were AISI 440C, D2 and 52100. All rolling simulations took place under smooth roll conditions, because this provided an opportunity to see both the clear deformation and morphological feature changes on the surface regions of the rolled aluminum alloys. From the literature review, it was evident that different roll materials, usually steel alloys, have different surface morphologies due to their inconsistent elemental distributions. 440C and D2 were found to experience carbide protrusions on their surfaces, but 52100 appeared to have none of the protrusions. The carbide protrusions observed appeared to be more prominent in 440C but appeared to have a higher population density and a larger size on D2, as shown in Figure 21 and Figure 28. The appearance of these carbides in 440C and D2 corresponded with the carbides mentioned in the Introduction; they were suspected to be $M_{23}C_6$ and M_7C_3 in 440C and M_7C_3 in D2. The M_7C_3 was larger than $M_{23}C_6$, confirmed by Figure 28. Carbides on the D2 roll contained C, Cr and V, and on 440C, they contained C and Cr, as shown in Figure 32. Since both the 440C and D2 had a high chromium content, the carbides were most likely chromium carbides. They were noted to form stable films of the metal oxide Cr_2O_3 around the carbide particles, which inhibited further oxidation; the carbides on both steel rolls were observed to contain O as well.

Three one pass hot rolling experiments were carried on the Al-Mn alloy aluminum alloy with 440C, D2 and 52100 for each simulation. The reason for only doing one pass for each experiment is that one pass was enough to cause localized shear deformations, since grain boundary sliding and cracks were observed on all the after rolled Al-Mn alloy surfaces, as shown in Figures 23-25. The one pass rolled Al-Mn alloy surface features showed a significant difference between the different roll materials of 440C, D2 and 52100, as shown in Figure 26,

where dark patches were observed on the aluminum surface rolled with 440C and D2 but not with 52100, These dark patches appeared more densely on the surface rolled with D2 than with 440C, and more than likely appeared at the areas that surrounded broken precipitates and that were rich in Mg and O. The carbide protrusions in 440C and D2 appeared to correspond with the rich Mg and O dark patches area on the Al-Mn alloy surface when comparing Figure 26 and Figure 28; the surface profilometry in Figure 22 also confirmed this. Furthermore, the EDS map in Figures 29-31 showed that over 50% Mg adhesion coincided with carbide protrusions and the carbide protrusions appeared to have a rich oxygen layer on the surface for both 440C and D2, However, for 52100, the Mg adhesion appeared just across the roll surface, and the oxide spread more across the surface. All the results of the one pass rolling experiments on the Al-Mn alloy pointed to the fact that the magnesium on the rolled aluminum surface was confirmed to be related to the carbides in the steel alloy rolls of 440C and D2. Therefore, the carbide protrusions on the 440C and D2 steel rolls were confirmed responsible for the dark rich Mg and O regions, and these carbides in the steel roll appeared to act as a catalyst for magnesium diffusion during the rolling of the aluminum alloy.

Since the carbide protrusions is the only variable parameter that correlate the Mg diffusion on rolled aluminum, another type of aluminum alloy, the Al-Mg alloy which has a higher magnesium content (3.2-3.7% higher, approximately), was used to carry out further investigations. In the rolling experiment of the Al-Mg alloy with the 440C roll, the surface showed rich Mg, and O dark patches featured as well. However, a new spherical bumps feature was observed to cover the Al-Mg alloy surface after rolling with 440C, as shown in Figure 34. These features could only be seen at a low voltage beam (5kV) condition in SEM, since it

provides a better topological view of the surface features than a high voltage beam (12 kV); otherwise, those features would appear as dark spots in SEM. These spherical bumps were more like balls of a size around 1 μm and they had the same Al, Mg concentrations as the surface from the EDS analysis showed in Figures 34f and h. However, none of the Al-Mg micro-ball features were observed on the Al-Mg alloy surface rolled with 52100; only dark depressions rich in Mg appeared on the surface after being rolled with 52100, as shown in Figure 33.

Moreover, from the SEM images and EDS map of 440C after the rolling simulation with the Al-Mg alloy, shown in Figures 35-36, the Mg adhesion coincided better with the carbides compared to the EDS map of 440C rolled with the Al-Mn alloy, shown in Figures 29-31. The more distinct correspondence of this magnesium adhesion was observed to be caused by the increased amount of Mg content in the Al-Mg alloy compared to the Al-Mn alloy.

All hot rolling simulations of the Al-Mn alloy and the two one-pass experiments on the Al-Mg alloy with the 440C and 52100 rolls (Figures 21-36) were conducted using lubricant A, and then the lubricant was changed to lubricant B for further investigation of the Al-Mg alloy, since the lubricant B used in this research work is the general lubricant for rolling the Al-Mg alloy in industrial areas. After the lubricant was changed to lubricant B, the Al-Mg micro-ball features appeared less frequently on the surface of the one-pass rolled Al-Mg alloy with 440C and D2, as shown in Figure 37a-b and Figure 38a-b; the ball features did not appear on the surface rolled with 52100 as they did when rolled with lubricant A. Although the Mg riched dark patches appeared as well on the Al-Mg alloy surface rolled with 52100, they were observed to be more apparent and have a higher density on the surface rolled with 440C and D2, as shown in Figure 37a-b, 38a-b and 39a-c. The Mg adhesion coincided more with the carbide protrusions in 440C with the Al-Mg alloy than with the Al-Mn alloy; as a result, it can be assumed that the

carbides' effect on the magnesium diffusion was not particular to the Al-Mn alloy but increased with the rising content of magnesium in the aluminum alloy.

After four passes with all three kinds of roll materials 440C, D2 and 52100, grain boundaries on the surface of the rolled Al-Mg alloy appeared darkened, and the surfaces rolled with 440C and D2 were observed to have a higher density of dark patches than the 52100 rolled sample, as shown in Figure 37d-e, 38d-e and 39d-f. No Al-Mg micro-ball features were observed after four passes with all 440C, D2 and 52100 rolls. All the darkened areas, despite grain boundaries or dark patches, were observed to be rich in Mg and O, as shown in the EDS analysis in Figures 40-42. These darkened areas could confirm that a surface evolution occurred on the surface area; hence, the Al-Mg alloy rolled with 440C steel roll was chosen to investigate the surface evolution on every pass up to four passes, since the 440C and D2 have similar carbide protrusion structures on their surfaces, and the only difference in morphology was the size of the carbide protrusions, which could be negligible. From the profilometry results, it was noted that the surface roughness decreased after the second pass but increased again at the third pass and then normalized after the fourth pass, as shown in Figure 43, the mechanism of the roughness fluctuation remains unclear. However, the grain boundaries and dark patches darkened further as the number of passes increased. It can be seen clearly in Figure 44 that they became darker with each pass.

Two lubricants were used in this research, both of them water-oil emulsions. The reason for conducting one hot rolling experiment on the Al-Mg alloy with lubricant A was to replicate the exact rolling conditions undergone for the Al-Mn alloy. This was done to determine the

effect of the Mg content of the alloy on the surface features during rolling with different steels, since the Al-Mg alloy possesses a higher proportion of Mg than does the Al-Mn alloy. Hence, the frequency of appearance of the Al-Mg micro-ball features on the Al-Mg alloy surface rolled with 440C with a different lubricant testified to the effect of lubricants on the surface morphology during rolling..

Since the Al-Mg micro-ball features were observed less often on the Al-Mg alloy surface rolled with 440C with lubricant B, as shown in Figure 37a-b and Figure 38 a-b, experiments with different lubrication conditions were conducted in order to provide more information on the appearance of surface ball features. One experiment was conducted with the lubricant nozzle at a close distance to the roll and the other with the lubricant nozzle at a far distance from the roll, as shown in Figure 45. The results in Figures 46-47 show no Al-Mg micro-ball features on the aluminum surface during the close nozzle distance condition, but they were still observed during the far nozzle distance condition. Therefore, the Al-Mg micro-ball features on the rolled Al-Mg alloy surface were suggested to be due to the lack of lubrication. The mechanism of formation of these balls needs further investigation; however, their formation can be hindered by better lubrication which lubricant B offers.

CHAPTER 6 CONCLUSION

Hot rolling simulation experiments were conducted using the aluminum alloys Al-Mn alloy (Al-Mn-Mg) and Al-Mg alloy (Al-Mg) in order to study the surface defects occurring during high temperature operations and to study the parameters that influence them. The experiments centred on the effects of different roll materials and the number of rolling passes on surface defects. The results show that:

- 1) Different roll materials do affect the morphology of the mating aluminum alloy surface with apparent surface defects.
- 2) The carbide protrusions in 440C and D2 steel rolls are confirmed to be responsible for the dark, rich Mg and O regions on the Al-Mn alloy rolled surface, and these carbides in the steel roll appeared to act as a catalyst for magnesium diffusion during the rolling of aluminum alloy.
- 3) The carbides' effect on magnesium diffusion is not particular to the Al-Mn alloy but increases with the rising content of magnesium in the aluminum alloy (Al-Mg alloy).
- 4) As the number of passes increases, Mg and O deposit in the form of patches and grain boundaries near the surface area.
- 5) The Al-Mg micro-ball features on the rolled Al-Mg alloy surface are suggested due to the lack of lubrication; however, the mechanism of formation of these features needs further research.

REFERENCES

- [1] Degarmo, E. Paul, JT Black, Kohser Ronald A. Materials and Processes in Manufacturing (9th ed.), Wiley. (2003).
- [2] R.E. Sanders. Technology Innovation in aluminum products, The Journal of Minerals. 53 (2001) 21-25.
- [3] WF Smith, J Hashemi. Foundations of Materials Science and Engineering (4th ed.), McGraw-Hill. (2006).
- [4] Joseph R. Davis. Aluminum and aluminum alloys, ASM International. (1993).
- [5] J. Gilbert Kaufman. Introduction to aluminum alloys and tempers, The Materials Information Society
- [6] A.S. Korhonen. On the work-hardening of AA 3104-H19 aluminum alloy, JMEPEG. 22 (2013) 505-511.
- [7] Polmear I. J. “Wrought Aluminium Alloys Light Alloys: Metallurgy of the Light Metals” , Butterworth – Heinemann, London. (1995).
- [8] Totten G. E., MacKenzie D. S. “Handbook of Aluminum Volume 1: Physical Metallurgy and Processes”, Marcel Dekker Inc. (2003).
- [9] Lu L., Man O. L. “Mechanical Alloying”, Springer. (1998).

- [10] Metals Handbook 10th Ed. Metallography and Microstructures, ASM International. 9 (2004) 1714.
- [11] Alankar, Mary A. Wells. Constitutive behavior of as-cast aluminum alloys AA3104, AA5182 and AA6111 at below solidus temperatures, Materials Science and Engineering A. 527 (2010) 7812-7820.
- [12] A.R. Riahi, A. Edrisy, A.T. Alpas. Effect of magnesium content on the high temperature adhesion of Al-Mg alloys to steel surfaces, Surface & coating technology. 203 (2009) 2030-2035.
- [13] Serkan Toros, Fahrettin Ozturk, Ilyas Kacar. Review of warm forming of aluminum-magnesium alloys, Journal of materials processing technology. 207 (2008) 1-12.
- [14] Alloys of 13 Aluminum, <http://chemsoc.velp.info/alloys.php?elementno=13>, DOA: March, 22, 2014, .
- [15] Frolich M.F., Walker J.C., Rainforth W.M., Benyon J.H. Formation and structure of a subsurface layer in hot rolled aluminium alloy AA3104 transfer bar, Tribology International. 38 (2005) 1050-1058.
- [16] Premendra., Philippe L., Terry H., de Wit J.H.W., Katgerman L. Understanding the electrochemical, microstructural and morphological changes during hot rolling from a corrosion perspective, Surface and Coatings Technology. 201 (2006) 828-834.
- [17] A.O. Adesola, A.G. Odeshi, U.D. Lanke. The effects of aging treatment and strain rates on damage evolution in AA 6061 aluminum alloy in compression, Materials and Design. 45 (2013) 212-221.

- [18] Specification of alloys steel:. AISI 52100/Gcr 15
- [19] Aircraft Materials. Alloy 440C, <http://www.aircraftmaterials.com/data/alstst/440c.html>. (DOA: March, 30, 2013).
- [20] Bohler Uddeholm. AISI D2, http://www.bucorp.com/aisi_d2_c.htm. (DOA: March, 30, 2013).
- [21] Syalons International, AISI 1010 Carbon steel (UNS G10100), <http://www.azom.com/article.aspx?ArticleID=6539>, DOA: March, 30, 2013, .
- [22] S. Peissi, G. Mori, H. Leitner, R. Ebner, S. Eglsaer. Influence of chromium, molybdenum and cobalt on the corrosion behaviour of high carbon steels in dependence of heat treatment, *Materials and Corrosion*. 57 (2006) 759.
- [23] Dennis W. Hetzner, William Van Geertruyden. Crystallography and metallography of carbides in high alloy steels, *Materials Characterization*. 59 (2008) 825-841.
- [24] D. Bombac, M. Fazarinc, A. Saha Podder, G. Kugler. Study of Carbide Evolution During Thermo-Mechanical Processing of AISI D2 Tool Steel, *ASM International*. 22 (2013) 742-747.
- [25] H. Torkamani, Sh. Raygan, J. Rassizadehghani. Comparing microstructure and mechanical properties of AISI D2 steel after bright hardening and oil quenching, *Materials and Design*. 54 (2014) 1049-1055.

- [26] Afseth A., Nordlien J.H., Scamans G.M., Nisanicioglu K. Effect of thermo-mechanical processing on filiform corrosion of aluminium alloy AA3005, *Corrosion Science*. 22 (2002) 2491-2506.
- [27] Zhou X., Liu Y., Thompson G.E., Scamans G.M., Skeldon P., Hunter J.A. Near-surface deformed layers on rolled aluminum alloys, *Metallurgical and materials transactions A*. (2010) 1-13.
- [28] Fishkis M., Lin J.C. Formation and evolution of a subsurface layer in a metal working process, *Wear*. 206 (1997) 156-170.
- [29] A.R. Riahi, O.A. Gali, K.R. Januskiewicz, D. Pattemore. Experimental study of the disturbed layer generation during hot rolling contact of aluminum with steel, *Tribology International*. 54 (2012) 42-50.
- [30] G. M. Scamans, A Afseth and G E Thomson, Y Liu and X Zhou. Corrosion of painted aluminum sheet, *Materials Science Forum*. 519-521 (2006) 647-654.
- [31] R. Shabadi, S. Suwas, S. Kumar, H.J. Roven, E.S. Dwarkadasa. Texture and formability studies on AA7020 Al alloy sheets, *Materials science & engineering*. 558 (2012) 439-445.
- [32] S. Das, A.R. Riahi, X. Meng-Burany, A.T. Morales, A.T. Alpas. High temperature deformation and fracture of tribo-layers on the surface of AA5083 sheet aluminum-magnesium alloy, *Materials Science and Engineering A*. 531 (2012) 76-83.

- [33] Y. Liu, T. Hashimoto, X. Zhou, G.E. Thompson, G.M. Scamans, W.M. Rainforth, Influence of near-surface deformed layers on filiform corrosion of AA3104 aluminum alloy, *Surface and Interface Analysis*.
- [34] Tamara McGill-Taylor, Charlie R. Brooks, Scott Goodrich. Effect of cold working and annealing on mechanical properties and microstructure of hot rolled Al Alloy 3104, *J. Heat. Treating*. 9 (1991) 5-25.
- [35] G. Buytaert, H. Terry, S. Van Gils, B. Kernig, B. Grzemba, M. Mertens. Study of the near surface of hot- and cold-rolled AlMg0.5 aluminium alloy, *Surf. Interface Anal.* 37 (2005) 534-543.
- [36] W.C. Liu, D. Juul Jensen, J. G. Morris. Effect of grain orientation on microstructures during hot deformation of AA 3104 aluminum alloy by plane strain compression, *Acta mater.* 49 (2001) 3347-3367.
- [37] W.C. Liu, P.P. Zhai. Characterization of microstructure near grain boundary in hot deformed AA 3104 aluminum alloy, *Materials Characterization*. 62 (2011) 81-89.
- [38] W.C. Liu, P.P. Zhai, C.-S. Man. Estimating local dislocation content near a grain boundary in hot deformed AA 3104 aluminum alloy, *Materials science and engineering*. 531 (2012) 178-181.
- [39] G. Buytaert, H. Terry, S. Van Gils, B. Kernig, B. Grzemba, M. Mertens. Investigation of the (sub)surface of commercially pure rolled aluminium alloys by means of total reflectance, r.f. GDOES, SEM/EDX and FIB/TEM analysis, *Surf. Interface Anal.* 38 (2006) 272-276.

- [40] Rong Hu, Tomo Ogura, Hiroyasu Tezuka, Tatsuo Sato, Qing Liu. Dispersoid formation and recrystallization behavior in an Al-Mg-Si-Mn alloy, ScienceDirect J. Mater. Sci. Technol. 26 (2010) 237-243.
- [41] Premendra, J.H. Chen, F.D. Tichelaar, H. Terryn, J.H.W. deWit, L. Katgerman. Optical and transmission electron microscopical study of the evolution of surface layer on recycled aluminium along the rolling mills, Surface & Coatings Technology. 201 (2007) 4561-4570.
- [42] Frolich M.F., Krzyzanowski M., Rainforth W.M., Benyon J.H. Oxide scale behaviour on aluminium and steel under hot working conditions, Journal of Materials Processing Technology. 177 (2006) 36-40.
- [43] G. Plassart, M. Aucouturier, R. Penelle. Microstructure and chemistry of an Al-4.7 wt.% Mg alloy subsurface after cold-rolling, Scripta Materialia. 41 (1999) 1103-1108.
- [44] Rajan Ambat, Alison J. Davenport, Andreas Afseth, Geoff Scamans. Electrochemical behavior of the active surface layer on rolled aluminum alloy sheet, Journal of the Electrochemical Society. 151 (2004) B53-B58.
- [45] S.I. Vooijs, S.B. Davenport, I. Todd, S. Van Der Zwaag. Monitoring the precipitation reactions in a cold-rolled Al-Mn-Mg-Cu alloy using thermoelectric power and electrical resistivity measurements, Philosophical Magazine A. 81 (2001) 2059-2072.
- [46] Takeshi Fujita, Zenji Horita. Characteristics of diffusion in Al-Mg alloys with ultrafine grain sizes, Philosophical Magazine A. 82 (2002) 2249-2262.

- [47] Rafal Pelka, Agnieszka Pattek-Janczyk, Walerian Arabczyk. Studies of the oxidation of nanocrystalline iron with oxygen by means of TG, MS, and XRD methods, *J. Phys. Chem. C.* 112 (2008) 13992-13996.
- [48] A. Shirizly, J. G. Lenard, J. Sauer, K. Januszkiewicz. Lubricant capture during hot rolling of an aluminum alloy, 45 (2002) 205-210.
- [49] M.S. Mirza, C.M. Sellars, K. Karhausen, P. Evans. Multipass rolling of aluminum alloys: finite element simulations and microstructural evolution, IoM Communications Ltd. (2001).
- [50] Baolute Ren. Evolution of rolling and recrystallization textures in a hot rolled can body stock alloy, Reynolds Metals Company, Muscle Shoals.
- [51] S.P. Timothy, H.L. Yiu, J.M. Fine, R.A. Ricks. Simulation of single pass of hot rolling deformation of aluminum alloy by plane strain compression, .
- [52] Guangjie Huang, Qing Liu, Lingyun Wang, Xiaohui Yin. Dynamic Recrystallization of 3104 Aluminum alloy during Isothermal Compression Deformation at Elevated Temperatures, *Materials Science Forum.* 546-549 (2007) 1061-1064.
- [53] Hakon Leth-Olsen, Jan Halvor Nordlien, Kemal Nisancioglu. Filiform corrosion of aluminium sheet. III. microstructure of reactive surfaces, *Corrosion Science.* 40 (1998) 2051-2063.
- [54] G. Buytaert, B. Kernig, H.J. Brinkman, H. Terryn. Influence of surface pre-treatments on disturbed rolled-in subsurface layers of aluminium alloys, *Surface & coatings technology.* 201 (2006) 2587-2598.

- [55] N. LeBozec, D.Persson, D. Thierry. In situ studies of the initiation and propagation of filiform corrosion on aluminum, *J. Electrochem, Soc.* 151 (2004) B440-B445.
- [56] de Wit J.H.W. New knowledge on localized corrosion obtained from local measuring techniques, *Electrochimica Acta.* 46 (2001) 3641-3650.
- [57] G.M. Scamans, A.Afseth, G.E. Thompson, Z Xiaorong. Ultra-fine grain sized mechanically alloyed surface layers on aluminum alloys, *Materials Science Forum.* 396-402 (2002) 1461-1466.
- [58] X. Zhou, G.E. Thompson, G.M. Scamans. The influence of surface treatment on filiform corrosion resistance of painted aluminium alloy sheet, *Corrosion Science.* 45 (2003) 1767-1777.
- [59] G. Buytaert, Premendra, J.H.W. de Wit, L. Katgerman, B. Kernig, H.J. Brinkman, et al. Electrochemical investigation of rolled-in subsurface layers in commercially pure aluminium alloys with the micro-capillary cell technique, *Surface & coatings technology.* 201 (2007) 4553-4560.
- [60] A. Bautista. Filiform corrosion in polymer-coated metals, *Progress in Organic Coatings.* 28 (1996) 49-58.
- [61] J.L. Delplancke, S. Berger, X. Lefebvre, D. Maetens, A. Pourbaix, N. Heymans. Filiform corrosion: interactions between electrochemistry and mechanical properties of the paints, *Progress in Organic Coatings.* 43 (2001) 64-67.
- [62] A.T.A. Jenkins, R.D. Armstrong. The breakdown in the barrier properties of organic coatings due to filiform corrosion, *Corrosion Science.* 38 (1996) 1147-1157.

- [63] S. Kuypers, G. Buytaert, H. Terryn. Depth profiling of rolled aluminium alloys by means of GDOES, *Surf. Interface Anal.* 36 (2004) 833-836.
- [64] Magnus Hanson, Sture Hogmark, Staffan Jacobson. Influence from tool roughness on the risk of work material adhesion and transfer, *Materials and manufacturing processes.* 24 (2009) 913-917.
- [65] A.R. Riahi, A.T. Alpas. Adhesion of AA5182 aluminum sheet to DLC and TiN coatings at 25 and 420, *Surface & coatings technology.* 202 (2007) 1055-1061.
- [66] A.R. Riahi, A.T. Morales, A.T. Alpas. Evaluation of vitreous and devitrifying enamels as hot forming lubricants for aluminum AA5083 alloy, *JMEPEG.* 17 (2008) 387-394.
- [67] Jianlin Sun, Guohong Ding, Lei Xia, Bing Yun, Zesheng Ji. Research on the color difference on surface of 3104 aluminum alloy stripes during cold continuous rolling process, *Advanced Materials Research.* 557-559 (2012) 1383-1386.
- [68] H.R. Le, M.P.F. Sutcliffe, J.A. Williams. Friction and material transfer in micro-scale sliding contact between aluminium alloy and steel, *Tribology Letters.* 18 (2005).
- [69] M. David Hanna. Tribological evaluation of a aluminum and magnesium sheet forming at high temperatures, *Wear.* 267 (2009) 1046-1050.
- [70] Paul E. Krajewski, Arianna T. Morales. Tribological issues during quick plastic forming, *Jmepeg.* 13 (2004) 700-709.

[71] Zhiping Chen, P.F. Thomson. Friction against superplastic aluminium alloys, *Wear*. 201 (1996) 227-232.

[72] R.S. Lee, G.A. Chen, Bing H. Hwang. Thermal and grinding induced residual stresses in a silicon carbide particle-reinforced aluminium metal matrix composite, *Composites*. 26 (1995) 425-429.

VITA AUCTORIS

NAME: Qi Zhao

PLACE OF BIRTH: Jinzhou, China

YEAR OF BIRTH: 1988

EDUCATION: Dalian Maple Leaf International High
School, Dalian, China, 2007
University of Windsor, B.A.Sc., Windsor, ON,
2011
University of Windsor, M.A.Sc., Windsor, ON,
2014